In-Silico Methods for De-Risking the Clinical Development of Subcutaneously Administered Therapeutic Macromolecules

by

Elliot Offman

A thesis

presented to the University of Waterloo

in fulfillment of the

thesis requirement for the degree of

Doctor of Philosophy

in

Pharmacy

Waterloo, Ontario, Canada, 2016

AUTHOR'S DECLARATION

I hereby declare that I am the sole author of this thesis. This is a true copy of the thesis, including any final revisions, as accepted by my examiners.

I understand that my thesis may be made electronically available to the public.

ACKNOWLEDGEMENTS

I would like to acknowledge first and foremost my doctoral supervisor, Dr. Andrea Edginton, without whom, I would not have reached this milestone. To my thesis committee, Dr. Dixon, Dr. Glerum and Dr. Edwards, I am truly grateful for all your support and input over the years. I would like to thank Dr. Colin Phipps, who provided support in the programming of some of the models described in this body of work and injected some humour into some of the more challenging days. I would like to thank the University of Waterloo for the opportunity to continue my education. Finally, to my wife Helen for your support and encouragement over the years. I literally could not have done this without you.

DEDICATION

I dedicate this thesis, as the capstone of my formal education, to my parents and grandparents.

ABSTRACT

Prediction of human pharmacokinetics (PK) following subcutaneous (SC) administration to animals is challenged by potential interspecies differences in skin anatomy and physiology. With respect to biologic or macromolecule drug development, the SC route is gaining substantial interest as a primary route of drug administration over intravenous due to convenience and cost factors. The bioavailability and time course of a SC administered macromolecule can potentially be influenced by local clearance (CL) processes in the SC space after injection, and due to size constraints, is subject to varying degrees of lymphatic uptake following injection. Traditional allometric techniques employed in interspecies scaling are limited to extrapolation of an average value for PK parameters such as clearance (CL) or volume (V), and provide no information on the time course of a drug after administration. In many cases, PK parameters are estimated using non-compartmental (NCA) methods which, in violation of the assumptions of NCA, requires CL to occur via the sampling compartment. Dedrick plots that have been employed to predict the time course of a drug after administration, do not consider species differences in extravascular drug absorption processes. In contrast, model-based methods such as population based compartmental methods allow for an estimation of absorption processes, along with CL and V, in animals, which can then be scaled to human values according empiric allometric relationships. Physiologically- based PK (PBPK) methods allow for a mechanistic means of accounting for the SC time course and further allow for incorporation of local CL processes and lymphatic transport. Model-based drug development has the potential to minimize reliance on animal data to inform human clinical trial design. Moreover, models developed with an intention to translate animal findings to human scale offer an opportunity to streamline clinical development through trial simulation, thus reducing the time and cost of developing a new therapeutic product. With an aim to de-risk biologic and biosimilar drug development, this thesis describes the development and evaluation of (1) a nonlinear mixed effect model incorporating allometric relationships and (2) a PBPK model incorporating an SC depot compartment, based on a single non-human primate (NHP) species, to predict the PK of a SC administered macromolecule. For reference, model-based methods are compared to traditional allometric and model-independent methods employing the same data used in the model-based approaches. Single-species allometric scaling of CL based on an empiric scaling factor previously demonstrated to support reasonable extrapolation from NHP to humans (i.e. 0.85) failed to predict human CL within a reasonable and pre-determined threshold fold error (i.e. predicted/observed falling with 0.7-1.3). Dedrick plots predicted secondarily-derived PK parameters such as Cmax and Tmax reasonably well, however clearly underperformed in predicting the early portion of the SC time course. Model-based approaches provided reasonable estimation of systemic exposure parameters and prediction of the time course, with PBPK models providing an opportunity to mechanistically appreciate influential factors in the SC time course of a macromolecule. As a novel development the SC time course of a macromolecule could be reasonably

simulated by a PBPK model incorporating lymphatic biodistribution and whereby the SC injection was parameterized as a depot compartment within the skin insterstitial space. Similarly for the first time in published literature, a population-based PBPK model was developed incorporating lymphatic system interindividual variability which was demonstrated to predict the time course of a macromolecule in a population of humans.

TABLE OF CONTENTS

LIST OF FIGURES

LIST OF TABLES

LIST OF ABBREVIATIONS AND ACRONYMS

Abbreviation/Symbol	Definition
AAFE	Absolute Average Fold-Error
AFE	Average Fold-Error
AUC	Area Under The Curve
$AUC_{0\text{-}inf}$	Area Under The Curve From Time Zero Extrapolated To Infinity
$AUC_{0\text{-}t}$	Area Under The Curve From Time Zero To The Last Measured Concentration
BMI	Body Mass Index
BW	Brain Weight Correction
CL	Clearance
CL/F	Extravascular Clearance
Cmax	Maximum Observed Concentration
CPT	Concentration vs. Time Profile
CV%	Coefficient Of Variation Expressed As A Percentage
EMA	European Medicines Agency
F	Bioavailability
FcRN	Brambell Receptor
FDA	United States Food And Drug Administration
FE	Fold-Error
FGFR	Fraction Of Glomerular Filtration Rate
FIH	First-In-Human
Fvic	Fraction Interstitial
Fvv	Fraction Vascular
G-CSF	Granulocyte Colony Stimulating Factor
GFR	Glomerular Filtration Rate
HED	Human Equivalent Dose
hGH	Human Growth Hormone
hr	Hour
ICH	International Conference On Harmonization
IM	Intramuscular
IOV	Inter-Occasion Variability
ISF	Interstitial Fluid/Interstitial Space
IV	Intravenous
Ka	First-Order Absorption Rate Constant
kDa	Kilodalton
kg	Kilogram
L	Numerical Value Blood Flow Was Divided By To Obtain Lymph Flow Value
LDC	Lymphatic Drainage Compartment .

Ln	Natural Log
LS	Numerical Value Blood Flow Was Divided By To Obtain Skin Lymph Flow Value
mAb	Monoclonal Antibody
MAD	Multiple-Ascending Dose
mg	Milligram
min	Minute
mL	Millilitre
MLP	Maximum Lifespan Potential Correction
MW	Molecular Weight
N	Sample Size
NCA	Non-Compartmental Analysis
NCE	New Chemical Entity
NHP	Non-Human Primate
nm	Nanometre
NOAEL	No Observed Adverse Effect Level
NRCL	Non-Renal Clearance
PBPK	Physiologically- Based Pk
PD	Pharmacodynamic
PEG	Polyethylene Glycol
PK	Pharmacokinetics
Pla	Plasma
PML	Pharsight Modeling Language
popPK	Population Pharmacokinetic
PPC	Pegylated Peptide Conjugate
Q	Blood Flow
R^2	Coefficient Of Determination
RCL	Renal
RO	Receptor Occupancy
ROE	Rule Of Exponents
SAD	Single-Ascending Dose
SC	Subcutaneous
$T_{1/2}$	Half-Life
TK	Toxicokinetic
Tmax	Time To Maximum Concentration
TMDD	Target Mediated Drug Disposition
V	Volume
V_c	Volume Of Distribution Of The Central Compartment
Vd	Volume Of Distribution
V_{ss}	Volume Of Distribution At Steady-State
Vz	Volume Of Distribution Based On The Terminal Phase

Vz/F	Extravascular Volume Of Distribution
WB-PBPK	Whole Body Physiologically-Based Pharmacokinetic
λ	Apparent Elimination Rate Constant
σ_{isf}	Lymphatic Reflection Coefficient .
σ_{v}	Vascular Reflection Coefficient .
$\sigma_{v,sf}$	Vascular Reflection Coefficient Scaling Factor

CHAPTER 1: INTRODUCTION AND BACKGROUND

1.1 Therapeutic Macromolecules

The use of therapeutic macromolecules, or biologics, is increasing globally and growing at a faster rate than small molecules as evidenced by global prescription sales for biotech drugs which, from a 2007 report, were increasing by 12.5% annually, to more than USD$75 billion (1). It has been estimated that one in eight prescriptions written globally is for a biologic drug and given an annual treatment cost per individual of more than USD$16,000, the consequence is that continued growth at such a rate will further increase the spending burden on payers of these therapies.(1) The term biologic drug requires distinction from chemically synthesized therapeutic product and includes compounds such as peptides, proteins, oligonucleotides, vaccines and blood products.(2) For the purpose of this thesis, only therapeutic macromolecules such as peptides, proteins and oligonucleotides will be discussed herein and the term therapeutic macromolecule and biologic drug should be assumed to be interchangeable. Therapeutic macromolecules can be contrasted with small, chemically synthesized molecules based on physico-chemical and biochemical characteristics. Table 1.1 summarizes some of the key differences between small and large molecule classes.

Table 1.1 Differences between small molecules and macromolecules

	Small Molecules	Macromolecules
Molecular weight	<1 kDa	>1 (generally >15-20 kDa)
Physiochemical properties	Well-defined	Complex (e.g. tertiary, glycosylation)
Synthesis	Chemical synthesis	Biotechnology (e.g. recombinant)
Purity	Single entity Chemical purity	Heterogeneous Mixture Broad specs
Administration	Oral (majority), IV, SC, IM.	Parenteral (IV, SC, IM)
Distribution	Various organs/tissues	Plasma and/or extracellular fluids Protein binding important
Metabolism	Phase 1 & 2 reactions to metabolites	Catabolized to smaller building blocks
Toxicity	Specific Dissociated from effect	Receptor mediated (endocytosis) Exaggerated PD responses
Antigenicity	Not typical	Yes

IV: intravenous; SC: subcutaneous; IM: intramuscular

Adapted from Baumann, 2006 (3)

The larger molecular weight of macromolecules is a key characteristic influencing the pharmacokinetics (PK) of the drug. In terms of biochemical processes, biologics are typically catabolized to smaller building blocks such as amino acids or nucleic acids, which alters the safety profile compared to synthetic compounds as these building blocks are similar, or identical to endogenous compounds in some cases. Due in part to molecular size as well as structural aspects that can be recognized as foreign by the human immune system, biologics have the potential to elicit an antibody response, which can in some cases alter the PK and pharmacodynamic (PD) properties of the drug.

1.2 Biologic Drug Development

No one single approach characterizes the development process for all biologics and each plan should be risk-based and consider the individual physico-chemical, biochemical and toxicological profile of the drug. There are however class-like properties of biologics that influence the regulatory requirements for many biologics in terms of advancing the drug from the preclinical stage to clinical, and onward to marketing authorization. Typically, small molecule drugs require toxicological assessment in a minimum of one rodent and one non-rodent species, substantial ADME (absorption, distribution, metabolism and excretion) characterization, genotoxicity evaluation and screening for drug-drug interaction potential. The safety profile of a biologic is typically influenced by the binding of the drug to a biological target and an exaggerated PD effect. Consequently, the safety of a biologic drug is to be evaluated in a relevant animal species. In many cases, only a single relevant species exists (e.g. non-human primate, NHP) and therefore a minimum of a single species is deemed necessary for toxicology testing for biologics. In part, due to the molecular size, restrictive biodistribution, and routes of catabolism, there is little need to extensively evaluate ADME properties of biologics. Exceptions of course exist, particularly for drugs with specific uptake into tissues such as with oligonucleotides and siRNA which demonstrate distribution into various organs (e.g. liver, kidney).(4) Also, due in part to the molecular size and similarity to native proteins, most biologics are assumed to not exhibit genotoxic potential, thus obviating the need for this evaluation in the drug development process. Lastly, biologic drugs have a lower potential for inhibiting drug metabolizing enzymes, and as these compounds are not typically metabolized to metabolites, are unlikely victims of PK drug interactions.(2)

Clinical (human) development of a biologic is similar to small molecules in that initial testing in humans is typically focused on evaluating safety and PK, followed by confirmation of biological effect and therapeutic efficacy and safety in larger clinical trials. However, as with the nonclinical development plan, extensive studies on the ADME properties and drug-drug interaction potential for a biologic are often unwarranted. Instead, greater importance is placed on the relationship between drug exposure and PD response or receptor occupancy (RO).

1.3 Biosimilar Development

An approach gaining popularity across the globe for reducing drug cost and improving access to otherwise out of reach therapeutic macromolecules is through the development of second entry biologic "copies" or biosimilars. The formal definition of a biosimilar may differ according to the regulatory jurisdiction or country; however it can be defined as a highly similar version of a previously approved therapeutic macromolecule. There is a consistent fundamental appreciation that although a high degree of physico-chemical characterization may be established between a biosimilar candidate and the reference innovative biologic (reference product), the two cannot be deemed identical.(5;6) This is in stark contrast to generic versions of small molecule drugs, where for the majority of compounds, when evidence of bioequivalence is presented, the two products are deemed interchangeable. For most orally absorbed drug products establishing bioequivalence is demonstrated through equivalence of systemic exposure, which is concluded when the 90% confidence interval for the geometric mean ratio of the pharmacokinetic parameters of interest (i.e. AUC and Cmax) for the test formulation over the reference formulation fall within the traditional bioequivalence margins of 80-125%.(7;8) The caveat of course is that the drug can be quantified bioanalytically, with reasonable sensitivity. The basis of this approach originates from the longstanding view that the concentration in the blood is related to the concentration at the site of action and that two drugs with equivalent systemic exposure are expected to have the same efficacy and safety profile provided the relative exposure falls within a predefined acceptance range. Since most macromolecules are complex in structure and PK relative to smaller, synthetically derived drugs, the "generic" approach to establishing bioequivalence does not apply and hence additional nonclinical and clinical testing is required.

1.4 Biodistribution and Other Important Pharmacokinetic Properties of Therapeutic Macromolecules

1.4.1 Biodistribution

Intravenous (IV) administration of a drug provides immediate access of a drug directly into the systemic circulation. From the venous blood circulation, the drug is then transported throughout the body and enters the vasculature of various organs and tissues. Further transport across the membrane of blood capillaries into the interstitial fluid (ISF) of an organ is restricted based on the physico-chemical properties of the drug. The endothelial surface of a blood capillary restricts movement of large and non-lipophilic molecules. Channels that exist in the membrane do however allow the passage of fluid and smaller non-lipophilic molecules.(9) Convective transport of endogenous and exogenous macromolecules through large pores as well as vesicular transport of macromolecules has both been proposed as mechanisms of transport of large molecules across the endothelial layer.(10;11) Morphologic evidence of large pores is lacking in the literature and in a comprehensive review focused on endothelial pore sizes, Sarin (2010) argued that based on ultrastructure analysis, the existence of a specific large pore is unlikely.(12) Instead, Sarin suggests that the transport of large macromolecules (as large as 60 nm in diameter) distribute to the interstitial space via a phago-endocytic route. Examination of extravascular tissue concentrations after IV administration of iodine-labeled human albumin confirms that macromolecules of high molecular weight (MW 69 kDa) and large spherical diameter (3.8 nm wide x 15 nm long) are indeed capable of crossing the endothelial membrane in humans into the interstitial space.(13;14) In mice, lymphatic uptake of the monoclonal antibody (mAb) bevacizumab was negligible after IV administration, suggesting only a small fraction of the administered dose crossed the endothelial surface (see next Section: Role of the Lymphatic System in the Pharmacokinetics of Therapeutic Macromolecules). In lymph cannulated rats, IV administered trastuzumab, another mAb molecule, resulted in more substantial lymphatic recovery (approximately 44%).(15) Such varying results with respect to lymphatic uptake of large molecules observed in these studies may suggest an experimental or interspecies dependency in passage across the endothelium. However, regardless of the precise mechanism, macromolecules (endogenous or otherwise) appear capable of traversing the vascular endothelial barrier from the vascular system into the interstitial space, in a size and potentially, species-dependent manner.

Macromolecules have similarly been demonstrated to cross from the interstitial space directly into the vasculature in an apparent size dependent manner. Following subcutaneous (SC) administration, Supersaxo demonstrated that with increasing size, a greater proportion of the administered macromolecule was taken up by the lymph.(16;17) While this demonstrates a size dependency in terms of lymphatic uptake, the corollary to this observation is that as the molecular weight, and presumably hydrodynamic radius,

increases, the less likely a compound would transit to the vasculature from the interstitial space. Whether this is strictly a size limitation or a result of convective flow and pressure forcing drug against the path of least resistance (see next section) has not yet been conclusively determined. Despite the low resistance offered by the lymphatic-interstitial interface, macromolecules with MW less than 16 kDa have been found to diffuse passively across the blood capillary endothelium when administered subcutaneously.(18) Thus, it can be inferred that macromolecule molecular size is an influential determinant of lymphatic uptake potential.

1.4.2 Clearance

Clearance (CL), a PK parameter that describes the rate of drug removal from a biological system, is one of the most important parameters used in the prediction of human PK based on animal values. As summarized above in Table 1.1, the CL of macromolecules differs from small molecules.

With small molecules, the majority of drug CL occurs via the hepatic (biotransformation or secretion into bile) or renal (filtration or active tubular secretion) routes, with a smaller portion of drugs being cleared by a variety of enzymes in plasma and other tissues. With macromolecules, CL mechanisms are likely highly compound or class of compound dependent, with mechanisms ranging from protein catabolism, proteolytic degradation by soluble peptidases, target-mediated internalization and degradation within a cell and renal elimination of smaller protein components.(2;3) Target-mediated internalization, termed target mediated drug disposition (TMDD), is of particular relevance with biologic macromolecules and interspecies scaling as animal models that do not express the target receptor may not process or clear the drug similar to those that do and consequently do not represent a reliable model for human prediction of PK. Moreover, the lack of target expression in a species does not allow for study of the PD response; an important parameter for safety assessment. Chapter 2 expands on these concepts and highlights the value of a single relevant NHP species in predicting the PK of therapeutic macromolecules based on animal data.

1.4.3 Bioavailability

When a drug is administered IV, the fraction of drug absorbed is equal to 100%. The relative bioavailability of an extravascularly administered drug is expressed as the fraction of the administered dose that is available for systemic action. As described in the section above, CL mechanisms of macromolecules include proteolytic degradation and cellular uptake. When these processes occur at a site of extravascular administration (e.g. following SC administration) there is the potential to reduce the bioavailability of the drug. Wang demonstrated that after SC injection of pegylated conjugates of erythropoietin in rats, CL occurred at the site of injection and by cells within the lymphatic fluid.(19) Similarly, Charman et. al.

observed that human growth hormone degraded prior to reaching the central lymphatics after SC administration.(20) Richter summarized the range of SC bioavailability's for a number of therapeutic macromolecules across various animal species.(18) The review concluded there was no obvious trend between molecular weight of a macromolecule and the bioavailability across various species. However it should be noted that the between species bioavailability within any particular molecule was obtained in some cases from different studies, with varying study designs, anatomical sites of SC administration and doses and consequently should be interpreted with caution. As will be addressed in Chapter 3, appreciation of local CL processes and interspecies differences in said processes is an important factor when scaling PK from animal models to humans.

1.5 Role of the Lymphatic System in the Pharmacokinetics of Therapeutic Macromolecules

As described in the previous section, lymphatic uptake of macromolecules from the interstitial space represents an important biodistribution process of said molecules, and an appreciation of lymphatic anatomy and function is an important consideration when employing *in silico* techniques to predict the PK of therapeutic macromolecules. Chapters 5 and 6, detail the development of PBPK models incorporating lymphatic distribution to improve the prediction of a new chemical entity (NCE) pegylated peptide conjugate's (PPC) PK properties based on a single NHP species. As such a brief overview of the lymphatic system as it pertains to macromolecule distribution is presented herein.

The lymphatic system is a parallel circulatory network consisting of capillaries, collecting vessels, lymph nodes, trunks and ducts, which vary in size and act as a one-way circuit for the transport of fluid, protein molecules and immune cells, draining from the interstitial space, eventually emptying into the venous circulation. (21) Lymph vessels do not possess tight junctions and therefore pose little resistance to macromolecule transport. As stated in the previous section, while in the interstitial space, macromolecules may undergo proteolytic degradation and phagocytic uptake prior to draining into the venous blood.(19;22) Transport of macromolecules within the lymph is facilitated by the unidirectional flow of lymphatic fluid, which is estimated to be 100 to 500 times slower than blood flow and influenced by ambient temperature, movement and massage.(21;23;24) In a comprehensive *in silico* PK analysis of SC administered mAbs, Zhao identified that lymph flow was an important determinant of the time to maximum concentration (Tmax). This finding is consistent with the research outlined in Chapters 3 and 5 of the current thesis, where lymph flow rate was an important determinant of the shape of the concentration vs. time profile (CPT), and interspecies differences may influence the potential to predict the shape of the CPT in humans.

1.6 Pegylated Therapeutic Peptides and Proteins

Pegylation is introduced at this point as the therapeutic macromolecule employed in the primary aims (as will be described later in this chapter) is a pegylated cyclic peptide with a molecular weight of approximately 44 kDa. To better appreciate subsequent Chapters, which describe the *in silico* methods used in the prediction of this model compound, a brief summary on pegylation of drugs is provided herein.

Pegylation of a compound involves conjugation of the drug portion to varying forms and chain lengths of polyethylene glycol (PEG).(25) PEG conjugation increases the drugs circulating half-life by reducing renal filtration and non-renal clearance routes of elimination, allowing for reduced dosing frequency of otherwise rapidly cleared peptides and proteins.(26) To date several pegylated versions of peptides have been approved and marketed in major regulatory jurisdictions (e.g. USA, Canada, and Europe). Conjugation of the granulocyte colony stimulating factor (G-CSF) prolonged the Tmax after SC administration 7-fold and more than doubled the circulating half-life relative to the unconjugated protein. (27) For cancer patients receiving myelosuppressive chemotherapy, pegylation of G-CSF allows for a single SC injection once per cycle as opposed to daily injections for the unconjugated version.(28;29) Similarly, pegylation of interferon α-2a for chronic hepatitis C infection requires once weekly dosing as opposed to the unconjugated form that was previously prescribed on a thrice weekly schedule. (30;31)

In addition to slowing systemic CL, pegylation can potentially alter the biodistribution of a peptide or protein beyond what would be predicted by the compounds molecular weight. Due to the propensity to randomly conform water molecules, pegylation may increase the hydrodynamic volume of a protein thus affecting its biodistribution to a greater extent than what the molecular weight would suggest.(32) The relevance of pegylation on the biodistribution and prediction of PK for a pegylated compound will be further explored in Chapters 5 and 6.

1.7 Subcutaneous Route as an Important Route for New Drug Development

The importance of the SC route to the drug development industry is evident in the growing number of drug products available for SC administration. In 2014, the U.S. Food & Drug Administration approved 41 new molecular entities and biological licensing applications, four of which had first approvals for SC administration(33). The industry has also witnessed conversion of IV to SC routes for a number of therapies where treatment that was previously relegated to a hospital can now largely be addressed in an ambulatory setting (e.g. IV heparin to SC low molecular weight heparins for treatment of deep vein thrombosis). With a growing emphasis on SC administration as the primary route for development, reliance on reliable PK scaling methods (nonclinical animal species to human) is correspondingly increasing.

1.8 Skin Anatomy and Physiology as it Pertains to Subcutaneous Drug Delivery

An important organ as a physical barrier against the environment, skin represents approximately 15% of total body mass and covers an average adult surface area of 2.2 m^2.(34;35) The skin also plays a vital role in sensory and touch, thermoregulation and biosynthetic regulation (e.g. vitamin D synthesis).(35)

An illustration of the various layers and structures of the skin can be found in Figure 2.1. The epidermis, which is the most superficial skin layer, is composed of various cell types including keratinocytes, dendritic cells, melanocytes, Langerhans and Merkel cells. Beneath the epidermis is the dermis layer that is a highly innervated and vascularized segment responsible for the elasticity and tensile strength of skin. The dermis is abundant in proteins such as collagen, hyaluronic acid and glucosoaminoglycans. At the interface of the dermis, lying between the dermis and the muscle tissue is the fatty subcutis, which is principally composed of adipocytes.

Figure 1.1: Cellular layers of the skin (Reprinted with permission for thesis purposes from Frost 2007)(36); drug administered by injection either via the subcutaneous or intramuscular (region) is taken up either via capillaries (red vessels) or the lymphatics (green vessels) based on size of the compound.

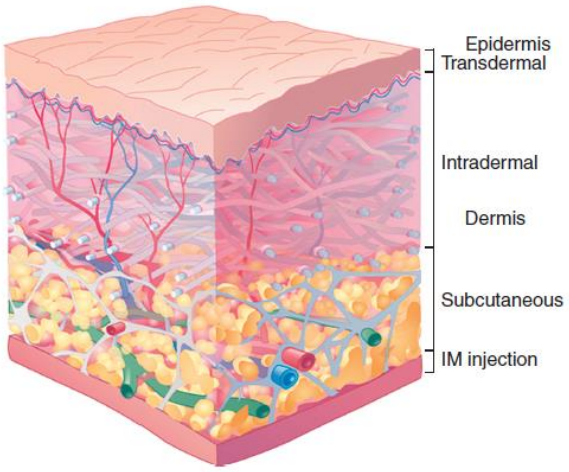

SC administration entails injecting a drug product into the subcutis layer of the skin (Figure 2.1).There is little blood flow in the fatty tissue layer of the skin and thus the injected medication is generally absorbed more slowly than the IV route.

Figure 2.1: Illustration of a subcutaneous injection (graphic obtained from the United States National Institutes of Health patient information leaflet on administration of subcutaneous injections)

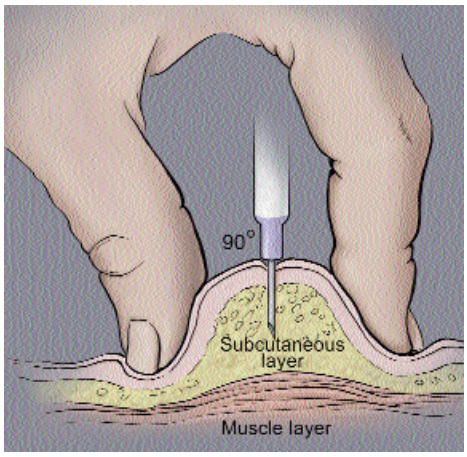

Common sites of injection include the back region, abdomen and thigh. Section 1.5 of this Chapter notes that physical movement can potentially influence lymphatic uptake of drugs due to altered lymph flow.(23). In a comparative bioequivalence study evaluating two formulations of a SC administered human growth hormone (hGH) inconsistent PK was observed.(37) In this initial study, the injection site was allowed to be rotated within the thigh region within and across subjects. Upon repeating the investigation, with stringent controls in terms of injection site consistency, within-subject variability in PK was reduced and the two formulations were concluded to be bioequivalent.

1.9 Extrapolating the Pharmacokinetics of Therapeutic Macromolecules from Preclinical Animal Species to Humans

A review of methods employed in scaling PK from animals to humans is addressed in part in Chapter 2: Contrasting toxicokinetic (TK) evaluations and interspecies pharmacokinetic scaling approaches for small molecules and biologics: applicability to biosimilar development. A brief introduction to this topic and a summary of the methods addressed in this thesis are described herein.

Scaling of PK from animals to humans serves several purposes in the overall drug development of a NCE. Perhaps the most important benefit is that it provides a method of relating toxicology findings in the animals species studies as part of the preclinical program, to humans. As per ICH and other relevant guidelines for drug development, selection of the maximum recommended safe starting dose for both small molecules and biologics requires at least some consideration of the systemic exposure in animal toxicology studies.(38) Nonclinical TK, which involved estimating systemic exposure parameters associated with toxicological observations in the tested animals, provides drug developers with some indication of the NCEs PK characteristics. In turn, this data informs future study designs. For example, in a first-in-human (FIH) investigation, blood is collected for bioanalytical quantitation and subsequent PK characterization following a range of doses administered to humans. The placement and temporal relationship of blood sampling related to the dosing time can be informed by observations in animals. Nonclinical TK assessments for NCEs typically include characterizing the PK in a rodent (e.g. mouse or rat) and non-rodent species (e.g. dog, monkey). In smaller mammals where blood samples are limited to 1-2 samples per animal, PK evaluation is often limited to systemic exposure based on the average (mean) concentration time profile from all animals in the study. Average data are of limited value in comparing treatments as they provide little information on the variability in the PK response. A method of obtaining full PK profiles in each animal, particularly when smaller mammals are used, is by limiting the number of samples being drawn per animal but employing a consistent sampling schedule among all animals tested. This approach however has limited utility, particularly for therapeutic macromolecules in the IgG-type monoclonal antibody class of compounds where the half-life is typically extended (e.g. ~20 days).(39). A long half-life coupled with a sparse sampling scheme is unlikely to allow for appropriate characterization of the concentration-time profile to an extent sufficient to be considered a thorough evaluation of PK. For larger mammals, although more blood samples over an extended duration may be possible, the total number of blood samples drawn may still be insufficient for adequately characterizing the PK of drugs with a prolonged absorption phase and/or a long terminal elimination half-life. Moreover, the number of animals in nonclinical investigations is

typically limited to 3-6 per treatment and in such cases, small sample sizes (n=3-6 per treatment) may be too low to estimate the PK parameters with any reasonable level of precision. The sample size and precise estimation of PK becomes especially important where detection of relatively small differences in PK (i.e. systemic exposure) is a primary objective (i.e. in the case of biosimilars).

1.9.1 Compartmental Pharmacokinetic Modeling

Information sourced for this section is influenced by Gabrielson and Weiner (2000).(40) *In silico* modeling methods have the potential to overcome some of the sparse data issues associated with nonclinical TK studies. One such method, employed in Chapter 4, is population-based compartmental modeling. Sometimes referred to as a "top down" approach, compartmental modeling condenses the biological system into a simplified mathematical representation of a biological system with a central or vascular compartment and one or more peripheral compartments. Each compartment in the model is associated with a volume that is either fitted or fixed at a theoretical value. Movement between compartments is represented by either micro rate constants or a distributional CL parameter. Similarly, CL of drug from the system is also parameterized as either a micro rate constant or CL, and typically for a typical small molecule CL occurs from the central compartment. Input into the system is either instantaneous into the central compartment for IV administration, or for extravascular administration, parameterized using a variety of different mathematical expressions, some of which are described in Chapter 4.

In compartmental modeling, observed data is simultaneously fit to a model with various parameters, and model parameters that best describe the data are optimized using an algorithm intended to minimize the difference between the observed and predicted data. In traditional compartmental PK modeling, the observed data are measured concentrations of drug in some biological matrix (e.g. blood, plasma, urine, tissue, etc.…)

With respect to therapeutic macromolecules, models can be adapted with receptor binding expressions to address TMDD and CL. Compartmental models with TMDD components have been demonstrated to describe the PK and PD response of interferon β-1a in both NHP and humans. (41;42)Receptor-mediated binding is a practical means of quantifying the non-linear nature of macromolecule CL where binding is saturable within the studied range. Models used for scaling macromolecules across species have also been parameterized with Michaelis-Menten expressions to characterize the non-linear nature of macromolecules.(43)

Population-based non-linear mixed-effect compartmental pharmacokinetic modeling, referred to in this thesis as popPK, is a sophisticated modification to compartmental modeling that allows for simultaneous estimation of a fixed-effect parameter (e.g. systemic CL), between-subject variability (random-effects), and residual or unexplained error. (44)This methodology also lends itself to quantification of factors that may explain the between-subject variability by way of covariates such as body weight, gender, age, concomitantly administered medications, to name a few.(44)

Once a popPK model is considered adequately qualified, the model inputs such as dose and frequency of dose can be varied and used to simulate future events. In the context of interspecies scaling from animal to human, as will be explored in Chapter 4, incorporation of species body weights in the form of an allometric scaling factor can be used to scale the model to predict PK parameter values and concentration values in humans for clinical study planning. Chapter 4 further explores the utility of employing empirically selected scaling factors incorporated into a popPK model in the prediction of PK and CPT of a novel therapeutic macromolecule after SC administration.

1.9.2 Physiological Based Pharmacokinetic Modeling

Similar to compartmental PK models, PBPK models include a series of differential equations describing the mass transfer of drug between compartments. PBPK models however are parameterized with values that represent the size of the overall and sub-compartments within each anatomical organ being represented. Movement of drug throughout the model is governed by flow rates that have physiologic meaning such as blood (or plasma) flow and in the case of macromolecules, lymph flow. Drug specific parameters such as molecular size, molecular weight, lipophilicity and pKa influence are incorporated into the structural model to describe biodistribution of a drug. Biochemical process such as in-vitro experimentally obtained CL can also be incorporated to address CL processes in the model. Several publications have demonstrated the value of PBPK models in terms of small molecule PK, however the predictive capacity was dependent on the methods and quality of the data used to inform the biodistribution and CL of the molecules studied.(45) Since the non-TMDD CL processes of therapeutic macromolecules are thought to be conserved across species(46), PBPK may offer advantages over single-species allometric and popPK approaches as PBPK facilitates the scaling across species by adjusting the anatomical and physiologic parameters in a species-dependent manner, independent of the drug's physical properties. For macromolecules, the scaling potential of the model is predicated on whether the animal species expresses the target with similar homology to humans. PBPK literature reports describing the prediction of human PK of therapeutic macromolecules from TK data are not as common as allometric approaches, however where it has been reported, PBPK has

demonstrated some promise. (47-51) Most of the available PBPK literature centres on mAbs, and following IV administration. Chapter 5 represents one of the few published PBPK models considering extravascular administration of a macromolecule and, at the time of publishing, was one of if not the first to propose a method of addressing SC administration of a therapeutic macromolecule. Moreover Chapter 6 extended the models capabilities to include simulations in a population on individuals. Since both chapters publishing as manuscripts, Gill has proposed a mechanistic PBPK approach for SC administration using the commercial platform, SimCyp®, however unlike the work addressed in Chapter 5, Gill and colleagues did not address the predictive capacity in terms of scaling to human based on animal data, nor predictions in a population.(52)

1.9.3 Interspecies Scaling Methods

In spite of the limitations of average animal TK, a commonly employed approach which utilizes this data for prediction of human PK is simple allometry and adaptations to the simple allometric technique. Simple allometry in drug development entails plotting the log of weight of multiple mammalian species vs. the log of a PK parameter of interest (e.g. CL) where the predicted human equivalent of the PK parameter is extrapolated based on Equation (1.1) (53;54):

$$\log y = \log a + b \bullet \log W \qquad (1.1)$$

$y = \text{PK parameter of interest (usually CL, volume of distribution or half} - \text{life)}$

$b = \text{allometric exponent for the PK parameter (slope)}$

$W = \text{Weight of the mammalian species}$

$a = \text{allometric coefficient (y} - \text{intercept)}$

While used extensively for small molecules prediction of human PK parameters from animal data, methods based on simple allometry, including correction for species brain weight or maximum lifespan potential (53), have performed inconsistently in terms of prediction accuracy when employed in therapeutic macromolecule predictions.(55-58) This may be a reflection of simple allometry requiring ≥3 different mammalian species(58) and as described earlier in this chapter (see 1.4.2 Clearance), not all of the species tested may be appropriate animal models for assessing the PK of macromolecules. Although mammals share common anatomy and physiological processes there are differences among mammalian species, particularly with respect to the skin and will be explored in more detail in Chapters 4 and 5. Given that therapeutic macromolecules contain human elements (i.e. humanized) or are fully human proteins, these compounds

may not bind with the same affinity, or at all, with the nonclinical species target. Since CL of proteins can occur through target mediated processes, it stands to reason that the greater the difference in sequence homology between the nonclinical and human species, the lower the utility (i.e. predictive potential) that species will display. Another consequence of the differences among species is that the more humanized the protein is, the more immunogenic the protein may be in a nonclinical species. (59) This is not to suggest that immunogenicity of a humanized protein does not occur in humans from humanized proteins, but rather the potential is greater with greater difference between the therapeutic macromolecule and the species' endogenous proteins. Should an immunogenic response be elicited in the animal species, altered systemic CL or biologic activity of the macromolecule in the nonclinical species may be observed and thus data obtained in this is species is consequently limited in terms of PK predictive capacity. (2) As such, there have been several investigations into the use of single-species allometric approaches, particularly employing NHP, for predicting PK of macromolecules in humans. (60-64)

The SC route offers a convenient means of administering parenteral solutions or suspensions of therapeutic macromolecules. However, predicting the PK in humans from animal data is challenged by interspecies differences in skin anatomy and CL mechanisms. This thesis proposes several single species methods for scaling the PK from a NHP to human following SC administration in an effort to de-risk biologic and biosimilar drug development. Chapter 2 represents a published article written by the PhD candidate which summarizes the prediction accuracy of methods using empiric scaling factors based on average PK parameters values.(55) In Chapter 3, applicable single-species model-independent scaling methods described in Chapter 2 are applied to prediction of human PK for a novel pegylated peptide conjugate (PPC) discussed earlier in this chapter. In Chapter 4, a representation of another published manuscript describes a popPK model based approach for predicting the human time course of the same PPC following SC administration to NHP.(65) Chapters 5 and 6 (both published manuscripts) propose novel modifications to a whole body PBPK approach, incorporating lymphatic uptake and local drainage from the SC injection space for predicting the SC time course of the same PPC described earlier, in a virtual human individual and human population.(66;67) In Chapter 7, the gamut of methods addressed in this thesis are contrasted and compared with recommendations as to which methods may provide the most useful *a priori* information in the context of predicting the human PK of a SC administered therapeutic macromolecule.

1.10 Research Topic

The principle objective of this thesis project was to develop a workflow for employing *in silico* approaches for de-risking the development of biologic and biosimilar therapeutic macromolecules through prediction of human PK after SC administration to nonclinical species. In the context of this proposal, de-risking implies concentration data obtained from nonclinical animal species can be employed to predict the PK in a human (or population of humans) with greater accuracy than previously reported methods, which rely principally on model-independent approaches and do not address interspecies differences in the absorption process of macromolecules following SC administration.

1.11 Objective

The research objective of this thesis was to develop a model-based workflow, and compare to model-independent methods, for translating macromolecule concentration data obtained from a single, non-human animal species, and use this data and workflow to predict the concentration vs. time course as well as important PK parameters, in humans.

1.12 Hypothesis

Model-based methods are superior in terms of predicting the time course and important PK parameters of a SC administered macromolecule, in humans, relative to traditional model-independent methods.

Aim 1: Comparison of existing empiric allometric and model-independent methods for predicting human pharmacokinetics based on preclinical animal evaluation

Addressed in Chapter 2, this research aim was intended to evaluate single-species allometric scaling methods which are commonly used with the additional intent of evaluating influence of a particular scaling factor exponent to yield the greatest accuracy in prediction of CL and volume of distribution (V_d) for therapeutic macromolecules. Single-species methods for predicting the PK of a therapeutic macromolecule in NHP were subsequently applied to the measured concentrations or non-compartmental analysis-derived PK parameters for a novel PPC in Chapter 3.

Aim 2: Evaluation of population pharmacokinetic models incorporating empiric scaling factors for predicting the subcutaneous pharmacokinetics of a therapeutic macromolecule in humans

As detailed in Chapter 4, population-based compartmental modeling was used to describe PK data obtained from a single NHP species for a novel PPC. Empiric and fitted scaling factors were then integrated into the model and used to predict the concentrations in a population of humans and compared to observed data in humans.

Aim 3: Development and evaluation of a PBPK model for subcutaneous administration of a therapeutic macromolecule

As detailed in Chapter 5, a whole body PBPK model with lymphatic and vascular flow integrated in the model was developed integrating a novel means of parameterizing the SC depot to predict the SC time course of a SC administered novel PPC in NHP with subsequent scale up and prediction of the PK in humans.

Aim 4: Incorporation of lymphatic biodistribution into a population PBPK model for a therapeutic macromolecule

Chapter 6 expands on the model developed in Chapter 5. The PBPK model was refined to incorporate interindividual variability elements with the intent of evaluating which model parameters exert the greatest influence on the variability of prediction of SC administered macromolecules in a human population.

Aim 5: Compare prediction capacity of published methods with methods developed in this thesis

The intention of this research aim is collate the results obtained across the various methodologies tested and compare and contrast the utility of each method as it pertains to the compound in question (Chapter 7).

CHAPTER 2: CONTRASTING TOXICOKINETIC EVALUATIONS AND INTERSPECIES PHARMACOKINETIC SCALING APPROACHES FOR SMALL MOLECULES AND BIOLOGICS: APPLICABILITY TO BIOSIMILAR DEVELOPMENT

The contents of Chapter 2 were initially published as an original contribution manuscript by the PhD. candidate (Elliot Offman). The original manuscript has been edited and formatted according to thesis publication requirements. For reference purposes, the original publication is as follows:

Offman E, Edginton AN. Contrasting toxicokinetic evaluations and interspecies pharmacokinetic scaling approaches for small molecules and biologics: applicability to biosimilar development. *Xenobiotic*; 43(6): 561-569.

The PhD candidate conducted all the pertinent research, conducted the analysis where applicable and wrote the manuscript.

2.1 Introduction

Global sales for biotechnologically-derived (biologic) drugs are increasing dramatically with an estimated one in eight prescriptions written globally at an annual treatment cost of more than USD$16,000.(1) By 2015, approximately USD$60 billion in global sales are [Note: original version of this manuscript was published in 2012] set to lose patent protection opening the market to competition and with it an opportunity to reduce drug cost and improve access to otherwise out of reach medicines.(68)

The formal definition of a biosimilar may differ according to the regulatory jurisdiction; however, it can be defined as a highly similar version of a previously approved therapeutic macromolecule. Regulatory bodies, such as the European Medicines Agency (EMA), have been proactive in developing a framework for the approval of biosimilar products. There is a consistent fundamental appreciation that although a high degree of physico-chemical characterization may be established between a biosimilar candidate and the reference innovative biologic, the two cannot be deemed identical. This is in stark contrast to small molecules where, for the majority of compounds, when evidence of bioequivalence is presented, the two products are deemed interchangeable.

At the time of writing, the EMA had issued guidelines for industry sponsors for the non-clinical and clinical development of several biosimilar compounds or classes such as recombinant human erythropoietin, human growth factor and monoclonal antibodies (mAbs).(69) Recently, the US Food and Drug Administration (FDA) issued a series of draft guidance documents outlining a pathway for submitting a biosimilar product through a 351 (k) application. This framework differs somewhat from the EMA and a review of the draft guidelines is available for review.(5)

Based on existing published guidelines, there is a high burden of evidence in the non-clinical phase to establish similarity between the biosimilar candidate and the reference biologic from a physico-chemical and biological characterization perspective.(70) This comparative characterization is usually performed through in-vitro methods comparing biological activity as well as through in-vivo methods such as pre-clinical toxicology and toxicokinetic (TK) studies. Following this characterization, development moves to the clinical phase typically requiring a combination of Phase 1 and comparative efficacy and safety studies. These comparative Phase 1 studies offer further opportunity to screen the candidate biosimilar product for similarity prior to proceeding to the larger, more expensive and time consuming Phase 3 trial(s).

The toxicity profile of some macromolecules, particularly in the mAbs class , may prohibit administration to healthy volunteers and the sponsor must consider whether to proceed directly to a Phase 3 study or to

conduct a smaller preliminary PK study in a relevant patient population.(71) Conducting such small "patient" PK studies are typically challenging to recruit, given that patients are not likely to derive clinical benefit from participating in a biosimilar PK/PD type trial, especially under a single-dose design. Moreover, these populations are not usually homogeneous in terms of co-morbidities and concomitant medications, further challenging the interpretation of results. Lastly there are ethical concerns with subjecting "sick" patients to intensive blood sampling when there is potentially no direct benefit. The alternative though entails proceeding directly to a comparative safety and efficacy trial without any comparative human data. This approach adds considerable risk to the overall clinical development for biosimilars should a difference in PK, or more importantly, a difference in the safety or efficacy profile which may be related to a difference in PK, wasn't identified during the in-vitro or animal comparability assessment.

Unlike with small molecules, small differences in manufacturing between the biosimilar and reference biologic may impart undetected differences that must be ruled out for the potential to result in significant safety and efficacy differences.(72;73) One potential means of overcoming the uncertainly of whether the test and reference biologic exhibit similar PK is to conduct robust comparative TK evaluations in a relevant animal species (if one exists). TK studies offer an initial picture of the potential for comparable human PK and particularly systemic clearance (CL). The PK for the biosimilar product can then be compared to PK reported in the public domain for the reference biologic in humans as well as to the data for the reference biologic generated in the comparative TK study. This provides additional confidence that the biosimilar will be comparable to the reference biologic in human trials. Limitations, however, in the number of blood samples which can be drawn from any one animal for PK evaluation and the cost per animal may limit the interpretation of the pharmacokinetic comparison.

2.2 Case Scenario

A biosimilar sponsor developed a product intended to be similar to the reference biologic, a recombinant therapeutic protein <25 kDA. As part of the toxicological evaluation both the test and reference biologic were assessed for comparative pharmacokinetics in 4 male and 4 female rhesus monkeys and serum samples for PK analysis of the protein were collected over 24-hours following a single dose. Based strictly on the mean derived pharmacokinetic parameters from standard non-compartmental analysis (NCA), the test values (e.g AUC, Cmax) were approximately 60% of the reference product. This was considered sufficiently similar in terms of PK similarity, given the entirety of the physico-chemical comparability package, to proceed to the phase 1 comparative human PK trial. The human trial was performed as a randomized, single-blind, 2-sequence, 2-period, crossover study in 126 healthy adult

subjects. The geometric mean ratio expressed as % for the Test/Reference overall exposure parameter was approximately 85% with the lower tail of the 90% confidence limit falling below 80%, the traditional regulatory threshold for establishing bioequivalence of comparable formulations.(7)

What this case illustrates is that basing the decision to proceed to human comparative PK studies on results from relatively small toxicokinetic evaluations can be a high risk venture because (1) the precision of the parameter estimate is low due to small sample size and (2) the criteria for scaling animal to human data may require a tighter threshold when the intention is to compare two formulations as the traditional 2-fold difference may not be sufficiently discriminating.

The purpose of this contribution is to address the second point above and consider the interspecies scaling approaches employed in predicting human PK and specifically CL for macromolecules and to determine which of those approaches may be most appropriate for guiding development of biosimilar compounds.

2.3 Methods

As CL is a key driver of systemic exposure, literature evaluating the relative prediction success of one or more methods of interspecies CL scaling was reviewed. PubMed was used to identify literature references for review from September 2011 through March 2012. Search terms used included: allometry/allometric, clearance, fusion protein, interspecies scaling, macromolecules, monoclonal antibodies, physiologic based pharmacokinetic modeling, therapeutic protein.

For each method, an explanation of the method is followed by an assessment of prediction accuracy for small and large molecules. We deliberately omitted methods that considered physico-chemical properties or correction factors not likely to be of use in macromolecules (e.g. in-vitro metabolism data, protein binding), despite these approaches potentially having merit in predicting human PK with reasonable accuracy in small molecules.(74-77) Also omitted were literature comparisons where oral CL was assessed since all currently available biologics are available only in parenteral forms. To ensure a robust assessment of the utility of any one particular method, only those literature reports comparing predictive approaches with greater than 5 compounds were included. The primary methods of interest for this review are listed in Table 2.1 including some caveats or instructions for use.

Table 2.1: Methods for the prediction of human clearance

Interspecies Method	Formula	Notes
Simple Allometry		
≥3 Species	$\log y = \log a + b \bullet \log W$	W represents weight. Use ≥50-fold weight range for species(58)
Maximum Lifespan Potential (MLP) Correction	$CL_{corrected\ for\ MLP} = CL_{species} \bullet MLP_{species}$ $MLP\ (years) = 185.4(BW)^{0.636}(W)^{-0.225}$	Plot the log of the product of CL x MLP for each species on y-axis as in simply allometry; BW and W are in kg(53)
Brain Weight (BW) Correction	$CL_{corrected\ for\ BW} = CL_{species} \bullet BW_{species}$	Plot as per MLP(53)
Rule of Exponents (ROE)	When $0.55<b<0.7$ use simple allometry; $0.71<b<0.99$ use MLP; $b\geq1$ use BW	Prediction error may not be acceptable when $b<0.5$ or >1.3; MLP not recommended; macromolecules; use BW when $b\geq1$ (57)
Species-Invariant Time Techniques		
Kallynochrons (Elementary Dedrick)	y-axis = concentration/(Dose/W); x-axis = $time/W^{1-b}$	b and c are the exponents derived from ≥3 species using simple allometry for CL and V (53)
Apolysichrons (Complex Dedrick)	y-axis = $concentration/(Dose/W^{c})$; x-axis = $time/W^{c-b}$	See notes on Kallynochrons
"Simplified" Allometry		
Single Species Fixed Exponent	$CL_{human} = CL_{animal}\ (W_{human}/W_{animal})^{b}$	See Ling(61)

Two-Species Allometric Techniques			
	Two-species fixed coefficient with optimized or fixed exponent	$CL_{human}=a_{two\text{-}species}\ (W_{human})^{b}$	$a_{two\text{-}species}$ is the coefficient obtained from conventional allometric scaling of the two-species data and b fixed is a fixed optimized value (78)

2.3.1 Evaluation of Interspecies Scaling Methods

Several approaches for evaluating the success of a particular method have been employed in the literature; (75) however, one of the more intuitive measures of evaluating the success of any single prediction is the fold-error (FE) criteria (Equation 2.1).

$$FE = (y_{predicted})/(y_{observed}) \quad (2.1)$$

To compare two or more methods for prediction success across a group of compounds either the average fold-error (AFE) (Equation 2.2) or the absolute average fold-error (AAFE) (Equation 2.3) can be used.(75)

$$AFE = 10[\sum \log \text{fold-error}/n] \quad (2.2)$$

$$AAFE = 10[\sum |\log \text{fold-error}|/n] \quad (2.3)$$

The advantage of AAFE is that it does not allow for an over-prediction to balance or cancel out an under-prediction and comparison of AFE to AAFE for the same dataset suggests that the AAFE results in a more conservative estimate of prediction success.(78) Comparison of prediction accuracy has also been based on the proportion of observations falling within 2-fold.(60;78) This 2-fold threshold is considered acceptable when used to estimate the starting dose for first-in-human (FIH) trials on new compounds. For this purpose a 2-fold threshold may be reasonable, as FIH safe starting doses also consider the no observed adverse effect level (NOAEL) where only a small fraction (e.g. 1/10) of the human equivalent dose (HED) is administered initially. However, more stringent criteria for success is warranted since accepting a 2-fold difference could potentially result in up to a 300%[1] difference between the PK parameters of two formulations. This would not provide sufficient confidence of equivalence according to the traditional regulatory threshold of the 90% confidence interval for the mean ratio of the PK parameter being within 80-125%. Given the low number of animals and sampling points in a TK study, it may be unrealistic to predict human CL within 20%. A more realistic range of acceptable error may be 30-50%.(79) Unlike recent reports that seek to assess the prediction accuracy for methods ultimately employed in predicting the human CL of macromolecules within 2-fold(60), this review seeks to examine which methods previously applied for small molecules and

[1] This was calculated by taking the % difference between predicted values of 200% and 50% (200-50/50)x100%.

macromolecules alike have the greatest potential to predict human CL within a tighter range of fold-error i.e. 0.7-1.3-fold.

2.4 Results

The following will provide a historical overview of each approach listed in Table 2.1 and provide comparative data on the strength of the approach to predict human CL. Since the methods were first employed in predicting CL of small molecules, brief reference to their relative prediction accuracy with small molecules is described.

2.4.1 Allometry

Allometry was first termed by Huxley and Tessier in 1936 where they agreed upon the algebraic formula :(54)

$$y = bx^a \quad (2.4)$$

Where:

y = some biological quantity

b = biological constant

x = mass of the animal

a = allometric exponent

This formula was initially used for describing the relationship between changes in relative dimension of parts of an organism and changes in overall size of the organism. This relationship has been reported for a number of biological functions, most notably by Kleiber where basal metabolic rate was related to species mass for mammals and birds with an allometric exponent of 0.74, and later by West and Brown who reported this relationship could be extended from mammalian cells, mitochondria and unicellular organisms through to whole mammalian species.(80;81)

2.4.2 Simple Allometry With and Without Correction Factors for Small Molecules

Plotting the weight of >1 mammalian species vs. PK parameters of interest is termed conventional or simple allometry and CL of the animal species of interest is derived from the double log plot of Equation (2.4). The naming convention for the parameters is typically reported as Equation 2.5:

$$\log y = \log a + b \bullet \log (W) \quad (2.5)$$

Where a is the allometric coefficient; *b* the allometric exponent or slope and W is body weight.

Following a linearized power function:

When $b<0$, y decreases as Weight (W) increases

When $0<b<1$, y increases as the species becomes larger

When $b=1$, y increases proportionally with W

When $b>1$, y increases greater than proportionally with W

A frequently employed approach relying on relatively easily obtainable data, simple allometry, has been shown to be inconsistent in terms of its prediction accuracy for small molecules.(75) Incorporating correction factors such as Maximum Lifespan Potential (MLP) or Brain Weight (BW) has demonstrated improved prediction accuracy relative to simple allometry when applied according to the rule of exponents (ROE) originally proposed by Mahmood and Balian(82)(see Tables 2.1-2.3 for formulas and average values for MLP and BW correction). Employing ≥3 mammalian species for predicting human CL appears to be the prevailing approach.(79) An alternative to simplified allometric approaches, where one- or two-species are used with a fixed coefficient and/or exponent has also been employed.(78) When we compared the prediction accuracy of the ROE and one- and two-species methods for small molecules administered via the IV route, only the ROE resulted in a prediction accuracy within the currently proposed AAFE range of 0.7-1.3 (Table 2.4), supporting the notion that simple allometry employing the ROE is a reasonable approach for human CL prediction of small molecules.

Table 2.2: Maximum Lifespan Potential (MLP) for species commonly used in allometric scaling

Species	MLP (Years)
Mouse	2.7
Rat	4.7
Rabbit	8.0
Monkey	20
Dog	20
Human	93

Adapted from Obach *et al.*(74)

Table 2.3: Brain weight as a percent of overall body weight for species commonly used in allometric scaling

Species	% Body Weight
Mouse	1.45
Rat	0.75
Rabbit	0.39
Monkey	1.14
Dog	0.531
Human	2.19

Adapted from Boxenbaum and Fertig(83)

Table 2.4: Absolute Average Fold-Error (AAFE) and proportion of small molecules within 0.7-1.3 fold-error (79)

Interspecies Scaling Approach	Number of Compounds Included in the Analysis (N)	AAFE	Number within 0.7-1.3 fold-error (N)
ROE	24	1.26	20
Single species Rat	24	1.85	9
Single species Dog	22	1.77	5
Single species Monkey	16	1.86	6
Rat-Dog (fixed exponent*)	10	2.12	2
Rat-Monkey (fixed exponent*)	10	2.29	3
Rat-Dog (allometry)	10	2.78	2
Rat-Monkey (allometry)	10	2.31	3

* Fixed exponent was derived from a training set as described by Tang *et al.* (78)

2.4.3 Species-Invariant Methods for Small Molecules

Where classic allometric techniques predict human PK parameters, methods exist where plasma concentration time-profiles can potentially be predicted based on animal species. The concept of "pharmacokinetic" time, as opposed to chronologic time, has been described in the literature (e.g. by Boxenbaum)(84) as a means of evaluating the interspecies similarities across species. The principle is based on the observation that chronologic time is arbitrary and that different species clear drugs at rates relative to their lifespan. By normalizing the timescale, plasma concentrations from different species could be approximately superimposable. Dedrick (85) observed that the half-life of methotrexate could be scaled across mammalian species with an exponent of 0.25 and that by normalizing the chronologic time to physiologic time specific to a particular species would result in superimposable plasma-concentration time profiles. A composite best-fit plasma-concentration time profile could then be converted back to a human time scale and the curve could be integrated to derive pharmacokinetic parameters of interest using either compartmental or non-compartmental approaches. Boxenbaum(86) extended this approach to clearance and volume parameters and assuming fixed exponents of 0.75 and 1 for clearance and volume, respectively, and proposed a new time scale "kallynochron" where species have cleared the same volume of plasma per kilogram of body weight. The resultant plot is referred to as an Elementary Dedrick Plot (see Table 2.1). Similar approaches, including Complex Dedrick plots (using Apolysichrons) where a species clears the same fraction of drug per kg of body weight, have been applied in the literature but does not necessarily improve prediction of human PK parameters relative to simple allometry for small molecules.(87) Other time scales considering MLP (Dienitichrons) and MLP with BW (syndesichrons) exist as well, however

these approaches have been infrequently reported in the literature in large scale comparisons of methods and are therefore not discussed here.

2.4.4 Simple Allometry and ROE for Macromolecules

Whereas many small molecules are extensively metabolized through processes which can vary across species, macromolecules are rapidly degraded in biological fluids via proteolysis, cleared through receptor mediated processes and, depending on the size of the molecule, filtered renally. These catabolic mechanisms are similar across mammalian species relative to humans and more so in those species sharing close genetic similarity (i.e. non-human primates).

The simple allometric relationship between body weight and CL for small molecules across multiple mammalian species typically results in an allometric exponent of approximately 0.75. (88) Mordenti *et al.* demonstrated that similar relationships exist with proteins with molecular weights ranging from approximately 6 to 60 kDa and with various mechanisms of CL.(58) Derived exponents for clearance ranged from 0.65-0.84 when log-log plots of CL vs. weight were regressed. It should be noted, that these exponents included observed human data in addition to pre-clinical species. When the regression was repeated, excluding the human observations to test the prediction accuracy, the resultant fold-error ranged from 0.7-1.04 with an AAFE of 1.16 suggesting that simple allometry can be employed with reasonable prediction error for macromolecules similar to small molecule application (Table 2.5). Similar allometric exponents and prediction accuracy have been observed with coagulation factors and tissue-type plasminogen activators (Table 2.5).(56)

Table 2.5: Comparison of interspecies scaling approach AAFE for clearance of macromolecules

Reference	Therapeutic Classification	Interspecies Scaling Approach	Number of Compounds (N)	AAFE	Number within 0.7-1.3 fold-error (N)
Mordenti *et al.* (58)	Various Therapeutic Proteins	Simple allometry[a]	5	1.16	5
Mahmood (79)	Various Therapeutic Proteins	Simple allometry	6	2.05	2
		Maximum Lifespan Potential (MLP)	6	3	1
		Brain weight (BW)	6	4.6	1
		Single species mouse, fixed exponent 0.75	6	1.77	1
		Single species rat, fixed exponent 0.75	5	1.77	1
Mahmood (56)	Coagulation Factors; Tissue-type plasminogen activators	Simple allometry	5	1.25	5
		2-Species Rat-Dog	5	1.40	3
		2-Species Rat-Monkey	4	1.98	2
Dong et al.(64)	mAb	Single species Monkey, fixed exponent 0.75	10	1.56	4
Ling *et al.* (61)	mAb	Single species Monkey, fixed exponent 0.75	13	1.54	3
		Single species Monkey, fixed exponent 0.80	13	1.38	8
		Single species Monkey, fixed exponent 0.85	13	1.26	11
		Single species Monkey, fixed exponent 0.90	13	1.18	11
		Single species Monkey, fixed exponent 0.95	13	1.23	11
		Single species Monkey, Dedrick, fixed exponent 0.8	6	1.36	4
		Single species Monkey, Dedrick, fixed exponent 0.85	6	1.29	5
		Single species Monkey, Dedrick, fixed exponent 0.90	6	1.24	4
Oitate *et al.* (89)	Mab Soluble target	Single species Monkey, Dedrick, fixed exponent	6	1.55	2

		0.79			
	Mab Membrane-bound target	Single species Monkey, Dedrick, fixed exponent 0.96	6	1.45	3
Deng *et al.* (63)	mAb	Simple allometry	11	1.91	1
		Rule of Exponents	8	1.64	0
		Single species Monkey, fixed exponent 0.85	13	1.18	11

[a] SA= simple allometry with ≥ 3 species not including human

SS=single species

MLP= Clearance X Maximum Life-Span Potential

BW= Clearance X Brain Weight

mAb=Monoclonal Antibody

ROE=Rule of Exponents

AAFE=Absolute Average Fold-Error

Mahmood also reviewed the performance of simple allometry for monoclonal antibodies with and without correction for MLP and BW. MLP correction did not improve prediction of human CL where the exponent was <1.(57) Mahmood did observe that BW correction improves the prediction error when the exponent ≥1, however the recommendation for BW correction when the exponent is >1 is based on a single compound's prediction accuracy upon BW correction and therefore the recommendation for BW correction when the exponent is >1 should be taken with caution.(57) A single-species approach using a fixed exponent of 0.75 for CL was also evaluated, however only 1 species (mouse) was reported for all 6 compounds and the fold-error was 0.37-2.15, with only one compound within ± 30% (Table 2.5).

When data from only 2-species is available, scaling for small molecules as well as therapeutic macromolecules has shown inconsistent results however this approach is infrequently reported in the literature. Mahmood examined the prediction accuracy of the 2-species approach previously described for small molecules as applied to macromolecules however this dataset only included 5 compounds (coagulation factors and tissue-type plasminogen activators, Table 2.5).(56) One of the major criticisms of the two-species approach for macromolecules is that different species have varying propensities for eliciting antibody generation. If relying on 2 species for biosimilar comparison, the approach should only be used when both the test and reference biologic have been demonstrated to have similar immunogenic potential in the animals employed, and as with simple allometry, the mechanism of CL should be conserved across the species.

2.4.5 Single-Species "Simplified" Allometry for Macromolecules

Examination of the proportion of compounds falling within the proposed fold error of 0.7-1.3 for single-species approaches for small molecules (Table 2.4) or for macromolecules (Table 2.5)(57) might lead one to assume that such an approach would not yield sufficiently reasonable CL prediction accuracy to confidently move forward in one's development plan. Although not included in Table 2.5, as it did not meet the minimum threshold of 5 compounds, Mahmood reported single-species monkey data for 3 compounds 2 of which fell within ± 20% (data not shown).(57) Larger scale comparisons of prediction accuracy from monkeys as a single-species model have more recently been published. Using a similar approach to that reported by Mahmood (i.e. single-species with a fixed exponent of 0.75) Dong *et al.* predicted CL within 2-fold for 8/10 antibodies exhibiting linear PK with 4 compounds within ± 30% in terms of fold-error (Table 2.5).(64) This supports the observation that monkey as a single-species results in overall reasonable prediction accuracy.

On the other hand there were a relatively large proportion of the compounds falling outside the 0.7-1.3 currently proposed threshold for prediction accuracy, which may have been improved by modifying the exponent value. The exponent used by Dong *et al.* was based on the assumed ¾ power rule, and has been shown to not work well for all types of therapeutic macromolecules, particularly coagulation factors .(56) Dong *et al.* reported that using an exponent of 0.85 (Table 2.5) did not consistently improve predictions for all 10 compounds exhibiting linear PK.(64) However when we calculated the AAFE (Table 2.5) of 13 monoclonal antibodies from a report by Deng *et al.*(63) with a fixed exponent of 0.85, the resultant AAFE was near unity with a majority of compounds falling with 0.7-1.3. The antibodies in the Deng *et al.* report consisted of humanized, human and chimeric IgG and 4 of the antibodies are marketed and include antibodies with soluble receptors (e.g. trastuzumab).(63) When we compared the single-species approach to conventional simple allometry and ROE in terms of fold-error within 0.7-1.3 the single species with fixed exponent of 0.85 was far superior (Table 2.5). Wang and and Prueksaritanont further explored the influence of the exponent in terms of prediction accuracy of a single-species (combination of mouse, rat, rabbit, monkey and dog) whereby they considering fixed exponents ranging from 0.7 to 0.9 with increments of 0.05 and confirmed that for 34 compounds, including monoclonal antibodies and fusion proteins, a fixed exponent of 0.8 provided the best overall prediction with 92% of compounds within 2-fold.(62) The authors did not report an overall prediction accuracy as the objective was to determine whether the predictions were reasonable for FIH dosing, however what is clear is that single species monkey can predict macromolecule CL for a reasonably diverse set of macromolecules and that the fixed exponent needed to achieve appropriate prediction accuracy, if used in biosimilar development, should be nearer to 0.8 or 0.85 as opposed to the previously assumed 0.75.

2.4.6 Species-Invariant Approaches for Macromolecules

In addition to comparing simplified allometric approaches using a single-species and fixed exponents, Ling *et al.* found that a fixed exponent closer to 0.85 improved prediction accuracy of CL when using the Dedrick plot approach (Table 2.5).(61) Oitate *et al.* however similarly considered the single species monkey employing both Elementary and Complex Dedrick Plot approaches for both soluble and membrane-bound target mAbs and found that although both Elementary and Complex Dedrick plots resulted in similar predicted CL values neither resulted in an AAFE within 0.7-1.3 for a group of 12 mAbs (6 soluble and 6 membrane-bound target) (Table 2.5 for Elementary Dedrick).(89) One explanation for the discrepancy between the two publications may be the method in which the CL values were estimated following normalization of the concentration time profiles. Ling *et al.* employed a non-compartmental analysis approach for deriving the human PK parameters whereas Oitate *et al.* employed compartmental analysis. The non-compartmental approach may not be as accurate when using TK data where sampling tends to be sparse. Further exploration of species-invariant approaches is warranted prior to suggesting this approach ahead of simplified allometry using non-human primates.

2.5 Discussion

If the mechanism of CL varies widely across species then using a single species which is different from humans may over- or under-predict. This may explain why simple allometry performs better in some cases than single-species, even when non-human primates are used as the single-species. In cases where the pharmacokinetics are linear and the mechanism of CL is thought or known to be conserved across the species based on the reference biologic compound, a single species, such as non-human primates may be the most efficient and appropriate model to scale the PK from animals to humans. Where the mechanism of CL is known to differ among the species, obtaining CL values from ≥ 3 species for both the biosimilar candidate and the reference biologic compound seems warranted however as previously stated, species selection must consider whether the degree of immunogenicity is similar across species. Where simple allometry is used with ≥ 3 species, the evidence suggests utilizing species with over a 50-fold or greater weight range as data clustered around a narrow range of species can affect the prediction.(58)

Single-species allometry has not been particularly useful for predicting CL in humans for small molecules, particularly when the compounds have been administered orally. Although monkeys have demonstrated reasonable predictive capacity for small molecules administered by IV, there is evidence to suggest that factors affecting oral bioavailability such a P-glycoprotein efflux and intestinal metabolism differ sufficiently between humans and monkeys such that the monkey is an insensitive model for predicting the oral CL of small molecules.(90) In contrast, for macromolecules, single-species, and particularly monkeys, have demonstrated reasonably good prediction of human CL across a variety of compounds including monoclonal antibodies and fusion proteins. There is less data available to support a universal application of single-species allometry for drugs exhibiting non-linear pharmacokinetics or for those administered via the subcutaneous route.

A limitation of the current evaluation, as well as other reports of this nature, is that prediction accuracy is based on a mean value for the exponent tested. With the exception a few report (e.g. Oitate 2011), the range of exponents are rarely reported.(89) A prediction interval (i.e. a range of prediction accuracies by product and method) is rarer, and this adds to the uncertainty, and limits the interpretation of the results. Inclusion of prediction intervals in future evaluations may allow for better discrimination between the different fixed exponent values as opposed to basing decisions on mean predicted values.

Another limitation of the current evaluation is that the compounds included in the simplified allometric approaches with fixed exponents tended to reside within the broader class of Mabs and thus the results may not be directly applicable to other therapeutic proteins such as fusion proteins and oligonucleotides. This is a consequence of the availability of literature reports which have been published to date evaluating single-

species interspecies scaling techniques with fixed exponents and likely reflects the reality that Mabs represent a significant proportion of therapeutic compounds either in development or on the market. Additional research is required to determine whether the prediction accuracy of the single-species allometric approaches in monkeys with fixed exponents can be extrapolated to a broader range of therapeutic compounds outside the Mab class.

The majority of the therapeutic macromolecules in the present review were administered IV for both animals and humans. Consideration of the subcutaneous route however is becoming increasingly important and many therapeutic macromolecules are available or are being tested currently for subcutaneous administration. This presents additional challenges for prediction of human pharmacokinetics from animal species as subcutaneous absorption of macromolecules such as mAbs follows uptake via the lymphatic pathway potentially imparting non-linearity in the subcutaneous absorption phase (through saturation of the proteolytic capacity or lymphatic transport).(72) There may also be interspecies differences in the mechanism of uptake of macromolecules from the subcutaneous compartment. Few literature reports are available on the interspecies scaling of macromolecules with subcutaneous administration. Dong *et al.* included data from macromolecules following subcutaneous administration where non-linearity in the pharmacokinetics has been observed.(64) For these compounds, derivation of the PK parameters was done following fitting data empirically to a pharmacokinetic model with parallel linear and non-linear elimination. A similar approach has been applied previously by Woo and Jusko in an interspecies comparison of the PK and PD of recombinant human erythropoietin.(91) When predictions of macromolecules known to exhibit non-linearity in the absorption phase are to be made as biosimilars, fitting the data to an appropriate PK model may be beneficial rather than utilizing the traditional non-compartmental approach, particularly when the animal data is derived from subcutaneous dosing. It should be noted that in some cases the comparison of human and animal PK was performed at saturating doses and, from a biosimilar perspective, it may be beneficial to include more than one dose level for each biosimilar candidate and the reference biologic to ensure the degree of non-linearity is similar between the two products.(62) Appropriate model development for a biosimilar may require the inclusion of factors such as the presence of soluble receptor targets, target-mediated clearance and neutralizing antibodies in the pre-clinical species (especially in the case of multiple-dose PK data).

Allometric approaches traditionally rely on either non-compartmental or some semi-mechanistic approach to assess CL and V, as such they are limited in their ability to extrapolate beyond the data being explained. There may be value in considering alternative approaches for scaling the PK of biosimilars. In contrast to allometric approaches, PBPK models consider anatomical spaces, physiologic processes as well as drug

specific characteristics to describe the PK of a given compound.(92;93) As PBPK models rely on well characterized physiologic processes and anatomy which are common across mammalian species, PBPK may offer advantages over traditional allometric approaches through limiting the number of different animal species for which in-vivo PK data is required for scaling up to human values. More work is required in this area as the literature supporting the use of PBPK in predicting human PK of macromolecules, and specifically application in biosimilars, is in its infancy.

2.6 Summary

Biosimilars have enormous potential for both generating revenue for industry and saving expenditures for payers of drug therapies. The development of a biosimilar candidate, although abridged relative to an innovative compound, is still fraught with risk particularly when the toxicity profile limits comparative testing in Phase I necessitating sponsors to make decisions to proceed to large scale patient trials based on pre-clinical testing. Access to methodologies for better prediction of PK equivalence based on pre-clinical data, and in particular animal TK data, may prove helpful to sponsors in making such decisions. Allometric techniques, which have had mixed success in the prediction of human PK for small molecules, may actually have better predictive success for macromolecules with greater promise for single species approaches using non-human primates than that previously observed with small molecules. Whole-body PBPK modeling may offer an alternative approach for both interspecies scaling of macromolecules for biosimilar purposes as well as incorporation of disease processes simulating the conditions used in comparative efficacy and safety trials. The 2-fold threshold, traditionally employed as a measure of prediction accuracy for interspecies scaling may be too liberal if such approached for the purpose of de-risking candidate selection in biosimilar development. A tighter threshold of 0.7-1.3 may be more discriminating in identifying biosimilar candidates which would be less likely to exhibit similar PK to the reference biologic in humans.

CHAPTER 3: MODEL-INDEPENDENT SINGLE-SPECIES ALLOMETRIC SCALING METHODS FOR A PEGYLATED PEPTIDE CONJUGATE

This chapter consists of unpublished works. The PhD candidate conducted all the pertinent research, conducted all described analyses, created all tables, plots and figures and wrote the entire chapter.

3.1 Introduction and Objectives

Simplified allometry as introduced and discussed in Chapters 1 and 2 provide for a means of extrapolating the systemic exposure from animals to humans to predict the dose required in humans corresponding to an exposure threshold below what is considered safe in animals. Pharmacokinetic (PK) parameters can be estimated via a number of computational methods and can be crudely divided into model-based and model-independent methods. Model-based methods can be further partitioned into mechanistic, semi-mechanistic models and empiric compartmental models, all of which employ a series of mass transfer equations to describe drug movement between compartments, with mechanistic models being more anatomically and physiologically representative relative to empirical models. Model-independent methods however, are far less computationally intensive, and potentially offer utility in the prediction of human PK following administration of a drug to a preclinical species early in drug development.

Model-independent methods rely on non-compartmental analysis (NCA) to estimate important PK parameters and exposure to drugs. Gabrielsson and Weiner (40) provide a detailed explanation of the principles of NCA, however a brief explanation is provided herein. The parameters of greatest interest following a single dose of a drug are defined in Table 3.1. The maximum observed concentration (Cmax) is the peak of the concentration vs. time profile (CPT), and literally involves identifying the highest observed concentration. The area under the curve (AUC) represents the overall extent of drug which is available for systemic action and is derived based on integral calculus theory. The CPT is partitioned into smaller areas and then the cumulative areas are summed to obtain a single value.(94) The linear trapezoidal method, involves dividing the CPT into discrete trapezoids and calculating the area of each trapezoid and summing the trapezoids to obtain a single AUC value. Another variation is the log-linear version which assumes a log scale for the CPT after the peak concentration, during the descending portion of the curve, which is assumed to mitigate the risk of overestimation of systemic exposure during the exponential decline in the concentrations over time. Regardless, both methods share underlying assumptions, being: (a) applicable to any typical route of administration (intravenous [IV], subcutaneous [SC], oral, etc.); (b) no specific biodistribution (i.e. compartmental) pattern is assumed and (c) clearance of the drug occurs from the sampling compartment.

The rate of disappearance of the drug from the sampling compartment is also an important PK parameter as it reflects how quick the body is clearing the drug. The term half-life ($T_{1/2}$) refers to the time the concentration in the sampling compartment divided by a factor of 2. In NCA, the $T_{1/2}$ is derived from the regression of the log-linear terminal (β) portion of the CPT, which describes the elimination phases of the

drug and is calculated as the natural log (Ln) of 2 divided by the apparent terminal elimination rate constant (λ), which is derived from the regression of the β portion of the CPT.(40)

Clearance (CL) and volume of distribution (V_d), as introduced in Chapter 1 are important PK parameters of a drug which inform key decision points related to drug, dose and regimen and. Said parameters can be estimated using NCA, or more computationally intensive methods that will be described in more detail in later chapters.

Formally, CL is the volume of plasma cleared of drug per unit of time. From a physiologic perspective, estimating CL following different dose levels or following different routes of administration helps inform whether the drug is cleared in a linear fashion or exhibits some degree of capacity-limited absorption or elimination. Based on a drug's physical and chemical properties, there is either a propensity or restriction on the tissue penetration of a drug after administration. The V_d is a parameter which is intended to quantify the volume required to explain the observed concentration in the sampling compartment after administration, and may not necessarily have an anatomic or physiologic basis.(95) The V_d is a parameter which attempts to describe the extent of distribution of a drug in the body, however depending on the analyst and data available, can potentially be expressed as: (1) V_c which relates that mass of drug in the blood immediately after instantaneous administration (i.e. IV administration); (2) V_{ss} which is the volume of distribution when equilibrium of the drug has been achieved between the blood and tissue compartments; (3) Vz, which is a proportionality constant which relates the distribution of a drug in the blood and tissue compartments at pseudo-equilibrium.

Following IV administration, CL and volume parameters can be estimated by NCA, however for extravascular administration, where the bioavailability (F) is unknown, these parameters are divided by "F" which is the fraction of drug dose that appears in systemic circulation. With NCA methodology, when the time interval between two data points is large, there is greater risk in over- or under-estimating the area of the trapezoid. In Chapter 1 and again in Chapter 2, limitations of PK evaluation in animal studies were raised, with one major limitation being frequency and duration of blood sampling from the animal. Thus, employing animal pharmacokinetic (referred to as toxicokinetics or TK in preclinical development) studies to obtain estimates of exposure can be fraught with considerable uncertainty.

Another model-independent approach to scaling PK based on allometric theory is the Elementary Dedrick plot (Dedrick plot for short). The theory underlying this approach is addressed in additional detail later in this chapter, however the principle of a Dedrick plot is to normalize the x-axis of a CPT such that time is

relative to the species size and the resultant x-axis is a dimensionless time scale referred to as kallynochrons.(53;86) An added benefit over traditional allometry that scales only the mean PK parameter value, Dedrick plots allow for visualization of the entire CPT. This approach has been employed for small and large molecule scaling with varying success, and has typically been used following IV administration.(87;89;96)

This chapter seeks to evaluate the prediction accuracy of single-species allometric scaling of model-independent derived PK parameters for a subcutaneously administered large molecule. The exemplary molecule is the same pegylated peptide conjugate (PPC) which is also the subject of Chapters 4-6. As this is the first chapter in this thesis for which computational analysis was performed on the data obtained for this molecule, some additional background is provided. Data for an investigation PPC was provided confidentially by a benefactor (pharmaceutical industry sponsor) wishing to remain anonymous for proprietary reasons. The unconjugated molecule is conjugated to a linear polyethylene glycol (PEG)-40 chain. Out of respect and wishes of the Sponsor, the investigational drug will be referred to as PPC throughout the chapters which are not versions of already published material (where the compound is referred to as a pegylated peptide conjugate).

PPC has currently just completed the initial phase of human development. Concentration vs. time data as well as some important study conduct information was provided for a first-in-human (FIH) dose escalation study as well as for preclinical exposure evaluation in a single, non-human primate (NHP) species. As such, the objective of this chapter was to test the prediction accuracy of single-species interspecies scaling methods for later comparison to the more computationally intensive, model-dependent methods described in Chapters 4-6.

3.2 Methods

3.2.1 Data

Drug concentration data for PPC was provided following IV and SC administration to a NHP cynomologus monkey species. Additionally, concentration data was provided for the same PPC following SC administration to humans by the Sponsor specifically for the purpose of this thesis research project. Nine non-naïve (previous exposure to other experimental treatments) female NHP (mean weight 3.4 kg) were evaluated for single- and repeat-dose exposure of PPC. Three NHPs each received a single 7 mg/kg IV dose and three received a single 7 mg/kg SC dose to the back region. Blood samples were obtained for PK evaluation at 0.083, 0.5, 1, 4, 8, 24, 48, 72, 120, 144, 168, 192 and 336 hours after the dose. An additional three NHPs received seven, daily, consecutive 7 mg/kg SC doses with an identical PK sampling schedule with the single-dose group (i.e. 0.083, 0.5, 1, 4, 8, 24, 48, 72, 120, 144, 168, 192 and 336 hours after the first dose).

The human data was obtained as part of the FIH dose escalation study where four healthy male subjects in each cohort (weight range 60-80 kg) received a single SC dose of either 45 mg, 90 mg, 180 mg, 360 mg or 720 mg to the abdominal region. Blood samples were obtained for PK evaluation immediately prior to the dose and 1, 4, 8, 12, 24, 48, 72, 96, 120, 144, 168, 240, 336, 408, 504, 576 and 672 hours after the dose, with an additional sample drawn 1008 hours after the dose for the 720 mg dose cohort.

The human study was conducted under good clinical practice and according the ethical principles outlined in the Declaration of Helsinki. Plasma was analyzed from both species employing an LC-MS/MS method with a limit of quantitation of 1 μg/mL for both NHP and human matrices.

3.2.2 PK parameter Estimation

For NHPs and humans, each individual's concentration data was subject to NCA to obtain estimates for those parameters listed in Table 3.1. Regression of λ was based on a minimum of three concentration observations and could not include the Cmax value. Regressions were only considered acceptable where there was an apparent terminal phase and where the coefficient of determination (R^2) value was >70%. Where an R^2 was not calculable, parameters dependent on λ were set to missing.

Table 3.1: Pharmacokinetic parameters derived in the current evaluation obtained by non-compartmental analysis using Phoenix WinNonlin (version 6.4, Certara)

Parameter	Definition	Calculation
AUC_{0-t}	Area under the concentration vs. time profile from dose time (0) to the last quantifiable time point	Measured by the linear trapezoidal method
AUC_{0-inf}	Area under the concentration vs. time profile from dose time (0) extrapolated to infinity	AUC_{0-t} + the ratio of the last measureable concentration/λ
Cmax	Highest observed concentration	Taken directly from the observed data
Tmax	Time of Cmax	Taken from time of Cmax
CL/F	Clearance after extravascular administration	Calculated as Dose/AUC_{0-inf}
Vz/F	Volume of distribution based on the terminal phase after extravascular administration	Calculated as Dose/λ•AUC_{0-inf}
λ	Apparent terminal elimination rate constant	Determined by the slope of the log-linear portion of the concentration vs. time profile
$T_{1/2}$	Apparent terminal elimination half-life	Calculated by dividing Ln(2)/λ

For parameters divided by F, F is equal to 1 for intravenous administration and may be less than 1 for extravascular administration.

Individual parameters were then summarized descriptively to obtain an arithmetic mean value for each of the two species.

NCA and descriptive statistics were performed using Phoenix ® 1.4 WinNonlin version 6.4® (Certara) and Excel (Microsoft). Prior to NCA, concentration values below the limit of quantitation (BLQ) were set to zero prior to Tmax and missing for any BLQ values afterwards.

As the observed human dataset consisted of 5 unique subject cohorts across 5 dose levels, linear regression of the log value of AUC and log value of Cmax, respectively vs. log of dose administered was performed. If the 95% confidence interval for the slope of the regression did not include zero, then a linear proportional relationship between PK parameters of interest with dose would be assumed. In such a case CL/F, Vz/F and $T_{1/2}$ would be assumed to be independent of dose and the mean PK parameters across all 5 dose levels would be calculated. Otherwise, comparison of the predicted PK parameters would be compared to the mean PK parameter by cohort/dose level.

3.2.3 Interspecies scaling methods

3.2.3.1 Fixed-exponent single-species scaling of clearance and volume

For single-species CL/F, Vz/F and $T_{1/2}$ scaling, the PK parameter value for humans (P_{human}) was obtained by multiplying the corresponding parameter obtained from NHPs (P_{monkey}) with a body weight ratio raised to a scaling factor exponent as per Equation 3.1. Body weight ratios assumed the arithmetic average of the NHPs (i.e. 3.4 kg) and the median of the per protocol range of humans (i.e. 70 kg).

$$P_{human} = P_{monkey} \bullet (Weight_{human}/Weight_{monkey})^{exponent} \quad (3.1)$$

Generally, and as described in greater detail in Chapter 2, volume of distribution parameters are assumed to scale proportionally with body weight and thus an exponent of 1 was assumed. Similarly, an exponent of 0.85 was assumed for clearance parameters. Consistent with the proposal by Boxenbaum and Ronfeld, $T_{1/2}$ can similarly be scaled across species according to Equation 3.1, where the exponent is the difference between the exponents for volume and clearance parameters(86); in our case 0.15.
As a sensitivity evaluation, the theoretical value was varied by ± 0.05 exponent increments.

Prediction accuracy for each predicted vs. observed value was performed by dividing the predicted by the observed value and reported as fold-error (FE). Consistent with the proposal in Chapter 2 (Equation 2.1), a prediction was determined reasonable where the FE, which is the ratio of a predicted parameter (P) over the observed parameter, falls between 0.7-1.3.

3.2.3.2 Elementary Dedrick Plot

Scaling of NHP to humans was performed by normalization of the CPT whereby plasma concentration and time scales following a single SC dose for NHPs were normalized to a human time scale and plotted as Elementary Dedrick plots similarly to the concentration-time transformations used by Lave et al.(46;89) Normalization of time and concentration were performed as per Equations 3.2 and 3.3 assuming empiric exponent values for c and b of 1 and 0.85 respectively, for apparent extravascular volume (Vz/F) and clearance (CL/F), respectively.

$$Time_{human,predicted} = Time_{monkey} \bullet (Weight_{human}/Weight_{monkey})^{c-b} \quad (3.2)$$

$$Concentration_{human,\ predicted} = Concentration_{monkey,observed} \bullet (Dose_{human}/Dose_{monkey}) \bullet (Weight_{monkey}/Weight_{human}) \quad (3.3)$$

As NHPs were dosed on a 7 mg/kg basis, doses were multiplied by the mean body weight to obtain an absolute dose prior to scaling. Following normalization, scaled concentrations obtained from NHPs were descriptively summarized to obtain an arithmetic mean concentration at each nominal time point and overlaid with the observed, concentration data obtained from humans. If the PK was determined to be linear across all dose levels, human observed concentration values were to be normalized to the lowest dose level (i.e. 45 mg). NCA was then performed on the mean observed human data and compared to the mean predicted human concentrations as scaled from NHPs.

3.3 Results

Although the methodology in this chapter is focused on the prediction accuracy methods following a single SC dose, for transparency and to provide a clear illustration of the PK of the test compound in NHPs, the CPT following single-dose IV administration as well as following single- and repeat-dose SC administration are provided. Figures 3.1a and 3.1b illustrate the linear and log scale CPT for in NHPs following the 7 mg/kg IV and SC doses. Figures 3.2a and 3.2b illustrate the same scales for 20 human male subjects over 5 SC dose levels. Single 7 mg/kg SC administered doses in NHPs achieved similar concentrations (1-100 μ/ml) observed in humans when considering the range of doses administered in the human population.

Figure 3.1: Concentration vs. time profiles (linear scale – 3.1a; log x vs. log y scale – 3.1b) of a pegylated peptide conjugate following a single 7 mg/kg IV administration (open circle), a single 7 mg/kg SC administration (open diamond) and a day-7 profile following seven repeat daily 7 mg/kg SC administrations (closed triangle) in cynomologus monkeys (n=3 monkeys per group).

Figure 3.1a

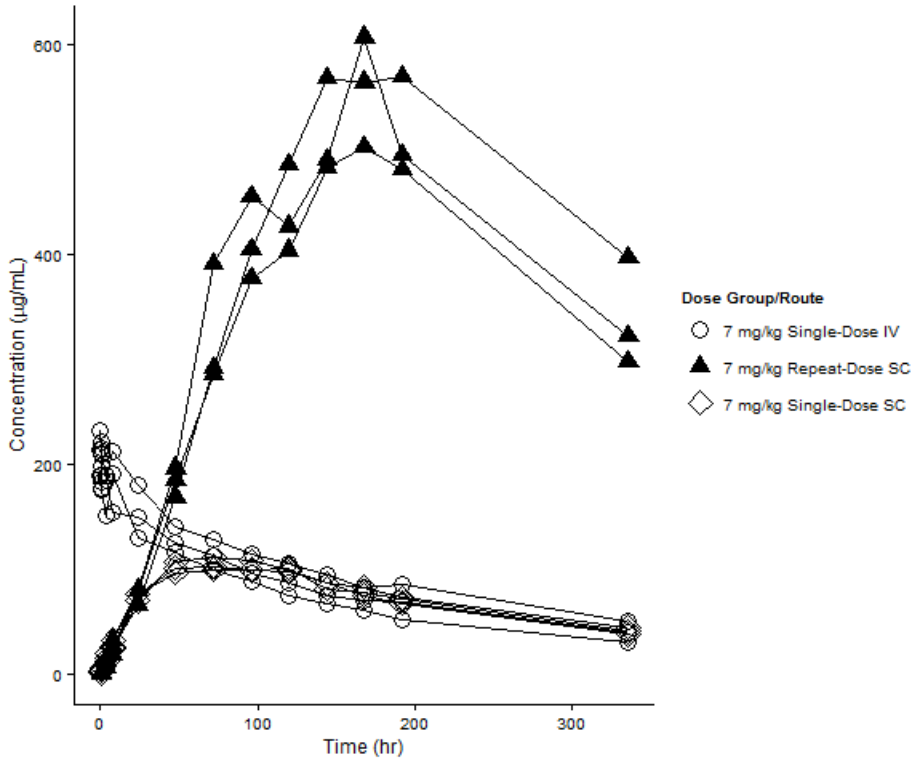

Figure 3.1b

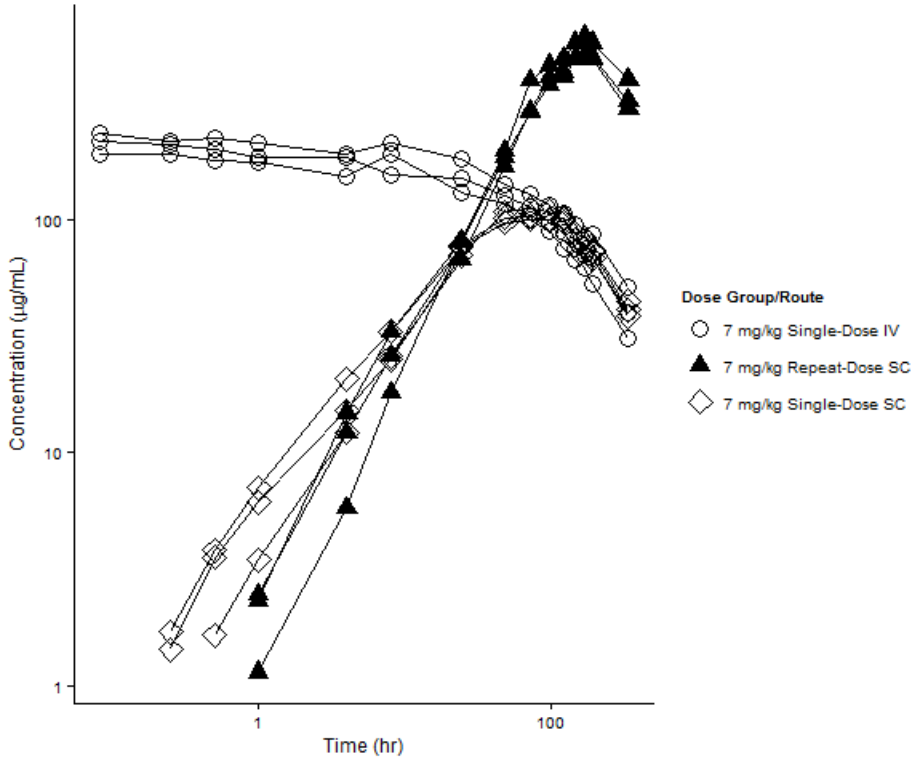
Concentration (µg/mL)
100
10
1
1
100
Time (hr)
Dose Group/Route
7 mg/kg Single-Dose IV
7 mg/kg Repeat-Dose SC
7 mg/kg Single-Dose SC

Figure 3.2: Concentration vs. time profile (linear scale – 3.2a; log x vs. log y scale – 3.2b) of a pegylated peptide conjugate following single-dose SC administration to healthy male subjects (n=4 per dose cohort) participating in a first-in-human single-ascending dose study.

Figure 3.2a

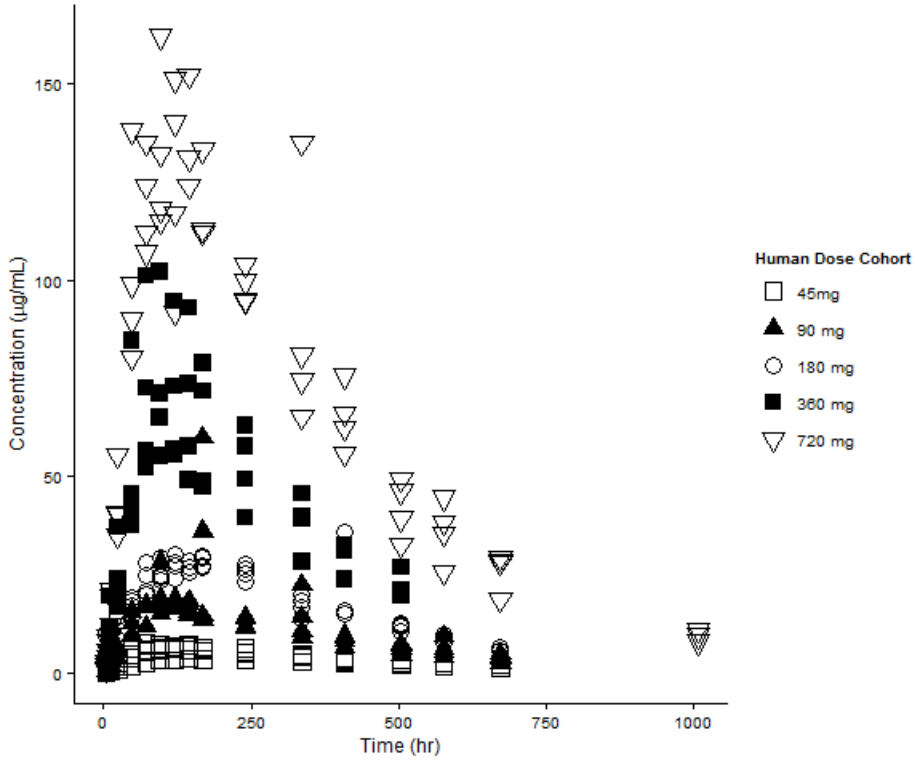

Figure 3.2b

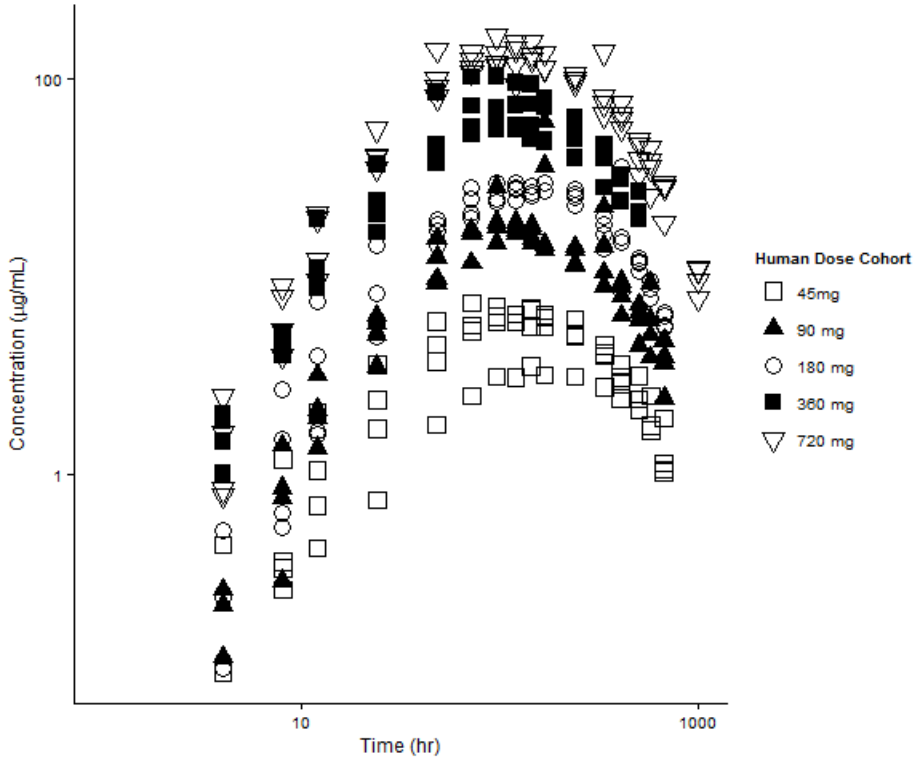
100
1
Concentration (µg/mL)
10
1000
Time (hr)
Human Dose Cohort
45mg
90 mg
180 mg
360 mg
720 mg

3.3.1 Fixed Exponent Scaling

Results of fixed-exponent scaling of PK parameters are presented in Table 3.2. An empiric scaling factor of 0.85 was assumed for CL/F, which resulted in an FE of only 0.67. This was outside of the ±30% pre-specified acceptance margin. In contrast, scaling factors closer to 1 resulted in a FE closer to unity, implying a proportional relationship of CL/F with body weight across species. With respect to volume, a scaling factor of 1 resulted in FE values well within the ±30% region suggesting V_d is proportional to body weight. An empiric allometric scaling factor of 0.15 somewhat over-estimated the observed $T_{1/2}$ with an exponent closer to 0.05 providing the FE closest to unity.

Table 3.2: Prediction accuracy of single-species simplified allometric scaling of extravascular clearance, extravascular volume of distribution and half-life from cynomologus compared to humans for a single, subcutaneous dose of a pegylated peptide conjugate

Parameter	Observed NHP	NHP body weight	Human body weight	Equation 3.1 Exponent	Predicted (Human)	Observed (Human)	Fold error	Criteria Achieved (between 0.7-1.3)
CL/F	0.20	3.4	70	0.7	5.62	13.16	0.43	No
CL/F	0.20	3.4	70	0.75	6.54	13.16	0.50	No
CL/F	0.20	3.4	70	0.8	7.61	13.16	0.58	No
CL/F	0.20	3.4	70	0.85	8.85	13.16	0.67	No
CL/F	0.20	3.4	70	0.9	10.29	13.16	0.78	Yes
CL/F	0.20	3.4	70	0.95	11.97	13.16	0.91	Yes
CL/F	0.20	3.4	70	1	13.93	13.16	1.10	Yes
Vz/F	51.78	3.4	70	0.85	2302.42	4054.96	0.57	No
Vz/F	51.78	3.4	70	0.9	2678.34	4054.96	0.66	No
Vz/F	51.78	3.4	70	0.95	3115.63	4054.96	0.77	Yes
Vz/F	51.78	3.4	70	1	3624.33	4054.96	0.89	Yes
Vz/F	51.78	3.4	70	1.05	4216.08	4054.96	1.00	Yes
Vz/F	51.78	3.4	70	1.1	4904.44	4054.96	1.20	Yes
Vz/F	51.78	3.4	70	1.15	5705.19	4054.96	1.40	No
$T_{1/2}$	180.73	3.4	70	0	180.73	214.34	0.84	Yes

$T_{1/2}$	180.73	3.4	70	0.05	210.23	214.34	0.98	Yes
$T_{1/2}$	180.73	3.4	70	0.1	244.56	214.34	1.10	Yes
$T_{1/2}$	180.73	3.4	70	0.15	284.49	214.34	1.30	Yes
$T_{1/2}$	180.73	3.4	70	0.2	330.94	214.34	1.50	No
$T_{1/2}$	180.73	3.4	70	0.25	384.97	214.34	1.80	No
$T_{1/2}$	180.73	3.4	70	0.3	447.82	214.34	2.10	No
$T_{1/2}$	180.73	3.4	70	0.35	520.94	214.34	2.40	No
$T_{1/2}$	180.73	3.4	70	0.4	605.99	214.34	2.80	No

CL/F: Extravascular clearance in mL/h; Vz/F: Extravascular volume of distribution in mL; $T_{1/2}$: Apparent terminal elimination half-life in hr; NHP: Cynomologus monkey

3.3.2 Dedrick Plot

As described in the methods section, if the human exposure was deemed proportional to dose, comparison of scaled concentrations from NHPs would be performed relative to the dose normalized CPT averaged across all five human dosing cohorts. Figures 3.3a and 3.3b demonstrate that exposure in humans, as measured by AUC and Cmax, increased proportionally with increasing dose with the 95% confidence interval for the slope including a value of one. Consequently, Dedrick plot prediction accuracy was based on human dose-normalized concentrations to the lowest (i.e. 45 mg) human dose cohort. Dedrick plots on the linear scale (Figure 3.4a) qualitatively suggest reasonable prediction of the human data, with slight over-prediction of the peak concentration. Due to truncation of the NHP observed data, the terminal elimination phase is not comparable between the two species. When comparing log scale plots (Figure 3.4b), it becomes evident that the Dedrick plot scaling could not account for potential interspecies differences in the absorption phase of the CPT. This obvious over-prediction in the mean CPT however did not translate to significant differences in the main PK parameters of interest. Table 3.3 presents the results of the NCA performed on the average predicted vs. observed CPT where exposure parameter FE (AUC_{0-t} and Cmax) and Vz/F were within ± 10%. In contrast, AUC_{0-inf} fell just outside; and CL/F fell just within the pre-specified acceptance boundary.

Figure 3.3: Log of pegylated peptide conjugate dose administered to healthy male subjects in the first-in-human single-ascending dose study vs. log of AUC (3.3a) or Cmax (3.3b) (obtained by non-compartmental analysis) for the corresponding subject, to evaluate proportionality of dose vs. exposure. Closed circles represent the individual values. The blue line and grey shaded region represent the regression slope and corresponding 95% confidence interval of the slope. Where the 95% confidence interval includes a value of 1, proportionality cannot be rejected.

Figure 3.3a

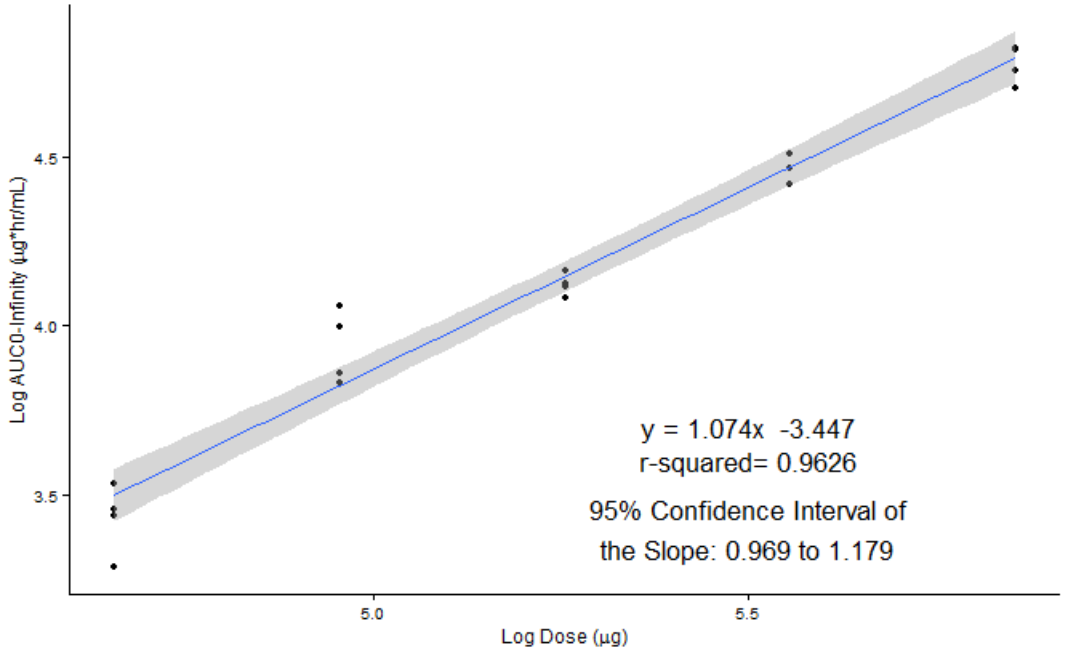

Figure 3.3b

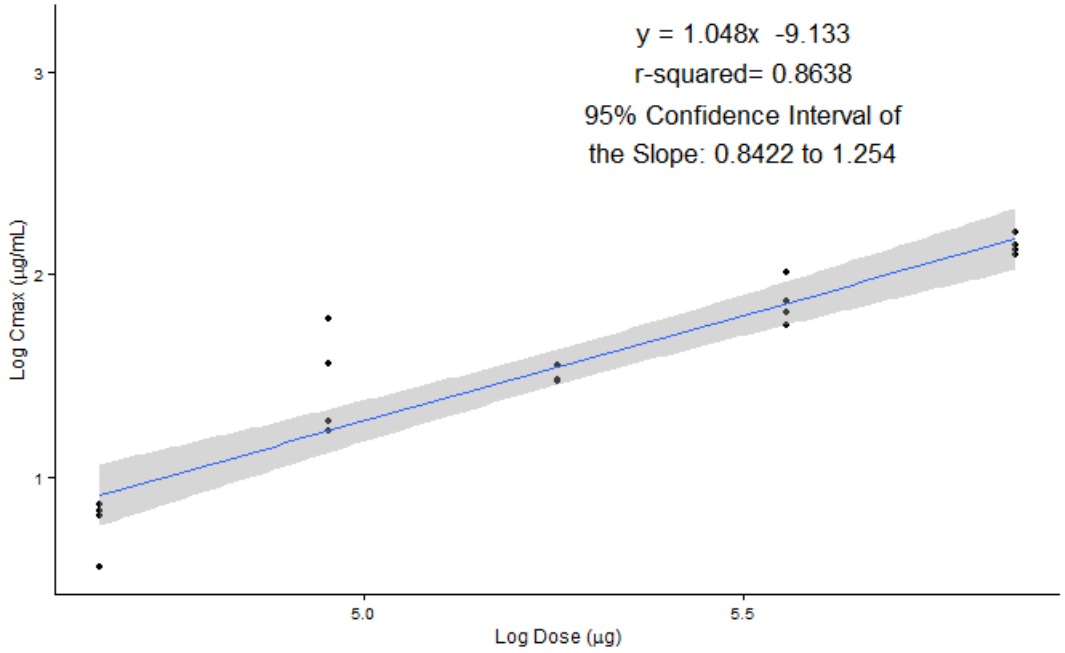
y = 1.048x -9.133
r-squared= 0.8638
95% Confidence Interval of
the Slope: 0.8422 to 1.254
Log Cmax (µg/mL)
3
2
1
5.0
5.5
Log Dose (µg)

Figure 3.4: Dedrick Plot (linear scale – 3.4 a; log x vs. log y – 3.4b). Dashed line represents the dose-normalized (to a 45 mg dose) arithmetic mean observed concentration of a pegylated peptide conjugate vs. nominal time profile in healthy human subjects following escalating doses in a first-in-human single-ascending dose study. The solid line represents the arithmetic mean concentration of pegylated peptide conjugate following a single, 7 mg/kg dose in cynomologus monkeys (n=3) scaled to human vs. nominal time from the cynomologus PK evaluation.

Figure 3.4a

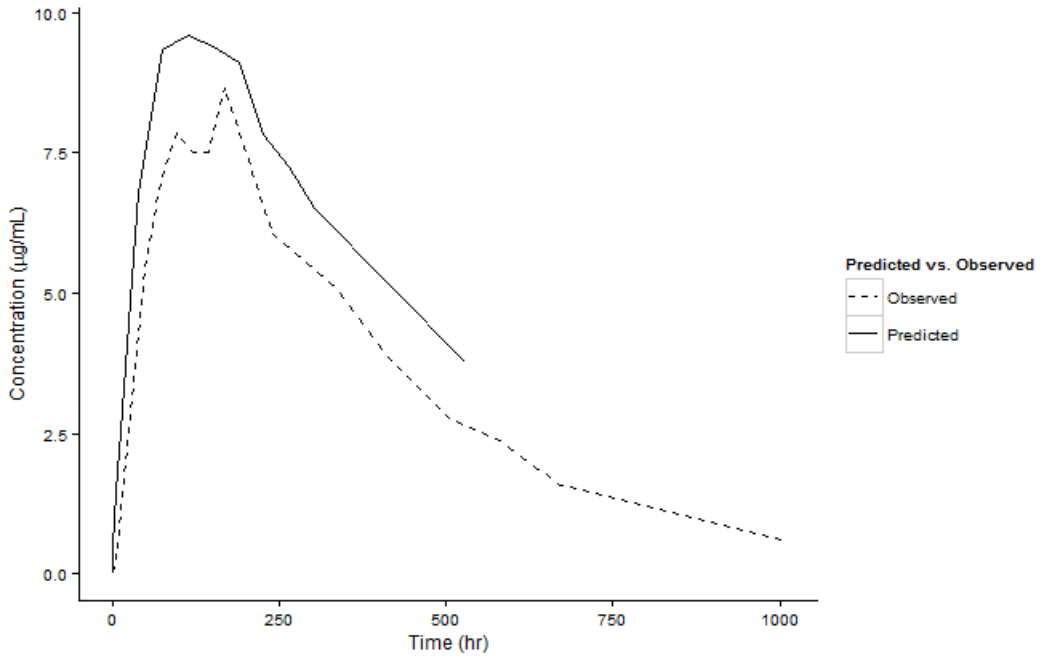

Figure 3.4b

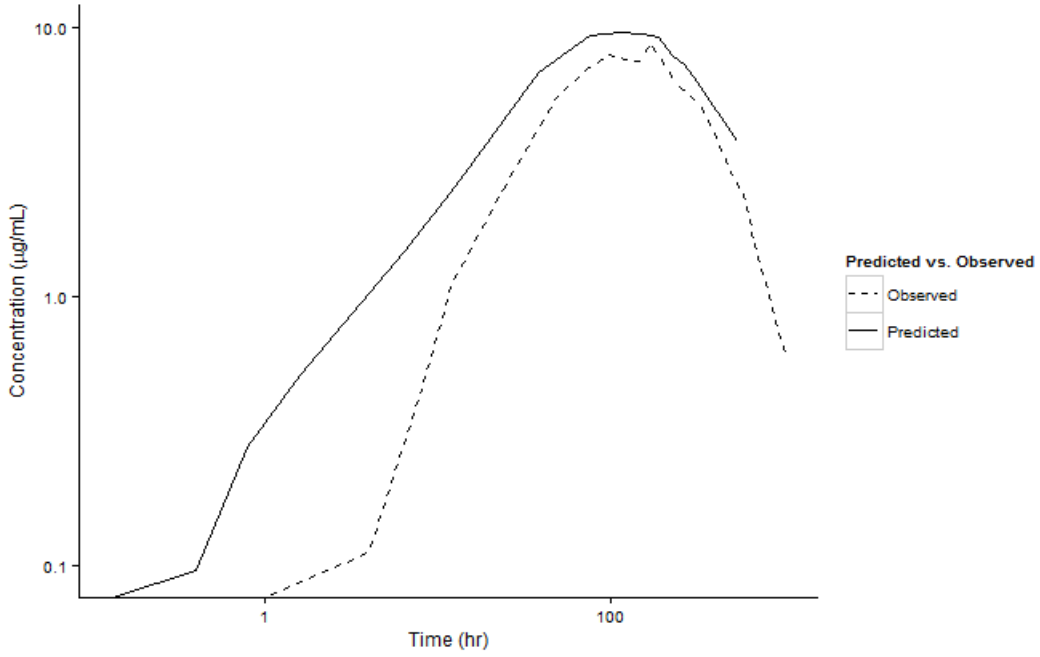
10.0
1.0
0.1
Concentration (µg/mL)
1
100
Time (hr)
Predicted vs. Observed
Observed
Predicted

Table 3.3: Prediction accuracy of non-compartmentally derived pharmacokinetic parameters obtained from Dedrick Plot scaling of the concentration vs. time profile in cynomologus monkeys to human scale for a single, subcutaneous dose of a pegylated peptide conjugate

Parameter	Units	Predicted (Human)	Observed (Human)	FE	Criteria Achieved
Tmax	hr	113.34	168.00	0.67	No
Cmax	µg/mL	9.61	8.65	1.10	Yes
AUC_{0-t}	µg·hr/mL	3539.14	3458.54	1.00	Yes
AUC_{0-inf}	µg·hr/mL	5099.09	3652.78	1.40	No
Vz/F	mL	3641.40	3916.80	0.93	Yes
CL/F	mL/hr	8.83	12.32	0.72	Yes
AUC%Extrap	%	30.59	5.32	NC	NA

CL/F: Extravascular clearance; Vz/F: Extravascular volume of distribution; AUC_{0-t}: Area under the curve to the last measurable time point; AUC_{0-inf}: Area under the curve extrapolated to infinity; AUC%Extrap: percent of the AUC extrapolated; Obs: Observed data; Pred: Predicted data; BW: Body weight; NC: Not calculated; NA: Not applicable

3.4 Discussion

Perhaps the most limiting characteristic of NCA when using this method to calculate PK parameters for macromolecules is the assumption that CL occurs via the sampling compartment. As briefly mentioned in Chapter 1, macromolecules are generally catabolized into smaller building blocks as opposed to biotransformed like small molecules.This breakdown can potentially occur within the interstitial space, lymphatic system and vasculature and thus the assumption of CL via the sampling compartment may be violated. Although macromolecules can be eliminated renally, due to molecular size restrictions, this is thought to be a minor pathway for most intact proteins and peptides. Pegylated compounds, such as the one studied in this thesis project, have been reported to be eliminated renally at approximately 0.1% of the glomerular filtration rate.(25;97) However, as with other pegylated therapeutic compounds, the likely pathway for the current peptide is likely a mixture of renal and non-renal extrahepatic processes which include uptake and digestion by immune cells and proteolytic breakdown of the intact pegylated peptide. (26) These processes may be occurring outside of the sampling compartment (e.g. in the interstitial space). Although compartmental PK modeling approaches, as employed in Chapter 4, have been reported in the literature for assessing prediction accuracy of single-species allometry,(62;63) Dong et al. employed NCA for estimating the PK parameters of macromolecules for the purpose of interspecies scaling of macromolecules with linear PK.(64) In spite of the obvious violation of a basic NCA assumption, such predictions yielded sufficiently reasonably accuracy for some of the tested compounds.

Another limitation of scaling NCA-derived parameters is the assumption of linear PK, which was only confirmed for the current evaluation upon receipt of the concentration data across five dose levels in humans. In the current evaluation, there was an *a priori* assumption of linear and stationary (lack of time-dependency) PK in NHPs prior to scaling. As only data following a single dose level (i.e. 7 mg/kg) in NHPs was available there was no way prove linearity *a priori*. However nonparametric superposition of the single SC dose was overlaid with the repeat-dose SC data and this suggested stationarity (superposition data not shown). Should evaluation of PK linearity yield a suggestion of non-linear CL/F, model-independent scaling of NCA-derived CL/F would not be reliable as clearance changes with exposure and no single clearance value could reliably be employed for translation from one species to another.

While the current analysis supported the *a priori* assumption for V_d and species body weight, an *a priori* allometric scaling factor assumption of 0.85 for CL did not achieve a reasonable FE (Table 3.2). As described in Table 3.1, NCA-derived extravascular CL/F is the quotient of dose and $AUC_{0\text{-}inf}$ where $AUC_{0\text{-}inf}$ is dependent on the ratio of the last observed concentration divided by the apparent terminal rate constant. For the NHP concentration data, the extrapolated area, which is defined as $1\text{-}(AUC_{0\text{-}t}/AUC_{0\text{-}inf})$ expressed as

a percentage, was approximately 30%. Large extrapolated areas can be associated with a poorly defined terminal elimination phase, and consequently greater uncertainty in the value for the λ and in any secondary parameters dependent on λ. As such, reliance on NCA-derived PK parameters for interspecies scaling may be limited by studies with different species and inconsistent or inequivalent sampling schedules used to define the PK.

With respect to the Dedrick plot analysis, based solely on the prediction accuracy of the main PK parameters, this method may be reasonable for scaling macromolecule PK, despite clearance processes not necessarily occurring via the sampling compartment. Oitate et. al. evaluated prediction accuracy of Dedrick plots for a group of IV administered mAbs with soluble and membrane bound targets using allometric exponents of 0.79 and 0.96 for CL, respectively and 1 for V_{ss}.(89;98) Of the twelve studied compounds, only five would have met the pre-defined ± 30% acceptance range of the current evaluation. It should be noted however that Oitate et al estimated CL and V_{ss} using an empiric 2-compartment model and not NCA. In contrast, using Dedrick plots and compartmental modeling for a group mAbs, Deng demonstrated good prediction accuracy of CL and V_{ss} when using exponents of 0.85 and 1 for CL and V_{ss}, respectively. In the current evaluation, Vz/F was used and not V_{ss}. NCA derived V_{ss} assumes that equilibrium between the sampling compartment and tissue compartments is achieved, and also that bioavailability is essentially complete. With extravascular administration, equilibrium cannot be assumed and thus the Vz/F method is used, which represents pseudo-equilibrium. However, the Vz parameter, as stated in Table 3.1, is dependent on λ being reliably estimated. Therefore some of the limitations in scaling NCA-derived clearance apply similarly to Vz/F.

In the current evaluation, upon graphical evaluation on the log scale (Figure 3.4b) there was an obvious difference between species in terms of the absorption profile which was further reflected by the FE in Tmax (Table 3.3). This observation however did not translate into a significant difference in the main exposure parameters. Although elimination or clearance of a drug can occur from the moment the drug enters the biological system, the duration of time from dosing to Tmax can be generally referred to as the absorption phase, where absorption processes predominate over elimination. For the scaled dataset, the time from dosing to Tmax represented approximately 21% or only $1/5^{th}$ of the total duration of sampling. As such, the duration where the over-prediction was most evident did not account for sufficient circulating drug exposure to result in an obvious difference in FE. Perhaps with a drug exhibiting a shorter elimination $T_{1/2}$, or a longer absorption phase relative to the elimination phase, where the absorption phase represents a larger proportion of the AUC, poorer prediction accuracy would be more evident.

Although the Tmax was under-predicted, Cmax was reasonably well predicted. This may be due to the fact that PPC has a similar V_d and F across the two evaluated species (i.e. monkeys and humans). The derived value for Vz/F was approximately 50 ml/kg regardless of species, which is consistent with plasma volume in mammals.(99)

The volume parameter derived was based on extravascular administration and thus Vz/F, meaning that the volume is dependent on the unknown bioavailability factor "F". The bioavailability after SC administration for this same compound in NHPs was previously estimated at approximately 90%.(66) Data following IV administration in humans was not available, however PBPK simulations (detailed later in this thesis) of IV administration in humans predicted a similar bioavailability in humans.(66) Thus the close agreement between predicted and observed exposure parameters may be partly a result of the similar bioavailability following SC administration across the two tested species. Bioavailability for SC administered macromolecules has been reported to vary widely across species.(18) As the SC bioavailability is unknown at the time of scaling from animals to humans for a FIH, the utility of empiric scaling methods are associated with a high degree of uncertainty.

3.5 Conclusion

Pharmacokinetic parameters derived using model-independent approaches may be scaled from NHP to humans assuming weight-based allometric functions with empiric scaling factors. However, prediction of parameters dependent on reliable estimation of an apparent elimination rate constant is subject to uncertainty. Moreover, this method must assume linear PK across a wide range of concentrations and near complete bioavailability if employed for extravascular administration. If the objective of scaling is to predict the time course of the drug after administration, it is not possible when simply relying on the mean value of a PK parameter such as CL. Combined, these factors limit the *a priori* utility of these computational methods in predicting the PK of a SC administered macromolecule. Dedrick plots, which are capable of predicting the time course of a drug after IV administration, do not account for interspecies physiologic and anatomic factors that influence the absorption of drugs. Although overall exposure parameters may have been reasonably predicted in the current evaluation, poor prediction in the absorption phase of the drug may limit the utility of this approach for other compounds. Moreover the unknown differences in SC bioavailability may limit the utility of empiric methods relative to more mechanistic, model-based methods.

CHAPTER 4: PHARMACOKINETIC TIME COURSE SCALING OF A SUBCUTANEOUSLY ADMINISTERED PEGYLATED PEPTIDE CONJUGATE FOR A FIRST-IN-HUMAN INVESTIGATION

The contents of Chapter 4 were initially published as an original contribution manuscript by the PhD candidate (Elliot Offman). The original manuscript has been edited and formatted according to thesis publication requirements. For reference purposes, the original publication is as follows:

Offman E, Edginton AN. Pharmacokinetic Time Course Scaling of a Subcutaneously Administered Pegylated Peptide Conjugate for a First-in-Human Investigation. *Eur J Drug Metab Pharmacokinet*. Feb. 2016 (epub ahead of print).

The PhD candidate conducted all the pertinent research, conducted all described analyses, created all tables, plots and figures and wrote the entire manuscript.

4.1 Introduction

As drug development transitions from preclinical to human phases, exposure and toxicology results obtained from preclinical animal species are used, in part, to inform the design of the first-in-human (FIH) investigation. For subcutaneously (SC) administered drugs, the time course, peak or maximum concentration (Cmax) and overall exposure as measured by area under the curve (AUC) in humans are important parameters for both study design (e.g. temporal placement of blood samples) and risk evaluation. Accurate prediction of the human pharmacokinetic profile can also mitigate the risk of protocol amendments associated with inadequate pharmacokinetic characterization and reduce the burden of interim pharmacokinetic evaluations throughout the FIH investigation.

Reports on the prediction of macromolecule pharmacokinetic in humans have largely focused on the monoclonal antibody (mAb) class and in particular, IgG type mAbs.(57;61-64;100) Moreover, many of these reports focus on prediction capacity of methods following intravenous administration (IV). Prediction methods rooted in allometric theory have demonstrated utility in predicting human clearance (CL) and volume of distribution (V_d) for mAbs as well as some other classes of macromolecules exhibiting linear pharmacokinetic. Whereas traditional allometric methods for scaling pharmacokinetic parameters suggest using data obtained from three or more species across a wide range of species body weight (82), single species methods employing non-human primates (NHP) have also yielded reasonable results for predicting drug exposure after IV administration of mAbs(63;63). These methods however rely on empirically selected scaling factors to explain the relationship between species body weight and a mean or averaged pharmacokinetic parameter value, obtained from a small number of animals. While scaling an averaged pharmacokinetic parameter such as CL may provide an estimation of overall systemic exposure of a drug, this method provides no information as to the time course after administration (e.g. temporal relationship between dose time and time to Cmax). Dedrick plots, which do allow for an evaluation of the time course have demonstrated reasonable prediction capacity for mAbs, however to date, the utility of this method following extravascular administration has not been reported, nor is expected, as this method does not consider absorption processes.(61)

More mechanistic, physiologically-based pharmacokinetic (PBPK) models incorporating lymphatic biodistribution facilitate prediction of the concentration vs. time profile after dosing and several authors have demonstrated the prediction capacity of these *in silico* approaches.(48;50;50;51;101;102) In most cases, however these reports are confined to the mAb class of drugs and following IV administration. More recently we reported the time course scaling of a pegylated peptide conjugate from NHP to humans after SC administration using a PBPK approach.(66)

While mAbs represent an important therapeutic class in pharmacologic treatment of disease, there remains a substantial collection of non-mAb macromolecules that exhibit varying biodistribution and CL properties. Cytokines, clotting factors, oligonucleotide derivatives and pegylated peptides represent important macromolecule classes in development for administration via the SC route. Although some reports suggest CL can be empirically scaled for these classes (56;58;103), reliable methods for predicting the time course of SC administered macromolecules are lacking, particularly for the non-mAb classes.

In order for empiric methods to be confidently employed in *a priori* extrapolation of pharmacokinetic following SC administration, the relationship between species size and drug absorption (if one indeed exists) requires further evaluation. Richter et. al. (18) highlighted challenges in predicting the SC absorption of macromolecules across species, noting interspecies differences in skin anatomy, local catabolism and bioavailability (F), which leads to difficulty in extrapolating across species. Woo and Jusko identified an inverse relationship between species body weight and first-order absorption rate constants following SC administration of erythropoietin to rats, monkeys and humans.(91) Similarly, Jolling et al. reported an inverse relationship for first-order absorption rate and body weight across several preclinical species in terms of a pegylated erythropoietin.(104) As such, and in spite of anatomical skin interspecies differences, there remains some potential to explain the relationship between species weight and absorption processes by an empiric relationship.

The objective of this work was to illustrate a model-based scaling workflow for *a priori* optimization of study design for a FIH trial of a SC administered macromolecule employing empiric scaling factors and a single non-clinical animal species.

4.2 Methods

4.2.1 Study Design

The exemplary molecule is a freely water soluble, linear PEG-40 conjugated peptide currently under clinical development, with a molecular weight of approximately 44 kDa. Drug concentration data was provided by the Sponsor of the research (withheld for commercial and proprietary purposes) following intravenous and SC administration in NHPs in a study not intended to meet compliance with good laboratory practices. . Nine non-naïve (previous exposure to other experimental treatments) female cynomologus NHP (mean weight 3.4 kg) were equally divided into three groups where each received either (1) a single 7 mg/kg intravenous dose (2) seven daily repeat SC 7 mg/kg doses or (3) a single 7 mg/kg SC dose. For SC doses, administration was to the back region.

The same drug was subsequently administered to a group of healthy male subjects participating in a FIH dose escalation study. Twenty healthy male subjects (weight range 60-80 kg) received a single SC dose of either 45 mg, 90 mg, 180 mg, 360 mg or 720 mg to the abdominal region (n=4 subjects per cohort). The human study was conducted under good clinical practice and according the ethical principles outlined in the Declaration of Helsinki.

4.2.2 Pharmacokinetic Sampling and Bioanalysis

The blood collection schedule for quantitation of the administered drug was identical for all 3 NHP groups with 0.5-1 mL collected from the femoral vein immediately prior to the dose and 0.25, 0.5, 1, 4, 8, 48, 72, 96, 120, 144, 168, 192, 216 and 336 hours after the dose (or after the first dose for the 7-day repeat-dose group). Following administration to humans, blood samples were collected from each subject immediately prior to the dose and 1,4,8,12,24,48,72,96,120,144,168,240,336,408,504,576,672 hours after the dose. Subjects participating in the highest dose cohort (720 mg) had an additional sample collected at 1008 hours post-dose. Serum was analyzed from both species employing an LC-MS/MS method with a limit of quantitation of 1 μg/mL for both NHP and human matrices.

4.2.3 Data Analysis and Population Pharmacokinetic Modeling

Prior to using the concentration data for model fitting and scaling, plotting of the raw data was performed followed by non-compartmental analysis (NCA) to obtain initial estimates of the relevant pharmacokinetic parameters. NCA and descriptive statistics were performed using Phoenix v 1.3 WinNonlin version 6.3® (Pharsight, a Certara Company) and Excel (Microsoft). Population pharmacokinetic model development was performed using Phoenix NLME version 1.2 (Pharsight, a Certara company) using the First-Order Conditional Estimation with Interaction algorithm. All plots presented in this manuscript were produced using R with ggplot2 package.(105;106) Concentrations below the limit of quantitation (BLQ) were set to missing in all instances.

4.2.4 Model Development

Prior to scaling to human exposure, concentration data obtained from NHPs was first fit to a compartmental pharmacokinetic model using population pharmacokinetic estimation methods. Between-subject (or inter-subject) variability was modeled assuming a log-normally distributed model as in Equation 4.1:

$$P_i = TVP^* \exp^{\eta_p} \quad (4.1)$$

Where P_i represents the pharmacokinetic structural parameter in the i^{th} individual and is equal to a typical value of the parameter (TVP, i.e. the population mean value) plus some deviation (η) from that population mean value. Each η_p was assumed to be log-normally distributed with a mean of 0 and a variance of ω^2.

Residual error was modeled as a proportional error model for the base model taking the form of Equation 4.2:

$$C_{OBS}=C_{PRED}*(1+\varepsilon) \quad (4.2)$$

Where C_{OBS} is the observed concentration, C_{PRED} is the population predicted value and ε is the deviation from the population predicted value and is assumed to be normally distributed with a mean of 0 and variance of σ^2.

Initially the IV route was modeled alone to obtain estimates for the systemic parameters of CL and V_d. Data was fit to 1-, 2- and 3-compartmental models.

4.2.5 Model Evaluation

The final model was selected based on individual data fit from diagnostic plots as well as the Akaike information criterion (AIC). Estimates for systemic parameters (i.e. CL and V_d) were then fixed to facilitate estimation of the parameters describing the absorption process for the SC route. Absorption processes tested included a single first-order absorption rate, dual first-order (with and without lag time) and mixed (zero- and first-order, with and without a lag-time on the first-order process). Based on the AIC and diagnostic plots the final model was selected for simultaneously fitting all available IV and SC data. As one group of NHP received daily dosing for 7 consecutive days, an inter-occasion effect was also tested for inclusion and influence on model diagnostics. Qualitative model discrimination was performed using visual predictive checks (VPC) where the model predicted median and 95^{th} percentile of the simulations are overlaid with the observed data and whereby adequate fit is judged when the observed data points fall largely within the 95^{th} percentile of the model predicted concentrations.

4.2.6 Model Based Scaling

Following final model development, human exposure following a single SC dose of drug was simulated by incorporating allometric scaling factors directly into the model prior to simulation. Population predicted typical values of structural parameters estimated in the NHP were multiplied by the weight-based ratio of human: monkey, raised to an exponent using the form in Equation 4.3:

$$TVP_{human} = TVP_{monkey} *(Weight_{human}/Weight_{monkey})^{exponent} \quad (4.3)$$

Prior to simulating the scaled concentrations for the human population, a population of 1000 unique individual body weights for humans was first simulated assuming a range of body weights corresponding to the human study.

Four scenarios were tested. The first scenario employed a fitting process, whereby the exponent was estimated in Phoenix NLME using the naïve pooled engine for the first dosing cohort (i.e. 45 mg) and then the estimated scaling factors were used to predict the concentrations for all 5 dosing cohorts simultaneously. Additional scenarios testing theoretical allometric scaling previously demonstrated to support allometric scaling of IV administered large molecules were applied to CL and V_d parameters. Scaling of the absorption processes assumed an inverse relationship with species body weight based on previous observations in SC administered macromolecules.

4.3 Results

4.3.1 Samples Included in the Analysis

In the NHP dataset, 144 samples were included in the population analysis of which 22 (15.2%) were noted as BLQ. For the human dataset, 355 samples were collected, of which 44 (12.3%) were noted as BLQ and four samples with no result available. As the database was not finalized, a demographic summary of the human male subjects who participated in the trial was not available at the time of writing.

4.3.2 Population Model Structure and Evaluation

The overall structural model for the pegylated peptide conjugate in monkeys was best described by a 2-compartment model with a single linear clearance process. The absorption aspect of the model, used to describe drug input into the body was best described with dual, parallel first-order processes, each rate associated with a fraction of the total absorbed dose and a lag-time associated with the slower of the two absorption processes (Figure 4.1). Initially a relative bioavailability term (Frel) was included; however the estimated Frel approached 1 suggesting essentially complete SC bioavailability, and therefore was dropped from the model with a corresponding improvement of the AIC. The amount of drug absorbed was then described as a fraction of the administered dose via each of the two first-order rate processes.

Figure 4.1: Structural population pharmacokinetic model for a pegylated peptide conjugate described as a 2-compartment model with parallel first-order absorption processes and linear elimination. Aa1 and Aa2 represent the mass of drug delivered to the SC tissue for absorption via the two independent absorption processes; Ka1, Ka2 are the first-order absorption rate constants; tlag represents the lag time associated with the first absorption compartment; F1 and 1-F1 represent the fraction of the absorbed dose associated with the respective absorption compartments; Vd, CL, Vd2, CL2 are the volume and clearance associated with the central and distributional compartments. Vd volume of distribution of the central compartment, Vd2 distributional compartment volume, CL clearance from the central compartment, CL2 distributional clearance, Ka1 absorption rate constant 1, Ka2 absorption rate constant 2, F1 and (1 - F1) are the relative proportions of absorbed dose via each of the absorption rates

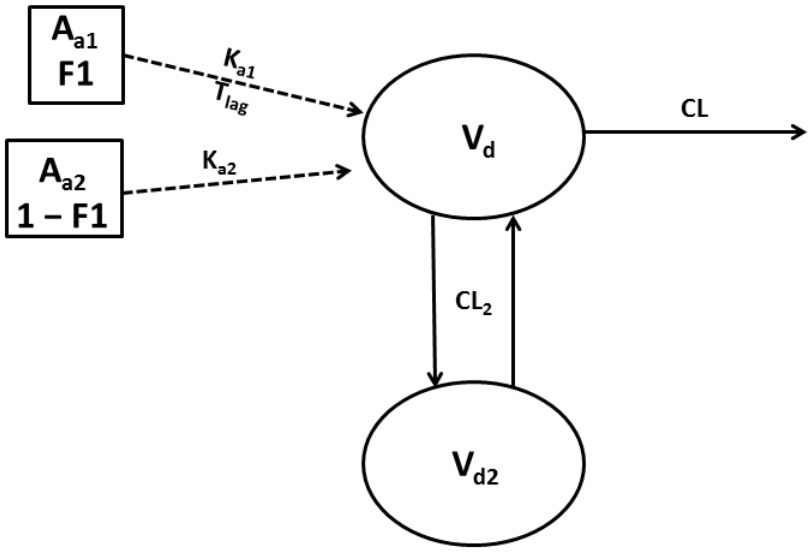

Final model parameters were estimated with good precision (Table 4.1). Random effects were included for both the central volume and clearance process. Inclusion of an interoccassion variability parameter (IOV) on the bioavailability parameter did not improve the model diagnostics and therefore was removed from the model. The impact of IOV on CL or V_d was not assessed as it was deemed unlikely that either parameter was time-dependent based on a comparison of single vs. repeat daily doses at the 7 mg/kg dose level (data not shown). As data for only a single dose level was available to test, it was assumed that non-linearity in either absorption or elimination processes could not be properly assessed. As the NHP were of similar age and body weight, no specific anthropometric covariates were tested in this analysis. Diagnostic plots and visual predictive checks (Figures 4.2 and 4.3) suggested reasonable model fit. Consequently the model was deemed appropriate for the model-based allometric scaling step.

Table 4.1: Population pharmacokinetic model derived parameter estimates for a pegylated peptide conjugate in cynomologus monkeys following simultaneous estimation of concentration data obtained after administration of single 7 mg/kg intravenous and SC doses and daily SC doses for seven days.

Parameter	Estimate	CV%
V_d (L)	0.11	8.77
CL (L/hr)	0.00059	7.84
V_{d2} (L/hr)	0.043	25.85
CL_2 (L/hr)	0.00092	46.70
K_{a1} (hr^{-1})	0.035	17.00
F1	0.87	3.10
K_{a2} (hr^{-1})	0.23	26.31
Lag-time (hr)	6.34	8.08
Residual Error	15	7.10

SC subcutaneous, V_d volume of distribution of the central compartment, V_{d2} distributional compartment volume, CL clearance from the central compartment, CL_2 distributional clearance, K_{a1} absorption rate constant 1, K_{a2} absorption rate constant 2, F1 relative proportion of absorbed dose, CV% coefficient of variation/relative standard error of the parameter estimate

Figure 4.2a: Model diagnostic plots for the final population pharmacokinetic model describing a single 7 mg/kg dose administered intravenously and single and multiple 7 mg/kg doses administered subcutaneously to cynomologus monkeys. Closed circles represent the observed vs. population predicted concentrations and the dashed line is the line of identity.

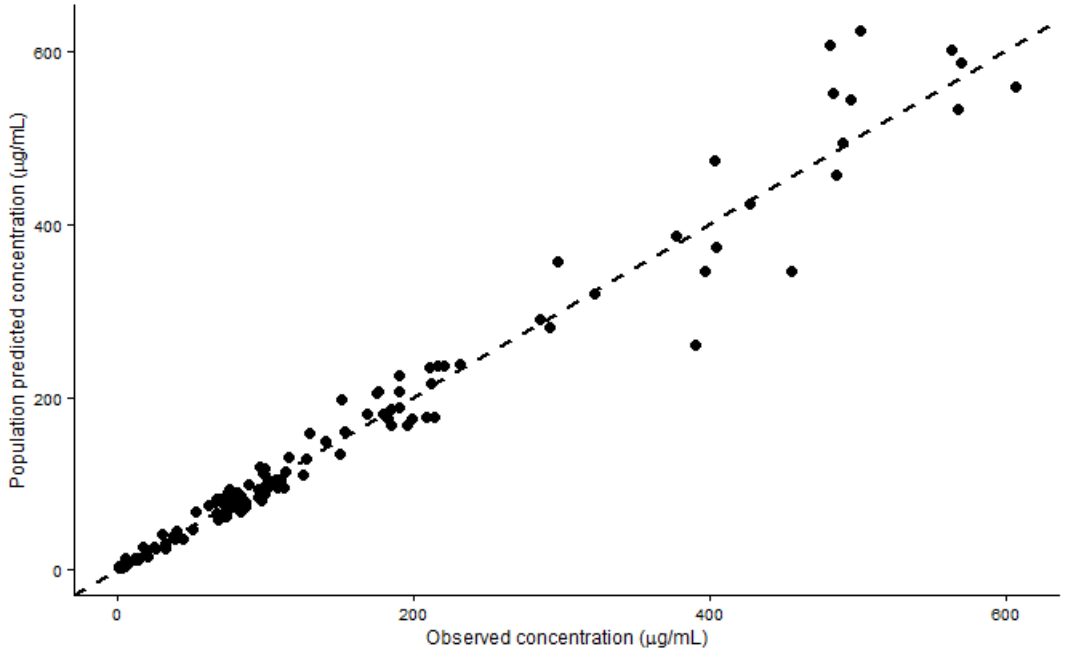

Figure 4.2b: Model diagnostic plots for the final population pharmacokinetic model describing a single 7 mg/kg dose administered intravenously and single and multiple 7 mg/kg doses administered subcutaneously to cynomologus NHPs. Closed circles represent the conditional weighted residuals vs. predicted concentrations with solid line as the loess fit.

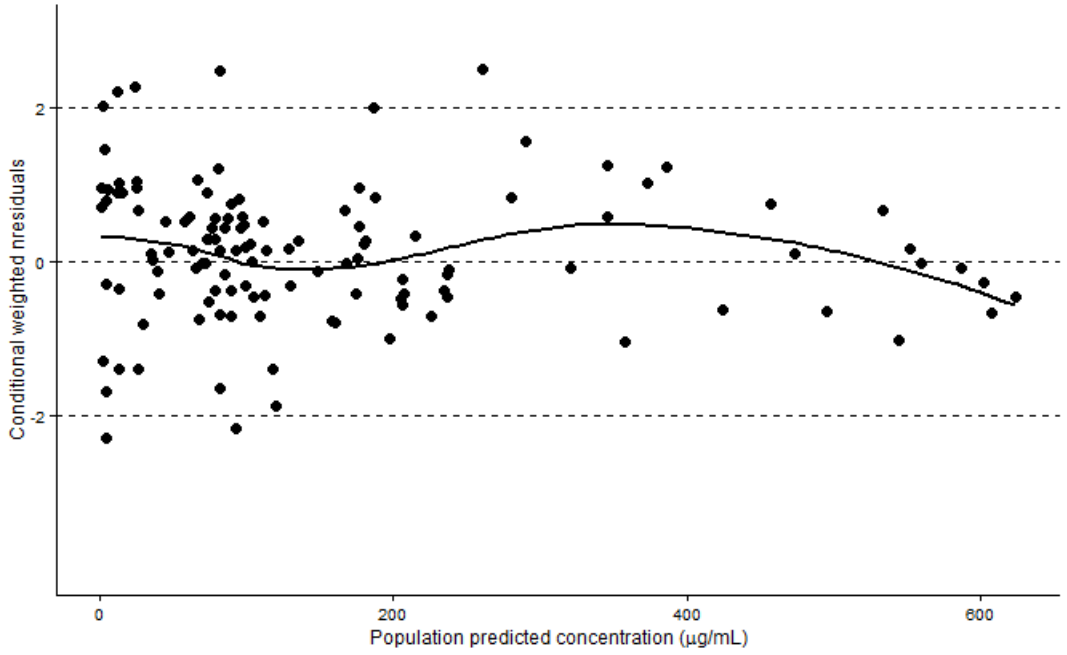

Figure 4.3: 5th, 50th and 95th percentile of simulated concentrations (solid lines) vs. observed concentrations (solid circles) in cynomologus monkeys following a single intravenous dose (top panel), seven daily repeated subcutaneous doses (middle panel) and a single subcutaneous dose (bottom panel). For single dose IV and SC groups, pharmacokinetic samples were drawn sequentially over a 336 hour post-dose period. For the seven daily repeat dose group, pharmacokinetic samples were drawn at 1, 4 and 8 hours after the first dose, then every 24 hours from days 2-9 with an additional sample drawn on day 15. IV intravenous, SC subcutaneous

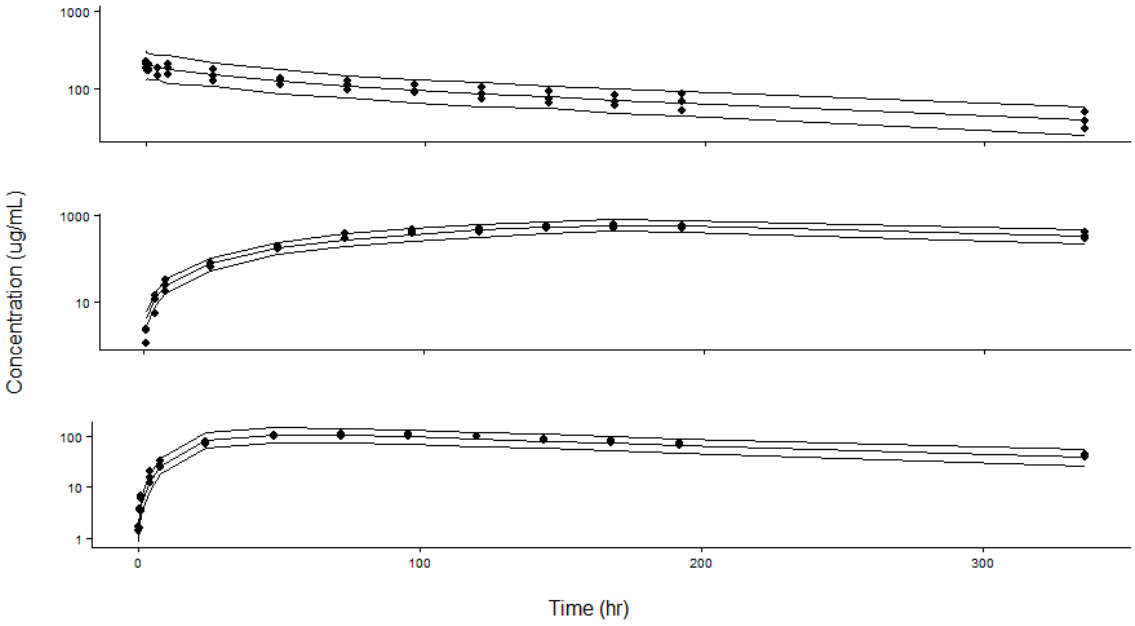

4.3.3 Model Based Scaling

Figures 4.4a and 4.4b graphically display the prediction accuracy of the four tested scenarios. Scenarios are presented in both linear-x/linear-y and log-x/log-y scales to allow for appreciation of prediction capacity in the various portions of the concentration vs. time profile. Specifically, in Figure 4.4a, the linear-x/linear-y scale allows the best appreciation of the prediction accuracy of the peak (Cmax), whereas in contrast, the log-x/log-y curve facilitates the best appreciation of prediction accuracy for the early time points critical in evaluating the full absorption phase. Overall, absorption, peak and elimination phases of the curve were best described in Scenario 3, which assumed empiric exponents of 1 on clearance and volume parameters and -0.4 on absorption parameters. Estimation of the scaling factor exponents in the first dosing cohort (Scenario 1) resulted in a reasonable prediction of the absorption phase across all 5 dosing cohorts with the exception of the initial 10-20 hours post-dose. Although not obvious from the log-log plot, linear scale plots suggest Cmax was under predicted in this case, which was particularly evident in the highest dose cohort. Assuming empiric scaling factors of 0.85, 1 and -0.4 (Scenario 2) for CL did not appreciably alter the absorption phase predictions however over-estimated the elimination phase of the curve, whereas assuming an exponent of 1 resulted in a poor prediction of the absorption and peak phases of the profiles.

Figure 4.4a (linear-x/linear-y) and 4b (log-x/log-y): Experimentally obtained concentrations across 5 dose cohorts in humans (symbols) and 5th-95th model scaled simulated concentrations (shaded region) for each corresponding dose level. Scenario 1: Scaling factors fit on lowest dose cohort (45 mg) and fitted exponents applied to simulations for all subsequent dosing cohorts; Scenario 2:exponent of 1 on Vd & Vd2; 0.85 on CL and CL2; -0.4 on Ka1 and Ka2; Scenario 3:exponent of 1 on Vd & Vd2, CL and CL2; -0.4 on Ka1 and Ka2; Scenario 4: assumes an exponent of 1 on all model parameters. Vd volume of distribution of the central compartment, Vd2 distributional compartment volume, CL clearance from the central compartment, CL2 distributional clearance, Ka1 absorption rate constant 1, Ka2 absorption rate constant 2

Figure 4.4a

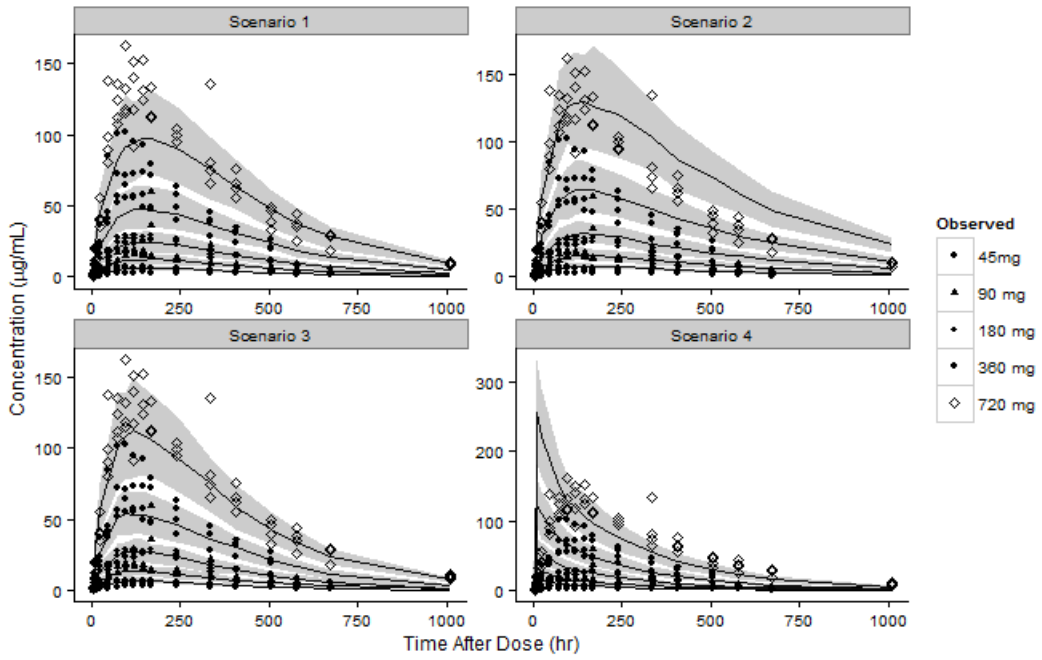

Figure 4.4b

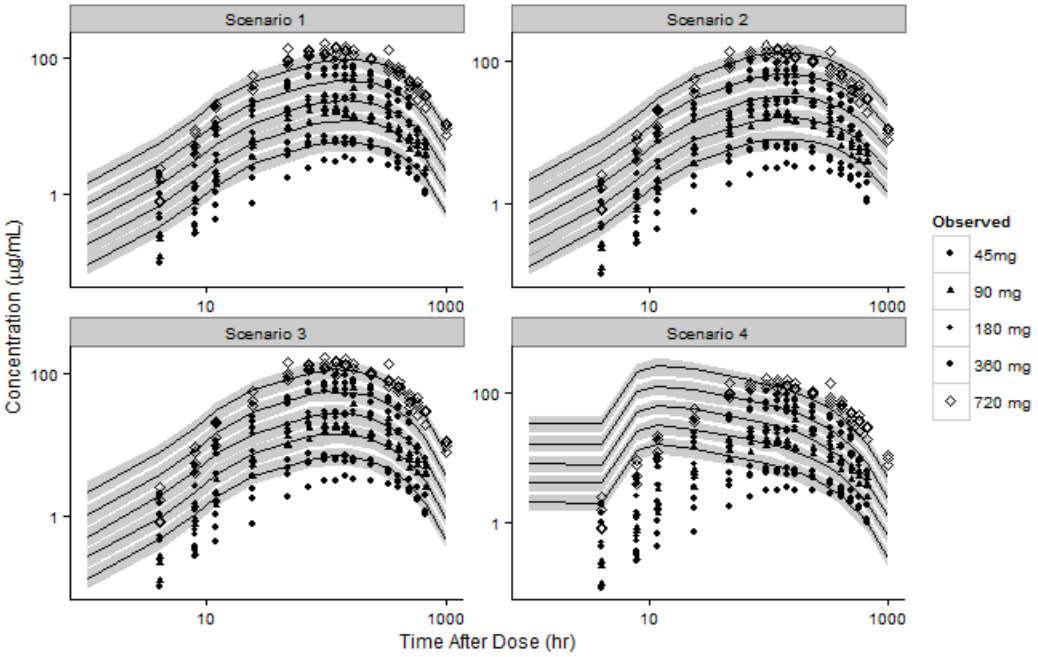
Scenario 1
Scenario 2
Scenario 3
Scenario 4
100
1
10
1000
Concentration (µg/mL)
Time After Dose (hr)
Observed
45mg
90 mg
180 mg
360 mg
720 mg

4.4 Discussion

Model-based approaches to support extrapolation of pharmacokinetic exposure is an important element of ensuring appropriate dose selection for testing in early human trials. Population pharmacokinetic model-based scaling may be particularly useful in estimating the pharmacokinetic parameters in animal studies where sparse sampling and a small number of individual animals is studied. Incorporating allometric scaling factors into a population pharmacokinetic model is a fairly commonplace methodology for describing pharmacokinetic within-species size relationships in adults and children. (107;108) However these evaluations have tended to be retrospective and interpolative in nature, describing the relationship among data from a range of individuals.

Although retrospective in nature, the current investigation considers an extrapolative workflow which has application in the prospective prediction of the pharmacokinetic time course of a SC administered macromolecule to guide study design for an FIH. We employed both fitted and empiric approaches for scaling exponents used to relate body weight to population model pharmacokinetic parameters to evaluate whether empiric exponents would have potential value in an a priori scenario.

There are challenges in extrapolating the SC pharmacokinetic from animals to humans particularly due to interspecies difference in the skin anatomy and physiology and potential differences in SC bioavailability where the drug may be broken down at the site of administration and/or prior to the initial appearance in the venous circulation. Bioavailability following extravascular administration of macromolecules may be, in part, a function of the lymphatic transit time.(109)

In the current investigation, the fraction of the absorbed dose (F), which is a surrogate for extravascular bioavailability, was assumed to scale directly across species. This assumption removed a significant level of complexity from the scaling step although, based on historical evaluation, this assumption would be unlikely to apply to all species and all macromolecules, (18) However for the current investigation, given that SC bioavailability in NHPs was essentially complete, human SC bioavailability was similarly assumed. Additional considerations in the model scaling step may be required to account for potential differences in SC bioavailability for different compounds where the bioavailability varies substantially across species.

The present investigation supports previously published reports where single-species NHP-derived macromolecule clearance and volume parameters were scaled with reasonable error to human values based on body weight raised to some empiric scaling factor. Successful predictions for macromolecules tend to be positive, ranging from 0.75 to 1 for clearance and approximately proportional to body weight for volume

parameters.(61-64) In contrast, the rate of input into the systemic circulation suggests an inverse relationship between species body weight and ka. Although few reports have examined this relationship our observations are also consistent in direction and magnitude with the scaling factor estimate across rat, NHP and humans for erythropoietin.(91) Jolling et. al. observed a similar relationship for a pegylated erythropoietin, where the first-order absorption rate constant scaled across several preclinical species and humans with an exponent of -0.149.(104) Neither physiologic nor anatomic explanations were provided in previous reports for an inverse relationship between body weight and absorption rate following SC administration. Absorption of large molecules from the SC space into the lymphatics is influenced by lymph flow.(18;109;110) Consequently, interspecies differences in lymph flow, particularly as it pertains to skin lymph flow, may underlie the slower absorption from the SC into the systemic circulation in humans relative to smaller mammalian species. Recently, using the same concentration data for both monkey and human as in the current manuscript, we developed a PBPK model in NHPs which was then demonstrated to scale the concentration vs. time profile to humans across a range of doses. In order to achieve line shape consistency with the simulated and observed data, a slower skin lymph flow was required in humans relative to NHPs.(66) A striated muscle, the panniculus carnosus, is located in the hypodermis of many preclinical animal species. This muscle is absent in humans and in higher order NHPs and has been suggested to at least in part, influence interspecies differences in drug absorption from the SC space.(18) Humans and furless animals also have fibrous bands that anchor the subcutaneous layer of skin and may reduce compliance and elasticity of the skin tissue, potentially resulting in slower transit from the SC space into the lymphatic transport system.(36) Although empiric in nature, an inverse mathematical expression relating absorption rate to species body weight seems to explain the observations in the current investigation and explains similar observations by others.(91;104) The precise numerical value for this inverse scaling factor may differ depending on the molecule and the number of different species included in the exponent estimation step. Pegylated and non-pegylated erythropoietin have molecular weights of 35 and 30 kDa, respectively, and yet estimated exponents were -0.149 and -0.349, respectively.(91;104;111) In these investigations however, several preclinical species including rat, rabbit, monkey and dog were included in the model parameter estimation process. Mager and colleagues independently fit recombinant human interferon β-1a to a target-mediated drug disposition model with first-order absorption in both human and rhesus monkeys.(41;42) Slow first-order rate constants of 0.104 hr^{-1} and 0.0414 hr^{-1} were estimated in monkeys and humans, respectively. Based on Equation (1) in the current manuscript, and considering an average body weight of approximately 3 kg for the monkeys and 70 kg for humans, a scaling factor exponent of -0.3 can explain the observed relationship in that publication.(91)

It should also be noted that the scaling factor obtained by fitting the first dosing cohort (-0.49, Table 4.2) in the human study was very close to the empiric value of -0.4 with only a modest improvement in the objective function for the fitted value. For future prospective extrapolation, a precise negative exponent cannot yet be proposed which would apply to all macromolecules. However in the context of predicting the exposure vs. time profile in humans based on a single NHP species, an inverse relationship between body weight and first-order rate constants appear to scale reasonably well within a range of -0.3 to -0.5. This relationship may be rooted in anatomical and physiologic interspecies differences such as skin lymph flow.

Table 4.2: Model-based scaling scenarios and corresponding prediction objective functions.

Scenario	Exponent Source	Parameter	Exponent Used in Simulation	Objective Function
(1)	Fitted Scaling Exponent fit from 1st human dose cohort	CL, CL_2	1.42	40.06
		V_d, V_{d2}	1.28	
		K_{a1}, K_{a2}	-0.49	
(2)	Empiric Scaling Exponent	CL, CL_2	0.85	74.12
		V_d, V_{d2}	1	
		K_{a1}, K_{a2}	-0.4	
(3)	Empiric Scaling Exponent	CL, CL_2	1	55.08
		V_d, V_{d2}	1	
		K_{a1}, K_{a2}	-0.4	
(4)	Empiric Scaling Exponent	CL, CL_2	1	497.11
		V, V2	1	
		Ka1, Ka2	1	

V_d volume of distribution of the central compartment, V_{d2} distributional compartment volume, CL clearance from the central compartment, CL_2 distributional clearance, K_{a1} absorption rate constant 1, K_{a2} absorption rate constant 2

4.1 Conclusion

In conclusion, predicting the full time course of a macromolecule following SC administration for a FIH trial first requires estimation of absorption processes in preclinical development. Simulations suggest that an inverse relationship exists between species body weight and first-order absorption processes. An *a priori* workflow integrating empirically selected scaling factors into a population pharmacokinetic model may provide for an adequate prediction of the time course for pegylated macromolecules exhibiting linear pharmacokinetic with essentially complete bioavailability.

CHAPTER 5: A PBPK WORKFLOW FOR FIRST-IN-HUMAN DOSE SELECTION OF A SUBCUTANEOUSLY ADMINISTERED PEGYLATED PEPTIDE

The contents of Chapter 5 were initially published as an original contribution manuscript by the PhD. candidate (Elliot Offman). The original manuscript has been edited and formatted according to thesis publication requirements. For reference purposes, the original publication is as follows:

Offman E, Edginton AN. A PBPK workflow for first-in-human dose selection of a subcutaneously administered pegylated peptide. *J Pharmacokinet Pharmacodyn*. 2015; 42(2):135-50

The PhD candidate conducted all the pertinent research, conducted all described analyses, created all tables, plots and figures and wrote the entire manuscript.

5.1 Background

Predicting the time course of drugs in humans from animal species following subcutaneous (SC) administration has been challenging. No single method has been demonstrated to be superior or even consistent in terms of prediction accuracy. Furthermore, none appear to be influenced by whether the compound is a peptide/protein or a smaller synthetic compound. This is in contrast to the intravenous (IV) route of protein administration, where human pharmacokinetics (PK) can be reasonably predicted within <2-fold based on single-species simplified allometric techniques using non-human primate data.(55;61;63) The PK following SC administration is complicated by the absorption into the systemic circulation via lymphatic and vascular pathways. Supersaxo et al (17) initially identified that interferon 2a appeared in significant mass when cannulating the efferent popliteal lymphatic duct in sheep following SC administration whereas lymphatic presence of drug was minimal when administered via the IV or intradermal route. Later, Supersaxo (16) reported that compounds with molecular weight (MW) less than 1 kDa exhibited little lymphatic absorption with increasing tendency for lymphatic transport as the MW increased above 16 kDa. These findings can potentially be extended to larger proteins and other mammalian species. Recently it has been reported that trastuzumab (15) was preferentially absorbed via the lymphatic route following SC administration in rats and Wang (19) has reported pegylated erythropoetin and inteferon exhibited significant lymphatic uptake from the SC space in rats and dogs. Richter (18) more recently reported that molecules with diameters less than 10 nm are capable of diffusing from the SC space into vasculature. However, molecules with diameters greater than 10 nm have a preferential and progressively greater proportion of lymphatic uptake with increases in size. The latter observations are consistent with a 2-pore theory where molecules of a certain size threshold become too large to diffuse from the SC space into the vasculature.(10;112)

There is value in developing mechanistic methods for not only predicting the time profile after SC administration, but also the SC bioavailability, for the purposes of scaling from animals to humans. Conventional allometric scaling of new chemical entities (NCE) has historically relied on evaluation of mean clearance (CL) values obtained in one or more preclinical species as a means of estimating exposure and dose selection for first-in-human (FIH)/single-ascending dose (SAD) studies. This approach provides little information on the time course of drug exposure after administration which may impact the safety and tolerability of the NCE. Moreover, allometric techniques employing clearance scaling are further confounded by non-linear PK and bioavailability (for extravascular administration). The SC exposure time course of therapeutic proteins has been particularly challenging to predict in light of the interspecies differences in skin anatomy and physiology as well as a general lack of understanding of factors impacting SC bioavailability differences.

Work by Zhao (109) and Kagan (113) have focused on the more mechanistic determinants of SC bioavailability, considering site of administration, volume of the injection site space and, in the case of mAbs, binding to the Brambell receptor (FcRN) at the site of injection. Such reports have either used compartmental modeling to describe the absorption process or employed a hybrid compartmental-physiologic model. Although predictions of observed data may have been successful, these methods are largely top down approaches. Meaning, the models are predicated on the assumption of having data describing the drug absorption to obtain an absorption rate constant and bioavailability fraction (113) which cannot be assumed to scale across species.

In most cases, the ultimate goal of studying the PK of a macromolecule is to translate findings to humans. There is no agreement on which species represents the best model for projecting the SC time course of therapeutic macromolecules, if one even exists. For SC administration, investigators have argued that the subcutaneous tissue of monkeys is dissimilar to human and have proposed the use of the minipig.(114) However, given the impact of target mediated drug disposition (TMDD), it is questionable as to whether the benefit of an animal model being employed due to similarity in skin anatomy overrides the overall benefit of using a species more inclined to express the drugs intended target. Regardless, where monkeys are employed, typically small sample sizes are used, thus limiting the interpretation of PK data, especially when variable.

Physiologically-based pharmacokinetic (PBPK) approaches have demonstrated utility in predicting the time-course of therapeutic proteins when administered intravenously.(47;48;50;51) However there is little published data supporting its success with SC administration in any species, and less evidence for scaling of SC bioavailability from an animal species to human using this method. Given the appetite for therapeutic macromolecules to be administered via the SC route there is particular utility in the application of PBPK modeling in the planning and conduct of FIH/SAD studies. This modeling technique allows for the results of non-clinical work to be extrapolated to humans based on interspecies differences in anatomy and physiology without necessarily testing an IV formulation in humans. Herein we present a workflow for translating single-dose IV and SC PK from a single non-human primate species to the human scale using a PBPK modeling approach for the purposes of planning and refining a FIH dose selection.

5.2 Methods

The workflow is comprised of 4 stages:

1) Simulation of the primate IV PK and optimization of the model parameters
2) Simulation of the primate SC PK to verify the model can adequately predict concentrations following SC administration
3) Scale up of the model to humans and simulation of the PK following SC administration under human clinical trial conditions
4) Optimize human model and simulate future dose cohorts

5.2.1 Observed Datasets

Observed data was obtained for 3 non-naïve (previous exposure to other experimental treatments) female cynomolgus monkeys (mean weight 3.4 kg), each receiving a single 7 mg/kg intravenous dose of a proprietary (name and target withheld for commercial proprietary purposes) freely water soluble, linear PEG-40 conjugated peptide, with a molecular weight of approximately 44 kDa. Drug was infused as a bolus in 5% dextrose in water. Serial blood samples were quantified for the pegylated conjugate at pre-dose and post-dose at 5, 15, 30 min, 1, 4, and 8 hours on Day 1; 0 hrs on Days 2-9 and Day 15 (360 hours post-dose). An additional 3 cynomolgus monkeys were administered the same dose via the SC route to the back region with the same sampling schedule.

As part of a single-dose escalation study in healthy volunteers, concentration data was provided by the Sponsor for the same peptide measured in 4 males (weight range 60-80 kg) receiving a single, SC fixed 45 mg dose into the abdominal region with sampling up until approximately 504 hours. This initial dose level was used to test the human model assumptions and two subsequent dose levels (90 mg and 180 mg) were used to confirm prediction potential.

A graphical depiction of a typical FIH combined SAD and multiple-ascending dose (MAD) and the overaching workflow in the context of a FIH program are presented in Figure 5.1.

Figure 5.1: Graphical depiction (top panel) of a first-in-human (FIH) combined single-ascending dose (SAD) /multiple-ascending dose (MAD) program in healthy volunteers (HV). Proposed workflow (bottom panel) for incorporating the PBPK model process for a FIH study.

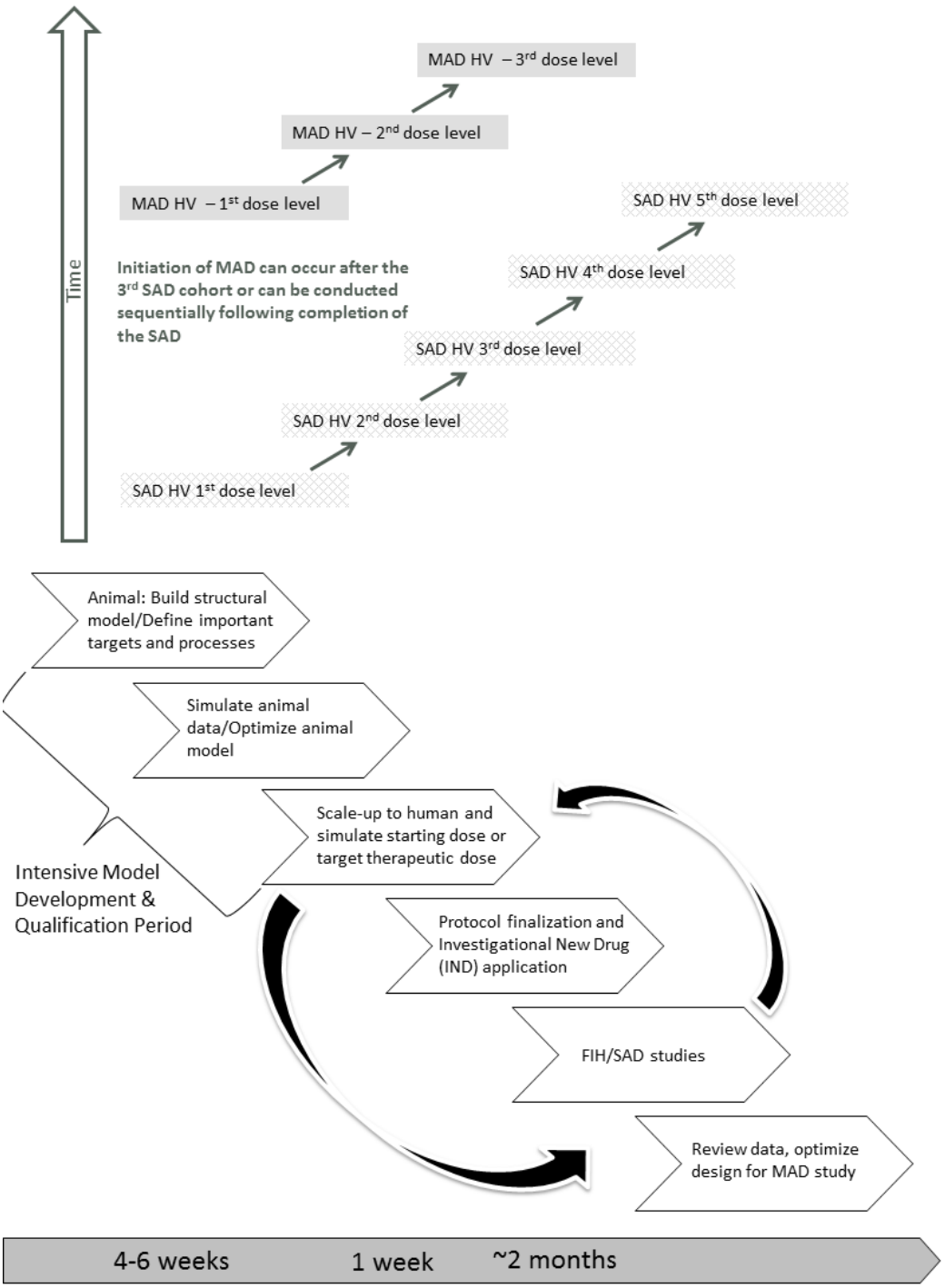

Non-compartmental analysis (NCA) was performed (Phoenix WinNonlin v 6.3, Pharsight) on the primate IV and SC data to obtain initial estimates of the PK parameters as well as to calculate absolute bioavailability of the SC route.

5.2.2 Development of the Base PBPK Model for IV Administration in Cynomolgus Monkeys

For ease of visualization of the simulated vs. observed IV & SC data, model building was performed using Berkeley Madonna (v8.3.1.8; http://www.berkeleymadonna.com). The model was then recoded in Pharsight Modeling Language (PML) for executing within the Phoenix NLME platform (v1.2, Certara). Select mass balance equations are presented in Appendix 5.1 and the full code for Berkley Madonna is provided in the Supplementary material section. All concentration vs. time profile figures were produced in R.(105)

5.2.3 Model Structure

The proposed overall and sub-compartment structures are based in part on the PBPK platform developed previously by Shah and Betts (50) and is depicted graphically in Figures 5.2a and 5.2b. The overall structure consists of a unique compartment for each of the venous and arterial circulation, a lymph node compartment and 15 individual organs where each organ consists of a vascular and interstitial sub-compartment. For IV administration, the drug is administered directly into the venous supply and is carried to the lung at a rate equal to hematocrit-corrected cardiac output. Once in the lung vasculature, a fraction of the drug is convectively transported from the plasma to the interstitial compartment; a process partially defined by a vascular reflection coefficient (σ_v). Drug in interstitium then transits into the lymphatic supply which is partially defined by a lymphatic reflection coefficient (σ_{isf}). The remaining drug is carried into the arterial supply for distribution into the remaining organs according to the plasma flow rate supplying each organ. Plasma flow from the intestines, pancreas and spleen empty into the liver. In each organ, convective transport from plasma to interstitial space and ultimately to lymph occurs, with lymph transit eventually returning drug to the venous system. The skin interstitial compartment is sub-divided further into a depot and residual space to account for SC administration. The volume of the depot interstitial compartment was set at the actual volume administered for each of the species tested, based on the assumption that as fluid is injected into the SC space expansion to accommodate the volume would occur due to the nature of the extracellular matrix components in the SC space. The proportion of lymph flow assigned to skin and depot interstitium was assumed to be proportional to the respective volumes relative to the total skin interstitial space.

Figure 5.2a: Structure of a whole-body PBPK platform (adapted from Shah & Betts 2012). Solid black arrows indicate plasma flow. Dark grey dashed arrows indicate lymphatic transport. S. Int. and L. Int. represent small and large intestines. Each organ compartment includes lymphatic flow emptying from the organ into the lymph node. For IV administration, drug is administered into the "Venous Supply". For SC administration, drug is administered into the "Skin Compartment" interstitium (see Figure 5.2b)

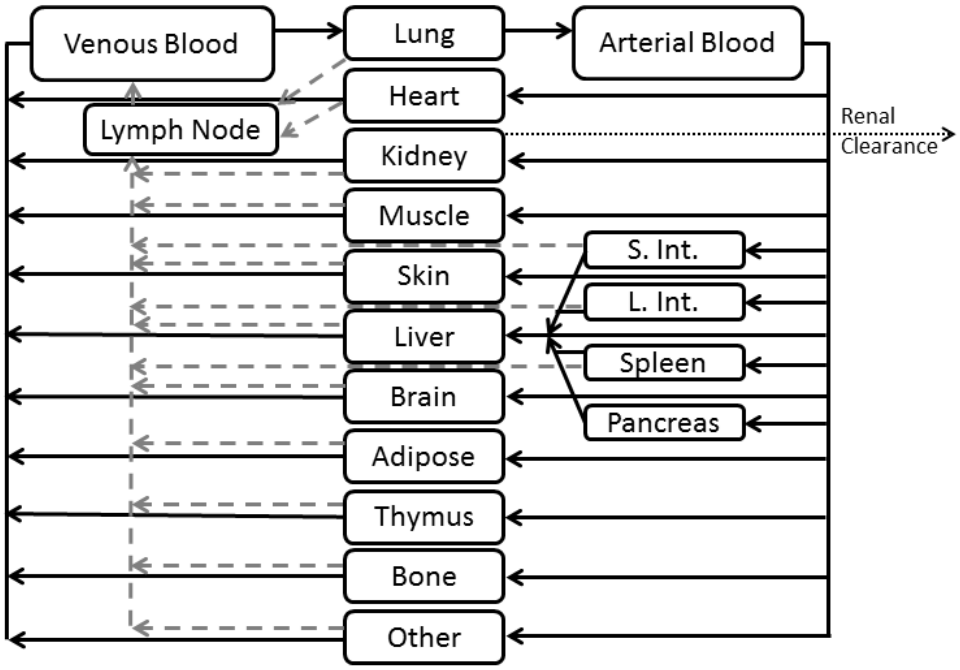

Figure 5.2b: Structure of the proposed subcompartment model. Drug enters the organ plasma vascular space via the arterial circulation. Q and L refer to blood flow and lymph flow. The symbol σ refers to a reflection coefficient, where σ v is the vascular reflection coefficient and σ isf is the interstitial reflection coefficient. For SC administration, drug is administered directly into a fraction of the skin interstitial space.

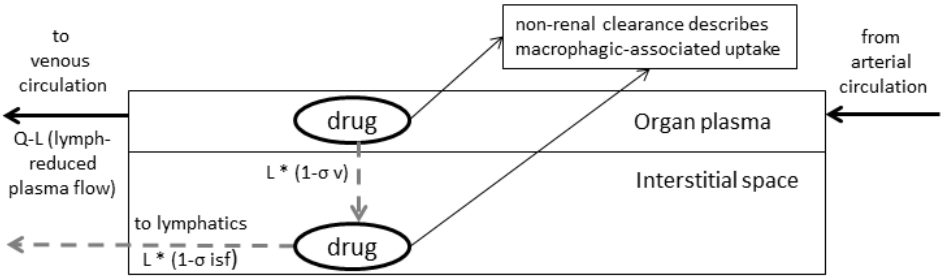

Organ volumes and blood flow rates for both primates and humans were obtained from the BioDmet database (http://pdsl.research.ge.com/BioDMET/).(115) The fraction vascular (Fvv) and interstitial (Fvic) were obtained from Kawai et al (116) and hematocrit values from Davies and Morris.(99) A listing of the anatomical and physiological values can be found in Appendix 5.2. Lymphatic flow (L) was set at a fraction of blood flow (i.e. where blood flow was divided by 500 to obtain the lymph flow) to each organ as per Swartz.(21) The vascular reflection coefficients for each organ (σ_v) were taken from Shah and Betts (50) however, each organ σ_v was scaled to a single scaling factor ($\sigma_{v,sf}$) to reduce the number of organ σ_v parameters needed to be optimized to 1. Lymphatic reflection coefficients (σ_{isf}) were set at 0.2 based on Garg and Balthasar.(102)

Although the clearance mechanism has not been formally evaluated for this pegylated conjugate, clearance is believed to occur via a renal and a non-renal pathway. A renal clearance process was incorporated into the kidney vascular compartment. Although the drug is considered a macromolecule, evidence suggests that high molecular weight pegylated compounds can be cleared renally at about 0.1% of the glomerular filtration rate (GFR).(25;97) Consequently, the fraction of GFR (FGFR) responsible for renal clearance was set at 0.1% of GFR. The value of GFR in cynomolgus monkeys was taken as the midpoint of previously reported values i.e. 2.41-2.61 mL/min/kg.(117) A non-renal clearance was also included to account for opsonisation whereby the drug-target complex acts as a signal for phagocytosis by macrophages. A non-specific, non-renal clearance (NRCL) was incorporated into the model within each organ vascular and

interstitial compartment. According to Gordon (118) macrophages do not enter efferent lymphatics or the thoracic duct and therefore the clearance process was not included in the lymphatic compartment. From the NCA of the primate IV bolus data, total clearance was estimated to be approximately 0.181 mL/hr/kg. Subtracting the renal component (i.e. 0.1 % of GFR, i.e. 0.12 mL/hr/kg) resulted in an initial estimated NRCL of 0.061 ml/hr/kg. NRCL was assumed to be uniform in each compartment where macrophagic-mediated clearance occurs and the total NRCL was then partitioned in a manner proportional to the volume of the compartment.

5.2.4 Primate IV model optimization

Parameters associated with the greatest uncertainty were estimated by fitting the observed concentration of drug in plasma using NLME assuming a proportional residual error model (Equation 5.1):

$$C_{observed}=C\bullet(1+\varepsilon) \qquad (5.1)$$

where $C_{observed}$ is the observed concentration, C is the fitted predicted value and ε is the deviation from the predicted value and is assumed to be normally distributed with a mean of 0 and variance of σ^2.

Due to the uncertainty in the parameters of L, σ_{isf}, $\sigma_{v,sf}$, and NRCL, these parameters were initially fit with all other parameters fixed at anatomical/physiological values. However due to the sparseness of the data and potential identifiability issues, precision could not be estimated for each of the four listed parameters. Of these four, the parameters assumed to have the greatest uncertainty that could be fitted with precision, (i.e. $\sigma_{v,sf}$ and NRCL) were the only two parameters allowed to fit in the initial IV model development step with all other parameters being fixed at literature or experimentally obtained values as described in Appendix 5.2 and Table 5.1.

Table 5.1: Parameter estimates following a single IV administration (7 mg/kg) to cynomologus monkeys and scaling of the model to humans for SC administration

Parameter/Species (units)	Definition	Estimate	Fitted	CV%
Cynomologus Monkey				
$\sigma_{v,sf}$	Vascular reflection coefficient scaling factor	0.96	Fitted	1.41
$NRCL_{cynomologus}$ (ml/kg/hr)	Non-renal/non-specific clearance mechanism in monkeys	0.196	Fitted	17.91
σ_{isf}	Interstitial reflection coefficient	0.2	Fixed	N/A
FGFR	Fraction of glomerular filtration rate	0.001	Fixed	N/A
L	Numerical value blood flow was divided by to obtain lymph flow value	500	Fixed	N/A
Residual Error	/	0.13	Fitted	10.67
Human				
Sigma_v_scaling factor	/	0.96	Fixed	N/A
$NRCL_{human}$ (ml/kg)	Non-renal/non-specific clearance mechanism in humans	8.71	Scaled	N/A

σ_{isf}	/	0.2	Fixed	N/A
FGFR	/	0.001	Fixed	N/A
L	/	500	Fixed	N/A
LS	Numerical value blood flow was divided by to obtain skin lymph flow value	1000	Fitted	11.29

N/A: Not applicable for fixed parameters

Fixed parameters imply the parameter was fixed at the literature or experimentally obtained value

Fitted implies the value was obtained through a minimization algorithm using Phoenix NLME

$NRCL_{human}$ was allometrically scaled according to body weight to an empiric exponent of 0.85

Sensitivity analysis was performed on the IV bolus model by perturbing the value of the parameters with the greatest uncertainty and re-simulating the concentration vs. time profile at each perturbation. For the parameters FGFR, NRCL and σ_{isf}, the null parameters were each perturbed by ± 10%. For $\sigma_{v,sf}$ the estimate could not be perturbed by more than 5% upwards as this would have increased the vascular reflection coefficient for the brain to >1.The parameter L was varied from 500 down to 100 as this is the range of reported values for this parameter.(21) Individual plasma concentration vs. time profiles for each of the 3 monkeys who received IV drug was simulated for each of the perturbed conditions. The mean area under the curve (AUC) calculated by NCA for each of the perturbed datasets ($AUC_{perterbed}$) was compared to the mean of the null (AUC_{null}) using % change [($AUC_{perterbed}$ –AUC_{null})/AUC_{null}].

5.2.5 SC Administration in Monkeys and Humans

For SC administration in monkeys, all systemic parameters defined or optimized in the IV model were held constant. The simulated bioavailability was calculated and compared to the observed bioavailability.

For translation to humans, the model was adapted to include human organ volumes, GFR, cardiac output, hematocrit and relative flow of blood to each organ. Fvv and Fvic were assumed to be constant across species. The non-renal clearance (NRCL) was scaled assuming the principles of simplified allometry with a fixed exponent of 0.85 which has been demonstrated to be a reasonable scaling factor from primates to humans in previous reports.(55;62-64)

At the time of this writing, the randomization scheme for the human study was still in a blinded stage and therefore the precise body weights of the subjects included was unknown and therefore an assumption of 70 kg (midpoint of the inclusion weight range for the study) was used for human simulations.

After comparison of the first human cohort observed data to the simulated profile, optimization was performed whereby skin lymph flow as a fraction of skin blood flow (LS) was fitted as a parameter rather than fixed to the previous value of 500. The optimized model was used to re-simulate the first dosing cohort (i.e. 45 mg single SC dose) as well as two subsequent dosing cohorts (90 mg and 180 mg) for which data was available at the time of this writing.

5.3 Results

5.3.1 IV Model Structure and Optimization

Prior to optimization, the model demonstrated reasonable fit with the observed data. However, through the fitting process, the NRCL was estimated with precision at a considerably higher value than initially estimated (Table 5.1). Goodness of fit plots (Figure 5.3) including an overlay of the observed and simulated profiles (Figure 5.4) demonstrate high agreement between simulated and observed IV data in all three cynomolgus monkeys included in this analysis.

Figure 5.3: Diagnostic plots for the IV model fit. Left panel illustrates the relationship between individual predicted concentrations (IPRED) obtained from a single-dose 7 mg/kg IV administration to 3 cynomologus monkeys. Closed symbols represent observed vs. predicted concentrations and dashed line represents the line of identity. Right panel illustrates the distribution of weighted residuals vs. IPRED (closed symbols) from the IV model in cynomologus monkeys.

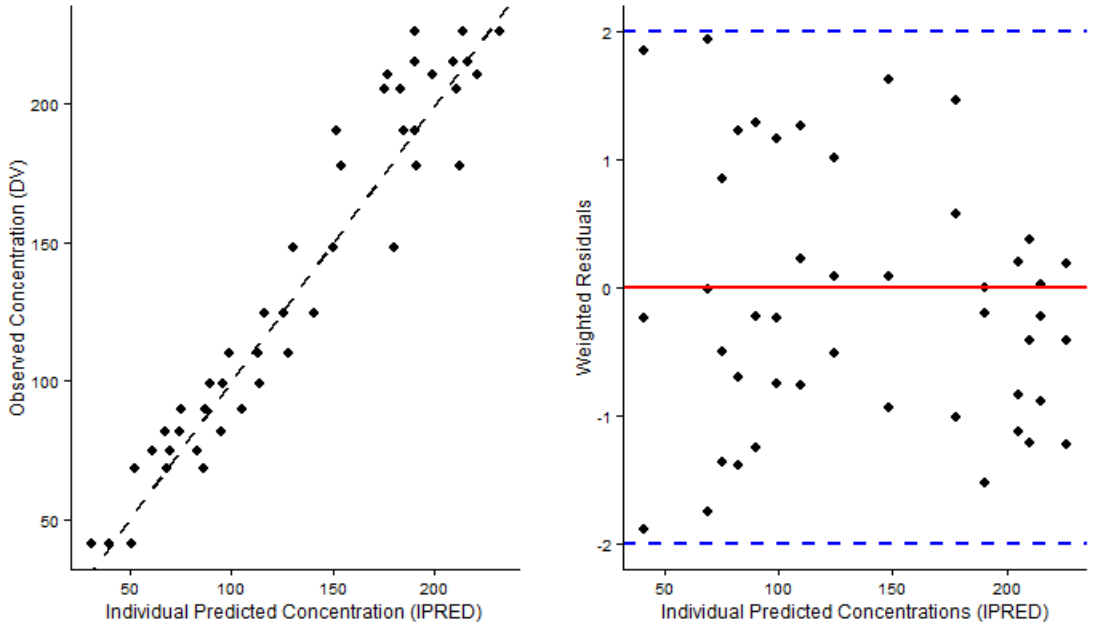

Figure 5.4: Plasma concentrations of a linear PEG-40 conjugated peptide versus time in 3 cynomolgus monkeys following a single 7 mg/kg IV dose, displaying a linear (top panel) and semi-log (bottom panel) scale for concentration . Closed symbols are measured values and lines are model simulations

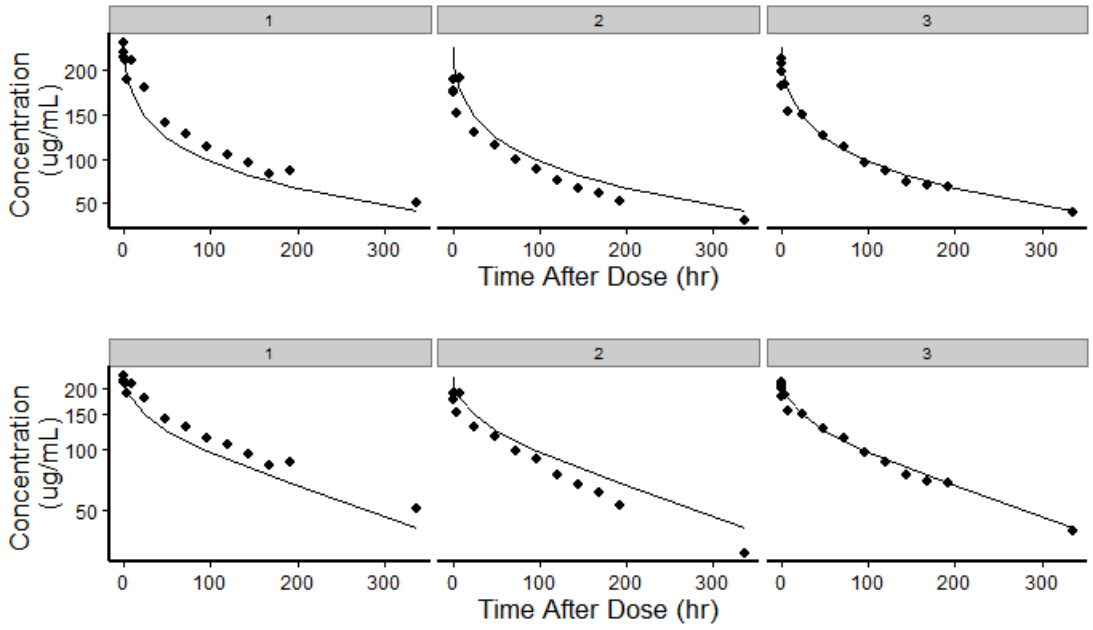

5.3.2 Sensitivity Analysis

The sensitivity analysis suggested that AUC was sensitive to each of the parameters tested, with the greatest sensitivity associated with $\sigma_{v,sf}$ (Table 5.2). Lymph flow as a fraction of blood flow (L), which when varied by 5-fold, changed the AUC by 4% demonstrating that for IV administration, lymph flow, which is uncertain, was not influential in describing overall exposure via the IV route in monkeys. Taken together, these results suggest that the most influential factor in the drugs overall exposure appears to be the convective transport across the vascular endothelium into the interstitial space.

Table5.2: Change in AUC as a result of parameter perturbation within the IV cynomologus monkey PBPK model.

Parameter & % Perturbation	Definition	AUClast (ug/mL*hr)	% Change from Null
Null/Base Model	Base human model without optimization	28550	-
FGFR +10%	Fraction of glomerular filtration rate	27612	3.3
FGFR -10%	/	29540	-3.5
NRCL +10%	Non-renal/non-specific clearance mechanism	28143	1.4
NRCL -10%	/	28955	-1.4
L100	Numerical value blood flow was divided by to obtain lymph flow value	27407	4.0
σ_{isf} +10%	Interstitial reflection coefficient	28409	0.5
σ_{isf} -10%	/	28687	-0.5
$\sigma_{v,sf}$ +5%	Vascular reflection coefficient scaling factor	31690	-11.0
$\sigma_{v,sf}$ -10%	/	23846	16.5

5.3.3 SC Administration in Monkeys and Humans

Simulating the concentration vs. time profile when the dose was administered into the SC depot also showed agreement with the observed data in monkeys (Figure 5.5). No optimization was performed in the generation of the SC monkey simulations. The absorption phase was well described by the model. Comparison of the simulated SC AUC relative to the simulated IV time course resulted in a similar bioavailability to that estimated by comparing the NCA-derived AUCs of the observed data (90% for simulated vs. 89% for observed). Therefore the model was considered adequate to scale to human by substituting organ size, blood flow rates, GFR and NRCL.

Figure 5.5: Plasma concentrations of a linear PEG-40 conjugated peptide versus time in 3 cynomolgus monkeys

following a single 7 mg/kg SC dose, displaying a linear (top panel) and semi-log (bottom panel) scale for concentration . Closed symbols are measured values and lines are model predictions.

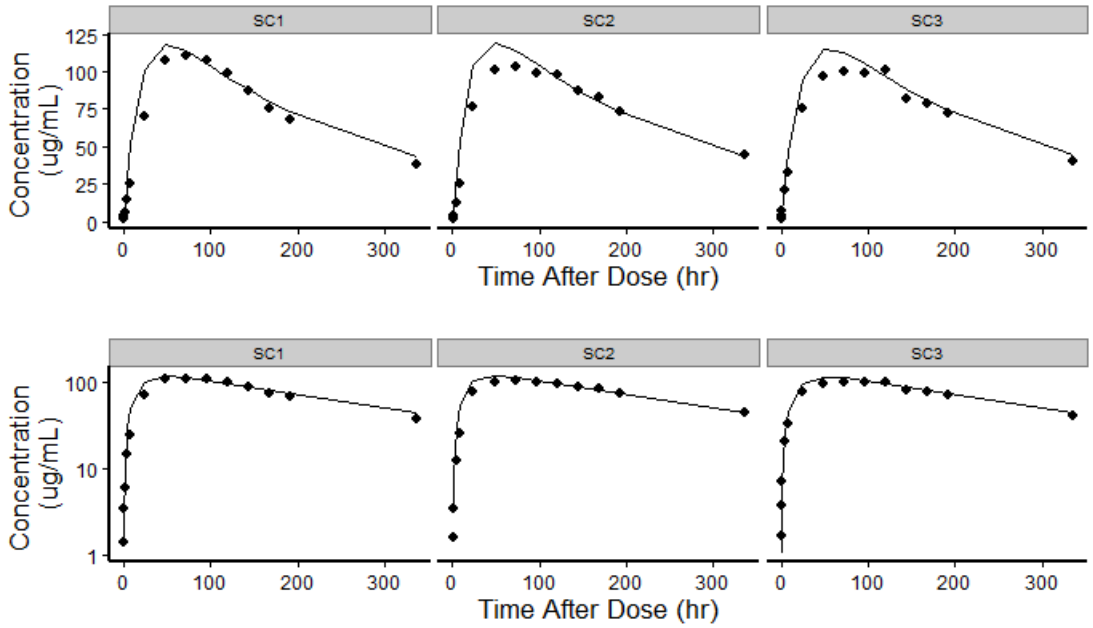

Figure 5.6 (solid line) presents the simulated human profile when administering a fixed 45 mg dose of the PEG-40 conjugated peptide to the SC depot compartment relative to the observed data from four healthy male participants in the first cohort of a FIH dose escalation study.

Figure 5.6: Model simulated and observed plasma concentrations of a linear PEG-40 conjugated peptide versus time in humans. The solid line represents the simulated concentrations from the null human model after scaling (as described in the methods section). The dashed line represents the simulated concentrations after adjustment for lymph flow from the skin (LS). Closed geometric symbols represent unique individual subjects in the first single-ascending dose cohort, receiving a single 45 mg SC dose to the abdominal region.

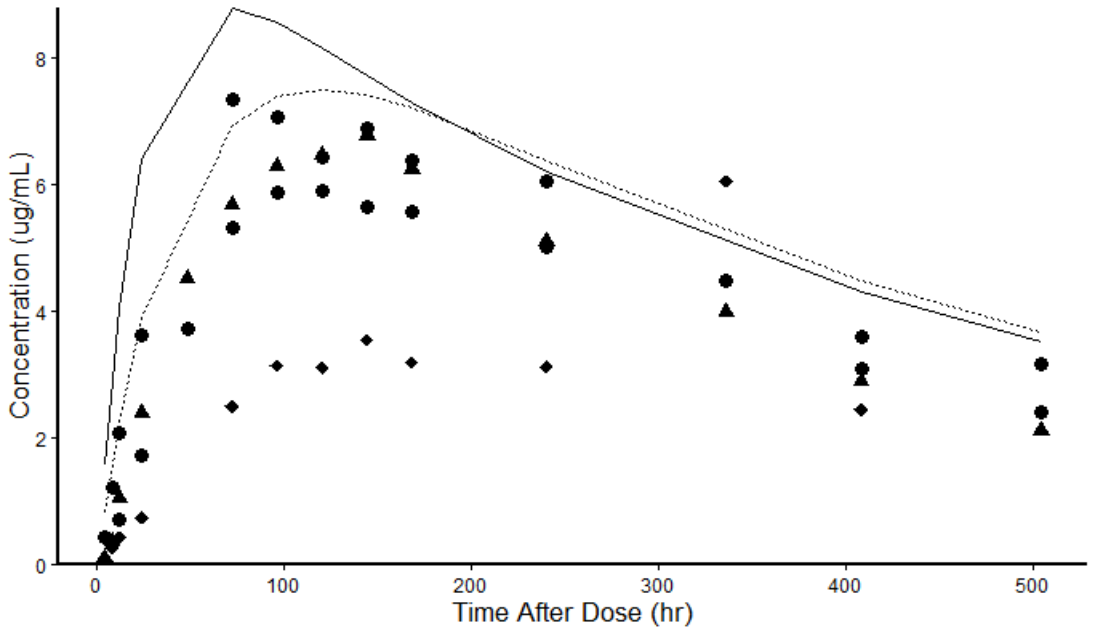

Although the observed data had a slower input than what was predicted from the model, the peak (Cmax) and overall exposure (AUC) as estimated by NCA, were within 24% and 30% of the mean observed data (Table 5.3), respectively, indicating that the time course was relatively well predicted. In line with the graphical comparison, the time to Cmax (Tmax) was somewhat earlier than what was observed, however the observed median value was influenced by one of the four subjects who had a distinguishably different profile than the other three subjects. Optimization of the parameter LS resulted in a value of 1000 with high precision (Table 5.1) and produced a simulation which described the observed data more closely than the null model (Figure 5.6 – dashed line). The simulated Cmax and AUC values differed by only 11% and 25%, respectively, from the observed values.

Table 5.3: Key NCA-derived pharmacokinetic parameter comparisons of observed human subjects receiving a single SC (45 mg) dose compared to simulated data obtained from the null human model and after optimization of skin lymphatic flow (LS)

Parameter (units)	Sample Size	Observed Dataset		Simulated Dataset	Simulated After Optimization of LS	%Difference Observed vs. Predicted	%Difference Observed vs Optimized
	N	Mean	CV%				
AUC (ug/mL*hr)	4	2035	22.1	2888	2714	30	25
Cmax (ug/mL)	4	6.64	8.34	8.78	7.50	24	11
Tmax* (hr)	4	156*	72.0-336*	72.0	120		

*Median (Min-Max reported for Tmax)

LS: Numerical value blood flow was divided by to obtain skin lymph flow value

Applying the same mechanistic principles as for estimating the monkey absolute bioavailability, human SC absolute bioavailability was simulated to be 94% and 88% based on the null and optimized models, respectively. As the LS optimized model appeared to better describe the absorption profile and overall time course of the SC administration, this version was used to simulate the next two dose cohorts (90 mg and 180 mg) which successfully predicted the proportionally higher dose levels in terms of the time course and peak concentration (Figure 5.7).

Figure 5.7: Model predicted (solid line) and observed (symbols) plasma concentrations of a linear PEG-40 conjugated peptide versus time in humans for subsequent cohorts at 2x and 4x the initial SC dose of 45 mg. Closed geometric symbols correspond to unique individual subjects in each cohort.

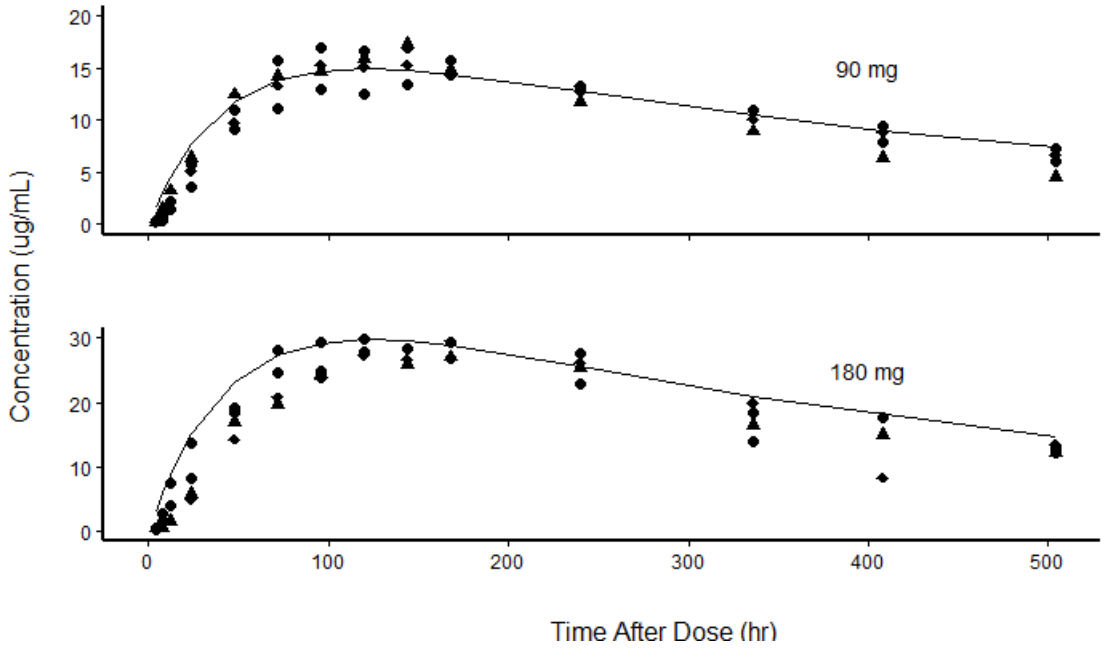

5.4 Discussion

We undertook this effort to further understand the mechanistic influences of SC bioavailability and interspecies differences in the context of scaling PK data obtained in the preclinical stages to predict the human time course and to support optimal study design of a FIH trial. The goal of this exercise was to develop a workflow to reduce the burden of preclinical development. An additional objective was to reduce the early human clinical work required to optimize the human dose through model-based drug development. The workflow entailed developing a fully body PBPK model with flexibility to incorporate mechanistic/semi-mechanistic elements to predicting the concentration vs. time profile for a broad range of SC administered therapeutics.

Prediction of the human PK profile after SC administration based on modeling of data from preclinical species has been challenging and inconsistent when allometry is employed in an a priori manner.(55) No single method is currently recommended for scaling the SC exposure from animals to humans as a result of the perceived lack of similarity in skin architecture across species. Anatomical differences in the skin architecture is hypothesized to be partially responsible for the inconsistency in interspecies SC bioavailability.(18) Although some work has demonstrated that the minipig may be a good model for scaling PK to humans for protein therapeutics administered SC (114), use of a minipig in protein therapeutics is questionable due to the potential difference in target expression and affinity.

A full body PBPK model was selected for scaling preclinical PK to human PK for several reasons. First, interspecies anatomical and physiological differences hypothesized to affect SC absorption are included as model components.(115) This allows for a biologically rational extrapolation to occur. Second, a full body PBPK model, as opposed to a reduced or lumped model, allows for the customization of clearance mechanisms based on a compound's therapeutic classification. Outside of mAbs, there exists a wide variety of therapeutic macromolecules which have entirely different clearance mechanisms from mAbs, and where SC administration is a desirable route of administration. The PEG conjugate in the current investigation could only be appropriately characterized by including a renal and non-renal component. Other classes of therapeutic macromolecules such as micro-RNA have been demonstrated to exhibit a differential uptake amongst the various tissue compartments.(119) In such cases a lumped model would not provide a true physiologic and anatomic representation of the drug's biodistribution. Furthermore, a PBPK approach has the advantage of overcoming limitations in sparse sampling and a low number of animals as it does not rely on the frequency or placement of the concentration samples to be useful in qualifying a model.

We hypothesized, prior to initiating this workflow that a PBPK model that could simulate the IV disposition of a therapeutic macromolecule would similarly result in a reasonable prediction of the time course following SC administration. Since the physiological factors driving drug distribution and CL were expected to scale across species, the SC time course and bioavailability would be influenced by the residence time of the drug within the SC space. Our hypothesis was further predicated on the assumption that since macromolecules are subject to lymphatic uptake from the interstitial space, any reduced bioavailability following SC administration would be a result of a longer duration of exposure to the non-renal clearance mechanisms in the SC milieu.

In the current model, the time course in plasma was sensitive to the parameter values for convective transport from the organ vasculature into the interstitium, and subsequent transit to the lymph. Parameter values for $\sigma_{v,organ}$ and σ_{isf} were adapted from previous reports by Shah and Betts (50) and Garg and Balthasar .(102) In the former, the values were based on a platform PBPK model which was demonstrated to have broad application across a range of monoclonal antibodies (mAbs) when tested in several preclinical species and humans. The latter obtained from Garg and Balthasar (10) was based on an assumption that transit to the lymphatics would not encounter substantial resistance. It should be noted that these values were evaluated with mAbs and that smaller macromolecules could exhibit a lower reflection coefficient of which more research is necessary to more precisely estimate. With respect to lymphatic transit, the current pegylated peptide with a molecular weight of approximately 44 kDa is considerably smaller than an IgG mAb. Due to the propensity to randomly conform water molecules, pegylation may increase hydrodynamic volume of a protein thus affecting its biodistribution to a greater extent than what the molecular weight would suggest .(26) To achieve slower lymphatic uptake than what our model produced, the σ_{isf} would have to be >0.5 (data not shown). A higher interstitial viscosity could also be responsible for the interspecies difference in the lymphatic uptake. Although we were unable to identify data describing differences in proteoglycan content differences between cynomolgus monkeys and humans, the density of the various skin layers is reported to be similar.(115) To account for a potential higher viscosity and thus slower transit of a macromolecule through the interstitium, we adjusted downward the lymph flow by increasing the LS in the human model and allowed it to fit through estimation. This adjustment allowed for better agreement between the observed and simulated data suggesting that perhaps a higher viscosity or lower skin lymph flow may be responsible for slower absorption into the systemic circulation in humans as compared to monkeys.

Supersaxo reported that compounds greater than 16 kDa tend to drain into the lymphatics from the application site.(16) The size, shape and charge of the molecule however, rather than the absolute molecule

weight, may exert a greater influence on the proportion of diffusive versus convective transport of the molecule with molecular diameters of 10 nm and greater having little to no diffusive capacity.(18) Sarin (12) reported that capillary pores range from 5-12 nm in most tissues. Considering that the hydrodynamic radii of a PEG-40 conjugated macromolecule would exceed the 10 nm diameter threshold for bi-directional flow across the capillary endothelium (32), it was assumed that the drug would follow a one-way circuit between the interstitium and organ vasculature. The hydrodynamic diameter for the pegylayted conjugate is similar to the approximately 9.3 nm diameter of IgG mAbs lending credibility to the observed scaling factor applied to the vascular reflection coefficients being similar to that employed in mAb PBPK models. (120;121)

For a mAb, Zhao (109) identified that bioavailability from the SC and intramuscular route was most sensitive to the lymphatic transit time followed by lymphatic flow rates and endosomal uptake. This publication also noted that the bioavailability increased with a reduction in the duration of transit through the lymph. This mechanistic observation is similar to our observations, where the absolute bioavailability appears to be driven by the lymph flow rate from the SC site of administration to the lymphatic space. In the current manuscript, the transit time from the SC space to the lymph node was influenced by the skin lymph flow rate which is derived as a fraction of skin blood flow. Reducing the lymph flow was necessary to slow the transit time from the SC space to the venous circulation in order to appropriately characterize the absorption phase and maximum concentration.

While the lymph flow from the SC space appeared to have an appreciable effect on PK of the drug, the site of injection cannot be ruled out as a source of variability in the current study. For the cynomologus studies, drug was injected SC into the back region while for humans the abdominal region was selected. Work by Kagan and Mager (113) have demonstrated, at least for rats administered a mAb, that there is a differential absolute bioavailability when administering to the back vs. abdomen with the abdominal region exhibiting a larger absorption rate constant (corresponding to a shorter duration of absorption). It is difficult to draw a comparison between the two reports due to different species and drug products having been administered, however if site of administration differences followed the observations of Kagan and Mager, one would expect that the absorption to be more rapid than what we observed in the human data.

Subjects participating in the human study were considered healthy and fell within a very narrow weight range (60-80 kg), consequently it is not expected that subcutaneous fat composition would be contributing to the observed differences between species. The body size alone of the species may account for the difference where the absorption may be slower in larger animals as has been observed by Woo and Jusko for

erythropoietin.(91) Further research into the interspecies mechanistic determinants of drug absorption from the SC space is warranted to improve our understanding of this observation.

Although the lymph flow to skin differed by 2-fold relative to the null human model once optimized, an informal analysis revealed that the model was not sensitive to lymph flow to the remaining organs when all organ L values including skin LS were adjusted in the human model upwards to 1000. Consequently, this affirms that skin lymph flow is a primary driver of both absolute SC bioavailability as well as the shape of the concentration vs. time profile. The fact that skin lymph flow was much slower than lymph flow to other organs is not a unique finding when considering Baxter's seminal PBPK evaluation of macromolecules where mouse skin lymph flow as a percentage of plasma flow was much slower than lymph flow for other organs.(47)

Zhao(109) also reported that the volume at the site of administration did not influence the shape of the concentration vs. time profile. In the current evaluation, the volume of the SC space was set at the injection volume. We hypothesized that the degree of spreading would be limited by the SC skin structure and would not exceed the volume that was administered, however in an informal analysis (data not shown) demonstrated that increasing the volume (whilst maintaining the same mass of drug) by 10-fold and 100-fold did not influence the shape of the profile in line with the observations by Zhao.(109)

Absolute bioavailability in monkeys was estimated from observed data using NCA. Although an underlying assumption of NCA is that clearance occurs via the central compartment and that macromolecules may not meet this assumption, employing NCA in the current scenario for estimation is justified when applying the same computation method to estimate relative exposure between two dosing conditions. In primates, exposure to the non-renal clearance mechanisms within the depot compartment accurately accounted for the reduced bioavailability. The simulated bioavailability was estimated at 90% and observed to 89% (obtained via NCA). It is expected therefore that for drugs exhibiting less than 100% absolute bioavailability, the residence time in the depot compartment is indirectly proportional to bioavailability. Confirmation of this hypothesis in humans would require IV data however this data is not forthcoming due to the desire to develop the drug for SC administration in the clinic.

PBPK model platforms as proposed by Shah and Betts (50) were principally developed for mAbs, incorporating recycling of the IgG mAb in the endosomal space, back to the plasma. In addition, these models incorporate elements such as pinocytosis and exocytosis mechanisms resulting in uptake and return from the interstitium to the endosomal and vascular spaces. Although pegylated therapeutics are reported to

be subject to pinocytosis and release from the cell either as intact or de-conjugated molecules (25), inclusion of an endosomal space with pinocytosis and exocytosis did not improve the disposition of the current molecule. This is not unexpected as the drug is not a mAb and not subject to binding by FcRn.

CL processes were defined as both renal and non-renal. Renal CL has been previously suggested to occur at a rate of approximately 0.1% of GFR for similar molecular weight pegylated drug molecules.(25;97). As pore size in renal glomeruli are reported to be approximately 15 nm (12) and the fact that PEG exhibits as high water solubility, a degree of renal filtration was not unexpected.

Renal elimination alone however was unable to account for the total body CL after IV administration. As the compound is a peptide, a degree of NRCL was also anticipated. However, identifying more than one route of CL when concentration data is only available in one biological matrix is challenging. As described in the results section, FGFR could not be estimated with precision during the optimization process and was fixed where the difference between total CL and renal CL was then attributed to the non-specific process. Through the sensitivity analysis, FGFR did not have an appreciable effect on the AUC when varied by 10% of the nominal value. The fact that the fitted NRCL value was nearly 4-fold greater than the initial estimated value may be a factor of using NCA to obtain the initial value and that the sampling interval did not adequately characterize the terminal phase of the profile for the monkey data.

An important distinction between the current proposed model and other PBPK models for therapeutic macromolecules is that the current model did not incorporate target binding and saturable clearance. While saturable binding is a hallmark of many mAbs and fusion proteins it is not necessarily applicable in all macromolecule models. For the current model, as previously mentioned, target binding data was not available for either species where the amount of target could be readily quantified, however based on initial toxicokinetic evaluations in primates, it was not assumed to be saturable. Consequently it was decided that the non-specific clearance, which was intended to account for a variety of potential clearance mechanisms (proteolytic degradation, macrophagic opsonisation) was the best choice for parameterizing the model in an *a priori* manner. This approach would have limitations where saturable CL is involved however evaluation of the preclinical data under single and repeat dosing suggested linear pharmacokinetics. For other compounds, the model is flexible in that where saturable binding data is available, it can be incorporated. At the time of this writing, three human cohorts covering a 4-fold difference in dose have been evaluated confirming approximately linear pharmacokinetics (Figures 5.6 & 5.7) supporting the assumptions of linear clearance in the animal model.

NRCL was scaled-up to human employing simplified allometric theory. An allometric method was selected based on the rationale that a mechanistically obtained value was not obtainable. In previous reports, a fixed exponent of 0.85 has been reasonably reproducible in scaling monkey CL to humans for therapeutic macromolecule. (55;62-64) Our own informal analysis (data not shown) suggests that an exponent ranging from 0.75-0.9 would have produced a similarly shaped curve, whereas exponents greater than 1 would result in an unacceptable level of under-prediction. This method of scaling accurately addressed the non-renal clearance component and resulted in a human SC bioavailability that was similar to that in primates. However, the preferable method, where possible, would be to include a mechanistic means of addressing all clearance processes.

It should be emphasized that the weight range in the human study was 60-80 kg and that the simulations were based on a 70 kg body weight. Adjusting the body weight for the simulations to the upper end of the range did result in slightly better fit with the observed dataset (data not shown) without adjusting the lymphatic flow to the skin. In the current workflow, and in the context of applying this workflow in predicting dose and exposure for a FIH study, actual body weight would not be obtainable without breaking the blind of these typically blinded studies. The workflow is intended to provide a reasonable estimation of the exposure and time course of a projected starting dose in humans and consequently an exact match of the simulation with the observed data is not an objective in the initial human data evaluation. Pauses in the availability of human data during the dose escalation provided an opportunity however to optimize the model and allowed for accurate prediction of the next cohort's concentration vs. time profile.

5.5 Conclusion

The workflow described above was developed specifically to address a process for selecting doses and regimens for SC administered therapeutic proteins in a FIH environment. We have demonstrated that through employing a PBPK model development process the SC absorption can be simulated with good precision in a commonly used preclinical species with particular relevance in biologic drug development. The model, which was developed for a pegylated peptide may be readily adapted to other non-mAb protein therapeutics exhibiting renal and non-specific linear CL with a similar high MW and a high degree of lymphatic uptake from the SC site. Scale-up to human demonstrated reasonable overlap with the first human dose cohort with peak and overall exposure within <30% of the observed data, and provided an opportunity to further optimize the model for more precise estimation of the time course for subsequent dose levels.

5.6 Chapter 5 supplementary material

Berkeley Madonna code for a macromolecule PBPK Model with Renal and Non-Specific Clearance in Each Organ Compartment

```
{Physiological Parameters}

{Constants to be set for average weight of the species being simulated}

{Body Weight}
BW = ___;enter per species (use average body weight)

{Hematocrit}
hct==___;enter per species

{Human Cardiac Output mL/hr}
CO==___;enter per species

{Total plasma volume}
PV=____*BW   ; = plasma volume per kg per species

{Glomerular Filtration Rate}
GFR=___;enter per species
;NOTE that units for GFR should be confirmed and if the GFR is entered in per body weight, then clearance must be multiplied by the body weight in the kidney plasma compartment.

{Organ Volumes}
Vheart=___;enter per species
Vlung=___;enter per species
Vmuscle=___;enter per species
Vskin=___;enter per species
Vadipose=___;enter per species
Vbone=___;enter per species
Vbrain=___;enter per species
Vkidney=___;enter per species
Vliver=___;enter per species
Vsmallintestines=___;enter per species
Vlargeintestines=___;enter per species
Vpancreas=___;enter per species
Vthymus=___;enter per species
Vspleen=___;enter per species
Vother=___;enter per species

{Organ Vascular Volume Fraction (Fvv)}
Fvvheart=___;enter per species
Fvvlung=___;enter per species
Fvvmuscle=___;enter per species Fvvskin=0.019
Fvvadipose=___;enter per species
Fvvbone=___;enter per species
Fvvbrain=___;enter per species
```

Fvvkidney=___;enter per species
Fvvliver=___;enter per species
Fvvsmallintestines=___;enter per species
Fvvlargeintestines=___;enter per species
Fvvpancreas=___;enter per species
Fvvthymus=___;enter per species
Fvvspleen=___;enter per species
Fvvother=___;enter per species

{Organ Volume of Interstitial Compartment Fraction (Fvic)}
Fvicheart=___;enter per species
Fviclung=___;enter per species
Fvicmuscle=___;enter per species
Fvicskin=___;enter per species
Fvicadipose=___;enter per species
Fvicbone=___;enter per species
Fvicbrain=___;enter per species
Fvickidney=___;enter per species
Fvicliver=___;enter per species
Fvicsmallintestines=___;enter per species
Fviclargeintestines=___;enter per species
Fvicpancreas=___;enter per species
Fvicthymus=___;enter per species
Fvicspleen=___;enter per species
Fvicother=___;enter per species

{Plasma Volume by organ (total organ volume * fraction vascular volume*1-hematocrit, mL)}

Vheart_pla= Vheart*Fvvheart*(1-hct)
Vlung_pla=Vlung*Fvvlung*(1-hct)
Vmuscle_pla=Vmuscle*Fvvmuscle*(1-hct)
Vskin_pla=Vskin*Fvvskin*(1-hct)
Vadipose_pla=Vadipose*Fvvadipose*(1-hct)
Vbone_pla=Vbone*Fvvbone*(1-hct)
Vbrain_pla=Vbrain*Fvvbrain*(1-hct)
Vkidney_pla=Vkidney*Fvvkidney*(1-hct)
Vliver_pla=Vliver*Fvvliver*(1-hct)
Vsmallintestines_pla=Vsmallintestines*Fvvsmallintestines*(1-hct)
Vlargeintestines_pla=Vlargeintestines*Fvvlargeintestines*(1-hct)
Vpancreas_pla=Vpancreas*Fvvpancreas*(1-hct)
Vthymus_pla=Vthymus*Fvvthymus*(1-hct)
Vspleen_pla=Vspleen*Fvvspleen*(1-hct)
Vother_pla=Vother*Fvvother*(1-hct)

{Venous Plasma Volume (mL)}
Vven_pla=(2/3)*(PV-
(Vheart_pla+Vlung_pla+Vmuscle_pla+Vskin_pla+Vadipose_pla+Vbone_pla+Vbrain_pla+Vkidney_pla+V
liver_pla+Vsmallintestines_pla+Vlargeintestines_pla+Vpancreas_pla+Vthymus_pla+Vspleen_pla+Vother_
pla))
;adapted from the assumptions in Peters(122)

{Arterial Plasma Volume (mL)}
Vart_pla=(1/3)*(PV-
(Vheart_pla+Vlung_pla+Vmuscle_pla+Vskin_pla+Vadipose_pla+Vbone_pla+Vbrain_pla+Vkidney_pla+V
liver_pla+Vsmallintestines_pla+Vlargeintestines_pla+Vpancreas_pla+Vthymus_pla+Vspleen_pla+Vother_
pla))
; adapted from the assumptions in Peters(122)

{Interstitial Volume by Organ, mL}
Vheart_isf = Vheart*Fvicheart
Vlung_isf=Vlung*Fviclung
Vmuscle_isf=Vmuscle*Fvicmuscle
Vskin_isf=(Vskin*Fvicskin)-Vdepot
Vdepot=____; define either based on injection volume or approximately 1 mL
Vadipose_isf=Vadipose*Fvicadipose
Vbone_isf=Vbone*Fvicbone
Vbrain_isf=Vbrain*Fvicbrain
Vkidney_isf=Vkidney*Fvickidney
Vliver_isf=Vliver*Fvicliver
Vsmallintestines_isf=Vsmallintestines*Fvicsmallintestines
Vlargeintestines_isf=Vlargeintestines*Fviclargeintestines
Vpancreas_isf=Vpancreas*Fvicpancreas
Vthymus_isf=Vthymus*Fvicthymus
Vspleen_isf=Vspleen*Fvicspleen
Vother_isf=Vother*Fvicother

{Human Volume of Lymph Node Compartment (mL)}
Vlymph=____;enter per species

{Blood Flow scaling factor (fraction of CO)}
QBheart= ___;enter per species
QBlung=___;enter per species
QBmuscle=___;enter per species
QBskin=___;enter per species
Qbadipose=___;enter per species
Qbbone=___;enter per species
Qbbrain=___;enter per species
Qbkidney=___;enter per species
Qbliver=___;enter per species
Qbsmallintestines=___;enter per species
Qblargeintestines=___;enter per species
Qbpancreas=___;enter per species
Qbthymus=___;enter per species
Qbspleen=___;enter per species
Qbother=___;enter per species

{Plasma Flow to Organs mL/hr}
{other than lung, each blood flow is defined as a fraction of lymph-flow reduced lung plasma flow so no need to include hematocrit}

Qlung=(1-hct)*CO

Qheart= QBheart*(Qlung-Llung)
Qmuscle=QBmuscle*(Qlung-Llung)
Qskin= QBskin*(Qlung-Llung)
Qadipose= QBadipose*(Qlung-Llung)
Qbone= QBbone*(Qlung-Llung)
Qbrain= QBbrain*(Qlung-Llung)
Qkidney= QBkidney*(Qlung-Llung)
Qliver= QBliver*(Qlung-Llung)
Qsmallintestines=QBsmallintestines*(Qlung-Llung)
Qlargeintestines=QBlargeintestines*(Qlung-Llung)
Qpancreas=QBpancreas*(Qlung-Llung)
Qthymus= QBthymus*(Qlung-Llung)
Qspleen= QBspleen*(Qlung-Llung)
Qother= QBother*(Qlung-Llung)

{Lymph flow from organs expressed in mL/hr}
L=500; lymph fraction of blood flow
Llung=QBlung*CO/L; except for lung which is defined as the fraction of the cardiac output divided by the lymph fraction
Lheart= (QBheart*(CO-Llung))/L
Lmuscle=(QBmuscle*(CO-Llung))/L
Lskin=((QBskin*(CO-Llung))/L)*0.99903
Lskin_depot=((QBskin*(CO-Llung))/L)* 0.00097
Ladipose=(QBadipose*(CO-Llung))/L
Lbone=(QBbone*(CO-Llung))/L
Lbrain=(QBbrain*(CO-Llung))/L
Lkidney=(QBkidney*(CO-Llung))/L
Lliver=(QBliver*(CO-Llung))/L
Lsmallintestines=(QBsmallintestines*(CO-Llung))/L
Llargeintestines=(QBlargeintestines*(CO-Llung))/L
Lpancreas=(QBpancreas*(CO-Llung))/L
Lthymus=(QBthymus*(CO-Llung))/L
Lspleen=(QBspleen*(CO-Llung))/L
Lother=(QBother*(CO-Llung))/L
Llymph=Lheart+Llung+Lmuscle+Lskin+Lskin_depot+Ladipose+Lbone+Lbrain+Lkidney+Lliver+Lsmallintestines+Llargeintestines+Lpancreas+Lthymus+Lspleen+Lother

{Vascular Reflection Coefficients}
Sigma_v_scalingfactor= 1; Can be optimized for each tissue or optimized as a scaling factor
Sigma_v_lung=0.95
Sigma_v_heart=0.95
Sigma_v_adipose=0.95
Sigma_v_muscle=0.95
Sigma_v_kidney=0.9
Sigma_v_bone=0.85
Sigma_v_thymus=0.9
Sigma_v_skin=0.95
Sigma_v_brain=0.99
Sigma_v_other=0.95
Sigma_v_smallintestines=0.9

Sigma_v_largeintestines=0.95
Sigma_v_spleen=0.85
Sigma_v_pancreas=0.9
Sigma_v_liver=0.85

{Lymphatic Reflection Coefficients}
Sigma_isf=0.2;

{Non-renal Clearance Code}
{Define the total volume where non-renal clearance occurs}
Vvascular_total= Vven_pla + Vart_pla + Vheart_pla+ Vlung_pla + Vmuscle_pla + Vskin_pla + Vadipose_pla + Vbone_pla + Vbrain_pla + Vkidney_pla + Vliver_pla + Vsmallintestines_pla + Vlargeintestines_pla + Vpancreas_pla + Vthymus_pla + Vspleen_pla +Vother_pla
Visf_total=Vheart_isf + Vlung_isf + Vmuscle_isf + Vskin_isf + Vadipose_isf + Vbone_isf + Vbrain_isf + Vkidney_isf + Vliver_isf +Vsmallintestines_isf + Vlargeintestines_isf + Vpancreas_isf + Vthymus_isf + Vspleen_isf + Vother_isf+Vdepot

Vtotal=Vvascular_total + Visf_total

{Define each volume space clearance occurs in as a fraction of the overall volume the total clearance occurs in}
VNRCL_ven_pla=Vven_pla/Vtotal
VNRCL_art_pla=Vart_pla/Vtotal
VNRCL_heart_pla=Vheart_pla/Vtotal
VNRCL_lung_pla=Vlung_pla/Vtotal
VNRCL_muscle_pla=Vmuscle_pla/Vtotal
VNRCL_skin_pla=Vskin_pla/Vtotal
VNRCL_adipose_pla=Vadipose_pla/Vtotal
VNRCL_bone_pla=Vbone_pla/Vtotal
VNRCL_brain_pla=Vbrain_pla/Vtotal
VNRCL_kidney_pla=Vkidney_pla/Vtotal
VNRCL_liver_pla=Vliver_pla/Vtotal
VNRCL_smallintestines_pla=Vsmallintestines_pla/Vtotal
VNRCL_largeintestines_pla=Vlargeintestines_pla/Vtotal
VNRCL_pancreas_pla=Vpancreas_pla/Vtotal
VNRCL_thymus_pla=Vthymus_pla/Vtotal
VNRCL_spleen_pla=Vspleen_pla/Vtotal
VNRCL_other_pla=Vother_pla/Vtotal

VNRCL_heart_isf=Vheart_isf/Vtotal
VNRCL_lung_isf=Vlung_isf/Vtotal
VNRCL_muscle_isf=Vmuscle_isf/Vtotal
VNRCL_skin_isf=Vskin_isf/Vtotal
VNRCL_adipose_isf=Vadipose_isf/Vtotal
VNRCL_bone_isf=Vbone_isf/Vtotal
VNRCL_brain_isf=Vbrain_isf/Vtotal
VNRCL_kidney_isf=Vkidney_isf/Vtotal
VNRCL_liver_isf=Vliver_isf/Vtotal

VNRCL_smallintestines_isf=Vsmallintestines_isf/Vtotal
VNRCL_largeintestines_isf=Vlargeintestines_isf/Vtotal
VNRCL_pancreas_isf=Vpancreas_isf/Vtotal
VNRCL_thymus_isf=Vthymus_isf/Vtotal
VNRCL_spleen_isf=Vspleen_isf/Vtotal
VNRCL_other_isf=Vother_isf/Vtotal
VNRCL_skin_depot=Vdepot/Vtotal

{Non-renal clearance value}
NRCL=_____; mL/kg

{Exposure Conditions}
AdminDose = _____; Enter Administered Dose
F=____; Relative Bioavailability Term if applicable (otherwise =1)
DOSE=AdminDose*F

{Mass Balance Equations}

{Venous Plasma Circulation}
;Aven_pla=amount in venous plasma circulation (ug); Aven_pla'=dAven_pla/dt
;Amount coming from each of the organs (difference between plasma and lymph flow) summed;with amount coming from lymph minus amount going to lungs
Aven_pla'= ((Qheart - Lheart)* Cheart_pla) + (((Qliver-Lliver) + (Qsmallintestines-Lsmallintestines) + (Qlargeintestines-Llargeintestines) + (Qspleen-Lspleen) + (Qpancreas-Lpancreas))*Cliver_pla) + ((Qadipose-Ladipose)* Cadipose_pla) + ((Qmuscle-Lmuscle)* Cmuscle_pla) + ((Qkidney-Lkidney)* Ckidney_pla) + ((Qbone-Lbone)* Cbone_pla) + ((Qthymus-Lthymus)* Cthymus_pla) + ((Qskin-(Lskin+Lskin_depot))* Cskin_pla) + ((Qother-Lother)* Cother_pla) +
((Qbrain-Lbrain)*Cbrain_pla)+ (Llymph*Clymph) - (Qlung*Cven_pla) - ANRCL_ven'
Cven_pla=Aven_pla/Vven_pla; relating concentration in the venous system to the amount and volume of the venous system.
INIT Aven_pla=0
ANRCL_ven'=NRCL*Cven_pla*VNRCL_ven_pla
INIT ANRCL_ven=0

{Arterial Plasma Circulation}
;Aart_pla=amount in arterial plasma circulation (ug); Aart_pla'=dAart_pla/dt
Aart_pla'= ((Qlung-Llung)*Clung_pla) - (Qheart*Cart_pla) - (Qadipose * Cart_pla) - (Qmuscle * Cart_pla) - (Qkidney * Cart_pla) - (Qbone * Cart_pla) - (Qthymus * Cart_pla) - (Qskin* Cart_pla) - (Qbrain * Cart_pla) - (Qliver* Cart_pla) - (Qsmallintestines* Cart_pla) - (Qlargeintestines* Cart_pla) - (Qspleen * Cart_pla) - (Qpancreas* Cart_pla)- (Qother*Cart_pla)-ANRCL_art'
Cart_pla=Aart_pla/Vart_pla; relating concentration of arterial plasma to volume of the arterial plasma.
INIT Aart_pla=0;
ANRCL_art'=NRCL*Cart_pla*VNRCL_art_pla
INIT ANRCL_art=0

{Lymph}
;Alymph=amount in Lymph (ug) ; Alymph'=dAlymph/dt

;isf = interstitial fluid
;Sigma_isf= interstitial reflection coefficient
Alymph'= (Llung*(1-Sigma_isf)*Clung_isf) + (Lheart*(1-Sigma_isf)* Cheart_isf) + (Ladipose*(1-Sigma_isf)* Cadipose_isf) + (Lmuscle*(1-Sigma_isf)* Cmuscle_isf) + (Lkidney*(1-Sigma_isf)* Ckidney_isf) + (Lbone*(1-Sigma_isf)* Cbone_isf) + (Lthymus*(1-Sigma_isf)* Cthymus_isf) + (Lskin*(1-Sigma_isf)* Cskin_isf) + (Lbrain*(1-Sigma_isf)* Cbrain_isf) + (Lliver*(1-Sigma_isf)* Cliver_isf) + (Lsmallintestines*(1-Sigma_isf)* Csmallintestines_isf) + (Llargeintestines*(1-Sigma_isf)* Clargeintestines_isf) + (Lspleen*(1-Sigma_isf)* Cspleen_isf) + (Lpancreas*(1-Sigma_isf)* Cpancreas_isf) + (Lother*(1-Sigma_isf)*Cother_isf)- (Llymph*Clymph) +(Lskin_depot*(1-Sigma_isf)* Cskin_depot)
INIT Alymph=0
Clymph=Alymph/Vlymph

{Lung}
;Alung=amount in lung (ug) ; Alung'=dAlung/dt
Alung'= (Qlung*Cven_pla) - (Llung*(1-(Sigma_v_scalingfactor*Sigma_v_lung))*Clung_pla) - ((Qlung-Llung)*Clung_pla)-ANRCL_lung_pla'
Alung_isf'= (Llung*(1-(Sigma_v_scalingfactor*Sigma_v_lung))* Clung_pla) - (Llung*(1-Sigma_isf)*Clung_isf)-ANRCL_lung_isf'
Clung_isf=Alung_isf/Vlung_isf
Clung_pla=Alung/Vlung_pla
INIT Alung=0
INIT Alung_isf=0
ANRCL_lung_pla'=NRCL*Clung_pla*VNRCL_lung_pla
INIT ANRCL_lung_pla=0
ANRCL_lung_isf'=NRCL*Clung_isf*VNRCL_lung_isf
INIT ANRCL_lung_isf=0

{Heart}
Aheart'= (Qheart* Cart_pla) - (Lheart*(1-(Sigma_v_scalingfactor*Sigma_v_heart))* Cheart_pla) - ((Qheart-Lheart)*Cheart_pla) -ANRCL_heart_pla'
Aheart_isf'= (Lheart*(1-(Sigma_v_scalingfactor*Sigma_v_heart))* (Cheart_pla)) -(Lheart*(1-Sigma_isf)*Cheart_isf)-ANRCL_heart_isf'
Cheart_pla=Aheart/Vheart_pla
INIT Aheart=0
Cheart_isf=Aheart_isf/Vheart_isf
INIT Aheart_isf= 0
ANRCL_heart_pla'=NRCL*Cheart_pla*VNRCL_heart_pla
INIT ANRCL_heart_pla=0
ANRCL_heart_isf'=NRCL*Cheart_isf*VNRCL_heart_isf
INIT ANRCL_heart_isf=0

{Adipose}
Aadipose'= (Qadipose* Cart_pla) - (Ladipose*(1-(Sigma_v_scalingfactor*Sigma_v_adipose))* Cadipose_pla) - ((Qadipose-Ladipose)*Cadipose_pla) -ANRCL_adipose_pla'
Aadipose_isf'= (Ladipose*(1-(Sigma_v_scalingfactor*Sigma_v_adipose))* (Cadipose_pla)) -(Ladipose*(1-Sigma_isf)*Cadipose_isf)-ANRCL_adipose_isf'

Cadipose_pla=Aadipose/Vadipose_pla
INIT Aadipose=0
Cadipose_isf=Aadipose_isf/Vadipose_isf

```
INIT Aadipose_isf= 0
ANRCL_adipose_pla'=NRCL*Cadipose_pla*VNRCL_adipose_pla
INIT ANRCL_adipose_pla=0
ANRCL_adipose_isf'=NRCL*Cadipose_isf*VNRCL_adipose_isf
INIT ANRCL_adipose_isf=0



{Muscle}
Amuscle'= (Qmuscle* Cart_pla) - (Lmuscle*(1-(Sigma_v_scalingfactor*Sigma_v_muscle))* Cmuscle_pla) - ((Qmuscle-Lmuscle)*Cmuscle_pla) -ANRCL_muscle_pla'
Amuscle_isf'= (Lmuscle*(1-(Sigma_v_scalingfactor*Sigma_v_muscle))* (Cmuscle_pla)) -(Lmuscle*(1-Sigma_isf)*Cmuscle_isf)-ANRCL_muscle_isf'
Cmuscle_pla=Amuscle/Vmuscle_pla
INIT Amuscle=0
Cmuscle_isf=Amuscle_isf/Vmuscle_isf
INIT Amuscle_isf= 0
ANRCL_muscle_pla'=NRCL*Cmuscle_pla*VNRCL_muscle_pla
INIT ANRCL_muscle_pla=0
ANRCL_muscle_isf'=NRCL*Cmuscle_isf*VNRCL_muscle_isf
INIT ANRCL_muscle_isf=0

{Kidney}
Akidney'= (Qkidney* Cart_pla) - (Lkidney*(1-(Sigma_v_scalingfactor*Sigma_v_kidney))* Ckidney_pla) - ((Qkidney-Lkidney)*Ckidney_pla) -(ACLR')-(ANRCL_kidney_pla')
Akidney_isf'= (Lkidney*(1-(Sigma_v_scalingfactor*Sigma_v_kidney))* (Ckidney_pla)) -(Lkidney*(1-Sigma_isf)*Ckidney_isf)-(ANRCL_kidney_isf')
Ckidney_pla=Akidney/Vkidney_pla
INIT Akidney=0
Ckidney_isf=Akidney_isf/Vkidney_isf
INIT Akidney_isf= 0
ACLR'=CLR*Ckidney_pla
CLR=(GFR*FGFR); renal clearance rate of a pegylated protein
INIT ACLR=0
FGFR=0.001; fraction of GFR at which a pegylated protein is renally excreted
ANRCL_kidney_pla'=NRCL*Ckidney_pla*VNRCL_kidney_pla
INIT ANRCL_kidney_pla=0
ANRCL_kidney_isf'=NRCL*Ckidney_isf*VNRCL_kidney_isf
INIT ANRCL_kidney_isf=0



{Bone}
Abone'= (Qbone* Cart_pla) - (Lbone*(1-(Sigma_v_scalingfactor*Sigma_v_bone))* Cbone_pla) - ((Qbone-Lbone)*Cbone_pla) -ANRCL_bone_pla'
Abone_isf'= (Lbone*(1-(Sigma_v_scalingfactor*Sigma_v_bone))* (Cbone_pla)) -(Lbone*(1-Sigma_isf)*Cbone_isf)-ANRCL_bone_isf'
Cbone_pla=Abone/Vbone_pla
INIT Abone=0
```

Cbone_isf=Abone_isf/Vbone_isf
INIT Abone_isf= 0
ANRCL_bone_pla'=NRCL*Cbone_pla*VNRCL_bone_pla
INIT ANRCL_bone_pla=0
ANRCL_bone_isf'=NRCL*Cbone_isf*VNRCL_bone_isf
INIT ANRCL_bone_isf=0

{Thymus}
Athymus'= (Qthymus* Cart_pla) - (Lthymus*(1-(Sigma_v_scalingfactor*Sigma_v_thymus))* Cthymus_pla) - ((Qthymus-Lthymus)*Cthymus_pla) -ANRCL_thymus_pla'
Athymus_isf'= (Lthymus*(1-(Sigma_v_scalingfactor*Sigma_v_thymus))* (Cthymus_pla)) -(Lthymus*(1-Sigma_isf)*Cthymus_isf)-ANRCL_thymus_isf'
Cthymus_pla=Athymus/Vthymus_pla
INIT Athymus=0
Cthymus_isf=Athymus_isf/Vthymus_isf
INIT Athymus_isf= 0
ANRCL_thymus_pla'=NRCL*Cthymus_pla*VNRCL_thymus_pla
INIT ANRCL_thymus_pla=0
ANRCL_thymus_isf'=NRCL*Cthymus_isf*VNRCL_thymus_isf
INIT ANRCL_thymus_isf=0

{Skin}
Askin'= (Qskin* Cart_pla) - ((Lskin+Lskin_depot)*(1-(Sigma_v_scalingfactor*Sigma_v_skin))* Cskin_pla) - ((Qskin-(Lskin+Lskin_depot))*Cskin_pla) -ANRCL_skin_pla'
Askin_isf'= (Lskin*(1-(Sigma_v_scalingfactor*Sigma_v_skin))* (Cskin_pla)) -(Lskin*(1-Sigma_isf)*Cskin_isf)-ANRCL_skin_isf'
Askin_depot'= (Lskin_depot*(1-(Sigma_v_scalingfactor*Sigma_v_skin))* Cskin_pla) - (Lskin_depot*(1-Sigma_isf)*Cskin_depot) - ANRCL_skin_depot'

Cskin_pla=Askin/Vskin_pla
INIT Askin=0
Cskin_isf=Askin_isf/Vskin_isf
INIT Askin_isf= 0
Cskin_depot=Askin_depot/Vdepot
INIT Askin_depot=DOSE
ANRCL_skin_pla'=NRCL*Cskin_pla*VNRCL_skin_pla
INIT ANRCL_skin_pla=0
ANRCL_skin_isf'=NRCL*Cskin_isf*VNRCL_skin_isf
INIT ANRCL_skin_isf=0
ANRCL_skin_depot'=NRCL*Cskin_depot*VNRCL_skin_depot
INIT ANRCL_skin_depot=0

{Brain}
Abrain'= (Qbrain* Cart_pla) - (Lbrain*(1-(Sigma_v_scalingfactor*Sigma_v_brain))* Cbrain_pla) - ((Qbrain-Lbrain)*Cbrain_pla) -ANRCL_brain_pla'
Abrain_isf'= (Lbrain*(1-(Sigma_v_scalingfactor*Sigma_v_brain))* (Cbrain_pla)) -(Lbrain*(1-Sigma_isf)*Cbrain_isf)-ANRCL_brain_isf'
Cbrain_pla=Abrain/Vbrain_pla

INIT Abrain=0
Cbrain_isf=Abrain_isf/Vbrain_isf
INIT Abrain_isf= 0
ANRCL_brain_pla'=NRCL*Cbrain_pla*VNRCL_brain_pla
INIT ANRCL_brain_pla=0
ANRCL_brain_isf'=NRCL*Cbrain_isf*VNRCL_brain_isf
INIT ANRCL_brain_isf=0

{Other}
Aother'= (Qother* Cart_pla) - (Lother*(1-(Sigma_v_scalingfactor*Sigma_v_other))* Cother_pla) - ((Qother-Lother)*Cother_pla) -ANRCL_other_pla'
Aother_isf'= (Lother*(1-(Sigma_v_scalingfactor*Sigma_v_other))* (Cother_pla)) -(Lother*(1-Sigma_isf)*Cother_isf)-ANRCL_other_isf'
Cother_pla=Aother/Vother_pla
INIT Aother=0
Cother_isf=Aother_isf/Vother_isf
INIT Aother_isf= 0
ANRCL_other_pla'=NRCL*Cother_pla*VNRCL_other_pla
INIT ANRCL_other_pla=0
ANRCL_other_isf'=NRCL*Cother_isf*VNRCL_other_isf
INIT ANRCL_other_isf=0

{Small intestines}
Asmallintestines'= (Qsmallintestines* Cart_pla) - (Lsmallintestines*(1-(Sigma_v_scalingfactor*Sigma_v_smallintestines))* Csmallintestines_pla) - ((Qsmallintestines-Lsmallintestines)*Csmallintestines_pla) -ANRCL_smallintestines_pla'
Asmallintestines_isf'= (Lsmallintestines*(1-(Sigma_v_scalingfactor*Sigma_v_smallintestines))* (Csmallintestines_pla)) -(Lsmallintestines*(1-Sigma_isf)*Csmallintestines_isf)-ANRCL_smallintestines_isf'
Csmallintestines_pla=Asmallintestines/Vsmallintestines_pla
INIT Asmallintestines=0
Csmallintestines_isf=Asmallintestines_isf/Vsmallintestines_isf
INIT Asmallintestines_isf= 0
ANRCL_smallintestines_pla'=NRCL*Csmallintestines_pla*VNRCL_smallintestines_pla
INIT ANRCL_smallintestines_pla=0
ANRCL_smallintestines_isf'=NRCL*Csmallintestines_isf*VNRCL_smallintestines_isf
INIT ANRCL_smallintestines_isf=0

{Large Intestines}
Alargeintestines'= (Qlargeintestines* Cart_pla) - (Llargeintestines*(1-(Sigma_v_scalingfactor*Sigma_v_largeintestines))* Clargeintestines_pla) - ((Qlargeintestines-Llargeintestines)*Clargeintestines_pla) -ANRCL_largeintestines_pla'
Alargeintestines_isf'= (Llargeintestines*(1-(Sigma_v_scalingfactor*Sigma_v_largeintestines))* (Clargeintestines_pla)) -(Llargeintestines*(1-Sigma_isf)*Clargeintestines_isf)-ANRCL_largeintestines_isf'
Clargeintestines_pla=Alargeintestines/Vlargeintestines_pla
INIT Alargeintestines=0
Clargeintestines_isf=Alargeintestines_isf/Vlargeintestines_isf
INIT Alargeintestines_isf= 0
ANRCL_largeintestines_pla'=NRCL*Clargeintestines_pla*VNRCL_largeintestines_pla
INIT ANRCL_largeintestines_pla=0

ANRCL_largeintestines_isf'=NRCL*Clargeintestines_isf*VNRCL_largeintestines_isf
INIT ANRCL_largeintestines_isf=0

{Spleen}
Aspleen'= (Qspleen* Cart_pla) - (Lspleen*(1-(Sigma_v_scalingfactor*Sigma_v_spleen))* Cspleen_pla) - ((Qspleen-Lspleen)*Cspleen_pla) -ANRCL_spleen_pla'
Aspleen_isf'= (Lspleen*(1-(Sigma_v_scalingfactor*Sigma_v_spleen))* (Cspleen_pla)) -(Lspleen*(1-Sigma_isf)*Cspleen_isf)-ANRCL_spleen_isf'
Cspleen_pla=Aspleen/Vspleen_pla
INIT Aspleen=0
Cspleen_isf=Aspleen_isf/Vspleen_isf
INIT Aspleen_isf= 0
ANRCL_spleen_pla'=NRCL*Cspleen_pla*VNRCL_spleen_pla
INIT ANRCL_spleen_pla=0
ANRCL_spleen_isf'=NRCL*Cspleen_isf*VNRCL_spleen_isf
INIT ANRCL_spleen_isf=0

{Pancreas}
Apancreas'= (Qpancreas* Cart_pla) - (Lpancreas*(1-(Sigma_v_scalingfactor*Sigma_v_pancreas))* Cpancreas_pla) - ((Qpancreas-Lpancreas)*Cpancreas_pla) -ANRCL_pancreas_pla'
Apancreas_isf'= (Lpancreas*(1-(Sigma_v_scalingfactor*Sigma_v_pancreas))* (Cpancreas_pla)) - (Lpancreas*(1-Sigma_isf)*Cpancreas_isf)-ANRCL_pancreas_isf'
Cpancreas_pla=Apancreas/Vpancreas_pla
INIT Apancreas=0
Cpancreas_isf=Apancreas_isf/Vpancreas_isf
INIT Apancreas_isf= 0
ANRCL_pancreas_pla'=NRCL*Cpancreas_pla*VNRCL_pancreas_pla
INIT ANRCL_pancreas_pla=0
ANRCL_pancreas_isf'=NRCL*Cpancreas_isf*VNRCL_pancreas_isf
INIT ANRCL_pancreas_isf=0

{Liver}
Aliver'= (Qliver* Cart_pla) + ((Qsmallintestines-Lsmallintestines)*Csmallintestines_pla) + ((Qlargeintestines-Llargeintestines)*Clargeintestines_pla) + ((Qspleen-Lspleen) * Cspleen_pla) + ((Qpancreas-Lpancreas)*Cpancreas_pla) - (Lliver*(1-(Sigma_v_scalingfactor*Sigma_v_liver))* (Cliver_pla)) - (((Qliver-Lliver) + (Qsmallintestines-Lsmallintestines) + (Qlargeintestines-Llargeintestines) + (Qspleen-Lspleen) + (Qpancreas-Lpancreas))*Cliver_pla)- ANRCL_liver_pla'

Aliver_isf'= (Lliver*(1-(Sigma_v_scalingfactor*Sigma_v_liver))* Cliver_pla)-(Lliver*(1-Sigma_isf)*Cliver_isf)- ANRCL_liver_isf'

INIT Aliver= 0
Cliver_pla=Aliver/Vliver_pla
INIT Aliver_isf= 0
Cliver_isf=Aliver_isf/Vliver_isf

ANRCL_liver_pla'=NRCL*Cliver_pla*VNRCL_liver_pla
INIT ANRCL_liver_pla=0
ANRCL_liver_isf'=NRCL*Cliver_isf*VNRCL_liver_isf

INIT ANRCL_liver_isf=0

{Quality Check for Mass/Flow Balance}

TOTAL=Alung+Aheart+Amuscle+Abone+Abrain+Askin+Athymus+Aother+Akidney+Aadipose+Aliver+
Apancreas+Aspleen+Alargeintestines+Asmallintestines+Alymph+ACLR+Aven_pla+Aart_pla+Alung_isf+
Aheart_isf+Amuscle_isf+Abone_isf+Abrain_isf+Askin_isf+Athymus_isf+Aother_isf+Akidney_isf+Aadip
ose_isf+Aliver_isf+Apancreas_isf+Aspleen_isf+Alargeintestines_isf+Asmallintestines_isf+ANRCL_ven+
ANRCL_art+ANRCL_heart_pla+ANRCL_lung_pla+ANRCL_muscle_pla+ANRCL_skin_pla+ANRCL_a
dipose_pla+ANRCL_bone_pla+ANRCL_brain_pla+ANRCL_kidney_pla+ANRCL_liver_pla+ANRCL_sm
allintestines_pla+ANRCL_largeintestines_pla+ANRCL_pancreas_pla+ANRCL_thymus_pla+ANRCL_sple
en_pla+ANRCL_other_pla+ANRCL_heart_isf+ANRCL_lung_isf+ANRCL_muscle_isf+ANRCL_skin_isf
+ANRCL_adipose_isf+ANRCL_bone_isf+ANRCL_brain_isf+ANRCL_kidney_isf+ANRCL_liver_isf+A
NRCL_smallintestines_isf+ANRCL_largeintestines_isf+ANRCL_pancreas_isf+ANRCL_thymus_isf+ANR
CL_spleen_isf+ANRCL_other_isf+Askin_depot+ANRCL_skin_depot
ERROR = (DOSE-TOTAL)/(DOSE+1E-30)*100; ERROR should be close to 0

CHAPTER 6: POPULATION PHYSIOLOGICALLY-BASED PHARMACOKINETIC MODEL INCORPORATING LYMPHATIC UPTAKE FOR A SUBCUTANEOUSLY ADMINISTERED PEGYLATED PEPTIDE

The contents of Chapter 6 were initially published as an original contribution manuscript by the PhD. candidate (Elliot Offman). The original manuscript has been edited and formatted according to thesis publication requirements. For reference purposes, the original publication is as follows:
Offman E, Phipps C, Edginton AN. Population physiologically-based pharmacokinetic model incorporating lymphatic uptake for a subcutaneously administered pegylated peptide. *In Silico Pharmacology*; (2016);4(1):3 (Open Access Journal)

The PhD candidate conducted much of pertinent research, wrote portions of the code for the described models, conducted the vast majority of described analysis, created all tables, plots and figures and wrote the entire manuscript.

6.1 Background

The importance of the subcutaneous (SC) route to the drug development industry is evident in the growing number of drug products available for SC administration. In 2014, the U.S. Food & Drug Administration approved 41 new molecular entities and biological licensing applications, four of which had first approvals for subcutaneous (SC) administration.(33) The industry has also witnessed conversion of intravenous (IV) to SC routes for a number of therapies where treatment that was previously relegated to a hospital can now largely be addressed in an ambulatory setting (e.g. IV heparin to SC low molecular weight heparins for treatment of deep vein thrombosis). With a growing emphasis on SC administration as the primary route for development, reliance on reliable pharmacokinetic (PK) scaling methods (pre-clinical animal species to human) is correspondingly increasing.

When designing clinical pharmacology (Phase 1) and in particular first-in-human (FIH) studies, there is considerable importance placed on predicting the peak (Cmax) and overall exposure (AUC). This is particularly critical when relating the exposure observed in pre-clinical species to observed adverse events. Appreciating the temporal relationship between dosing time and Cmax, as well as an estimate of the drug's plasma half-life (T1/2), are useful for *a priori* design of early human research studies to mitigate the need for protocol amendments and reduce the burden of interim PK assessments.

In traditional allometric theory, prediction of human PK from animals has largely focused on estimating mean human exposure by scaling the mean clearance value of three or more preclinical species.(82;123) For macromolecules, and particularly for monoclonal antibodies (mAbs) exhibiting linear PK, single-species (primates) simplified allometric techniques have yielded useful predictions.(55;61-64) These methods however, provide no information as to the time course of a drug after administration, and have principally been employed for the IV route of administration. Dedrick plots have been demonstrated to have some utility in predicting the time course of IV administered monoclonal antibodies (mAbs), but have not yet been reported to yield similar predictive capacity for SC administered proteins.(61)

Predicting the SC time course of a drug in a population of humans from animal models is considerably more complex compared to prediction for a "mean human". For macromolecules, this is further complicated by a lack of knowledge regarding extravascular bioavailability and/or non-linearity in PK.

Whole body physiologically-based PK (WB-PBPK) modeling provides a rational mechanistic approach for predicting the time course of drugs in the vasculature and potentially other tissue compartments, and has demonstrated utility in describing the mean time course of IV administered macromolecules in both pre-

clinical and human species.(47-51) To extrapolate to SC administration however, these models may require modification to better account for local lymphatic drainage from the SC depot site.

The lymphatic system provides unidirectional transport for fluid and protein by collecting constituents from the interstitial space and returning them to the blood.(21) While transport is convective in nature, movement of lymphatic fluid and macromolecules transported into and by the lymphatics can be influenced by muscle contractions and ambient temperature.(21;23;24) Lymphatic vessels are categorized into capillaries, larger collecting vessels, nodes, trunks and ducts, and likely, many capillaries drain a single injection site.(21;22) Cannulation techniques in animal models have allowed for the quantitation of macromolecule uptake into the lymphatics, and whilst seminal in confirming lymphatic involvement in biodistribution and contributing to our understanding of how macromolecule size influences uptake, they do not address the actual local drainage dynamics from the depot into the immediate lymphatic capillaries.(16;17;22) Skin lymphatics include superficially spread, subpapillary fine mesh and deeper vessels which empty into larger vessels draining the SC space before reaching the collecting ducts.(124) Mathematical modeling lymphatic drainage remains challenging, as there is no non-invasive method for differentiating the volume of lymphatics attributed to local drainage at the site of drug administration and that attributed to the remainder of the lymphatic vessels.

WB-PBPK models for macromolecules and particularly mAbs have universally incorporated a lymph node compartment with convective transport dragging drug across the organ vascular-interstitial interface, into the lymph node compartment and subsequently into venous circulation.(47-51;66) Although mean values for a lymph node compartment are reported, it is unclear as to whether the reported volumes relate to the sum of all nodes, ducts, collectors and capillaries or to what extent these vary among individuals. Furthermore, population PBPK algorithms, available in the public domain, have not reported compartment characteristics (i.e. mean, variance) for the lymphatic system or lymph flow, and consequently don't readily lend themselves to the study of SC administration of macromolecules in a population of individuals.(125;126)

Employing a WB-PBPK modeling approach, we previously characterized the SC time course of a novel pegylated peptide conjugate in primates which was then scaled to humans at three different dose levels in a FIH single ascending dose (SAD) trial.(66) Upon further examination across a wider range of doses, the model predictions suggested further model refinement in the lymphatic uptake processes would improve predictive capacity of the model, particularly in the very early portion of the concentration vs. time profile.

To further investigate the contribution of local lymphatic capillary drainage from the SC space on the time course and shape of the plasma concentration vs. time profile (CPT), and to improve our understanding as to which parameters influence the variability of the CPT in a population, we endeavored to expand on our previous work and develop a population PBPK model which incorporates both lymphatic drainage and overall lymphatic system compartments.

6.2 Methods

6.2.1 Observed Datasets

CPT data was obtained for a novel pegylated peptide conjugate (approximately 45 kDa) as it transitioned from preclinical to early clinical development. The compound (name and target withheld for commercial proprietary purposes), predominantly consists of a freely water soluble, linear PEG-40 conjugated to a small (approximately 1 kDa) peptide portion. The current evaluation includes concentration and anthropometric data from 20 healthy Australian male subjects, 18-55 years of age and within a weight range of 60-80 kg who participated in a FIH, SAD investigation. The investigation was conducted under good clinical practice and according to the ethical principles outlined in the Declaration of Helsinki. Each subject received a single SC dose between 45 mg and 720 mg into the abdominal region with sequential PK sampling post-dose until approximately 1050 hours. The concentration of the injection ranged from 100 mg/mL to 150 mg/mL with multiple injections for some dose levels such that the volume in any single injection would not exceed 2 mL. Plasma was analyzed employing an LC-MS/MS method with a limit of quantitation of 1 ug/mL.

6.2.2 Model Structure

The base model structure has been previously described (66), and was slightly modified to better characterize the SC drainage into the lymphatics. Representative mass balance equations are provided for reference in Appendix 6.1. The proposed overall and sub-compartment structures are based in part on the PBPK platform developed previously by Shah and Betts and is depicted graphically in Figure 6.1a-b.(50) The overall structure consists of a unique compartment for each of the venous and arterial circulation, a lymph node compartment and 15 individual organs where each organ consists of a vascular and interstitial sub-compartment. The skin interstitial compartment is further sub-divided into a depot and residual space where the SC dose inputs directly into the depot. The SC depot volume was parameterized as being equivalent to the total injection volume, which varied from 0.45-4.8 mL depending on the dose level and concentration injected. Transport from the interstitium into the lymphatic space is via a convective flow with a small degree of resistance parameterized as lymph flow and a lymphatic reflection coefficient (σ_i), as proposed by Garg and Balthasar.(102) In our previously developed model based on primates,, drug in the SC depot space emptied directly into a lymphatic compartment.(66) In the current model, an intermediate anatomical volume was added in order to include the localized lymphatic drainage from the SC depot into adjacent lymph vessels, which we will refer to as the lymphatic drainage compartment (LDC). The LDC subsequently drains into the greater lymphatic system compartment. Lymphatic flow empties from the lymph compartment into the venous circulation and re-enters the interstitial space in a one-way circuit via the same lymphatic convective flow. Transfer from the organ plasma vascular space to the interstitial space

is similarly driven by convective flow and constrained by vascular reflection coefficients (σ_v) that were initially set at values proposed by Shah and Betts.(50) However, as per the previous model, all organ vascular reflection coefficients are scaled by the parameter σ_{sf}, which was previously optimized.(66) Fraction vascular (Fvv) and interstitial (Fvic) were retained at the same values as in the original model.(66)

Figure 6.1a: Structure of a whole-body PBPK platform (adapted from Shah & Betts 2012). Solid black arrows indicate plasma flow. Dark grey dashed arrows indicate lymphatic transport. S. Int. and L. Int. represent small and large intestines. Each organ compartment includes lymphatic flow emptying from the organ into the lymph nodes. For IV administration, drug is administered into the "Venous Supply". For SC administration, drug is administered into the "Skin Compartment" interstitium.

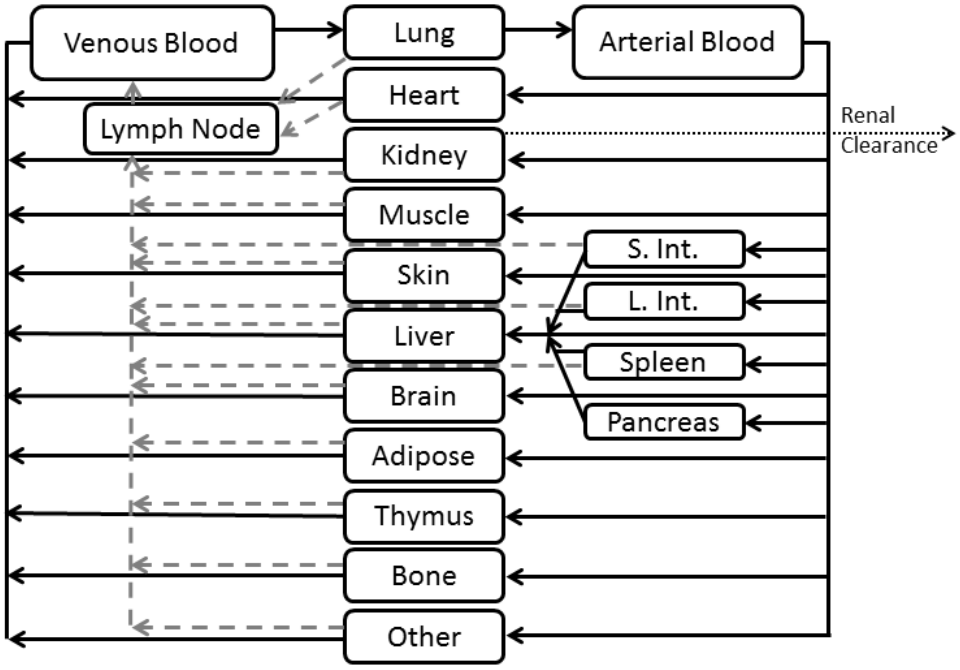

Figure 6.1b: Sub-compartment model for all organs other than skin (top) and skin (bottom).

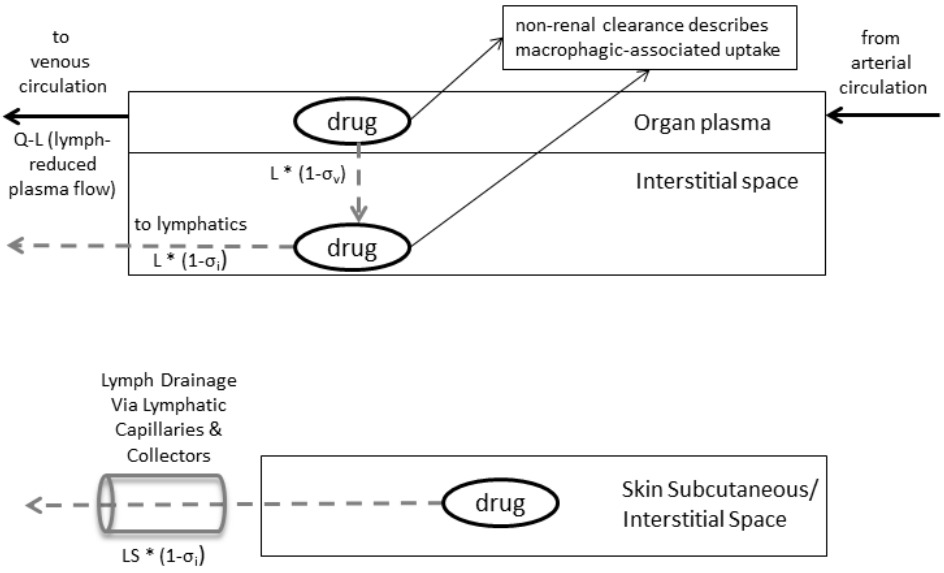

6.2.3 Virtual Population Development

Prior to simulation of a virtual population, the target population for simulation needs to be defined. Since the observed PK data was obtained in a group of Caucasian Australian men, average height and weight and corresponding coefficients of variations for these anthropometric measurements in non-obese Australian males were obtained from Craig et al.(127) As described by Willmann et al., first, height values were randomly drawn from a normal distribution for a population of 1000 male subjects followed by sampling of each organ compartment mass for each individual in the virtual population.(126) To mitigate the likelihood of individuals with the same height being allocated identical organ weights, organ masses were drawn either from a normal or log-normal distribution (Table 6.1) that was re-centered to the size of the individual employing an allometric scaling factor according to the ¾ power rule.(126) To avoid the selection of extreme outliers, organ mass distributions were symmetrically truncated to the 95th percentile and, when necessary to prevent negative masses, constrained at the lower bound to one tenth the re-centered mean value. A visual check was then performed to evaluate the impact of truncation and constraining the lower bound by repeating the simulations for all dose levels in the observed data where parameters initially drawn from a normal distribution were then drawn from a log-normal distribution.

Table 6.1: Anatomical and physiologic parameters with distributions used in the population PBPK model

	Mean*	CV%	Distribution	CV% Source
Mean Weight	71 (kg)	/	/	/
Compartment Mass	% Body Weight	/	/	/
Adipose	18.540	0.43	Log-normal	(128)
Brain	1.968	0.10	Normal	(128)
Blood (Arterial/Venous)	8.005	0.22	Log-normal	(129)
Bone	13.952	0.14	Normal	(128)
Heart	0.448	0.19	Normal	(130)
Kidney	0.421	0.25	Normal	(130)
Large Intestines	1.52	0.2	Normal	(125)
Liver	2.707	0.23	Normal	(130)
Lung	1.569	0.36	Log-normal	(130)
Lymph	0.359	0.22	Log-normal	Empirically assumed to be similar to circulatory system variability
Muscle	40.702	0.16	Log-normal	(128)
Other	Remainder not accounted for by	0.2	Normal	Empirically

	other organs			selected
Pancreas	0.136	0.27	Normal	(130)
Skin	4.477	0.1	Log-normal	Empirically selected
Small Intestines	1.068	0.12	Normal	(125)
Spleen	0.244	0.56	Log-Normal	(130)
Thymus	0.008	0.05	Log-Normal	Empirically selected
Hematocrit	0.42	0.02	Normal	(131)
Renal Filtration Fraction	0.20	0.0294	Normal	(132)
Vfrac	0.25	0.68		Fitted Parameter

*Mean organ mass was obtained from the BioDMET database(115)

All model compartments, with the exception of skin, blood and lymph were scaled according to Equation 6.1, where the mean mass of each organ O, denoted M_O^{mean}, is dependent on a single variable, in this case the body height of the individual, H_{indiv}, via an equation of the form $M_O^{mean} = cH_{indiv}^p$, where c is a sex- and race-dependent constant and p is a chosen exponent. Organ masses for a reference individual (M_O^{ref}) were obtained from the BioDmet database where H_{ref} is the height of a reference individual weighing 71 kg with a body mass index of 24 kg/m^2 (corresponding to a height of 172 cm).(115) Where organ volume and or mass were to be interconverted, density values for organs were obtained from ICRP references.(133)

$$M_0^{mean} = M_0^{ref} \times \left(\frac{H_{indiv}}{H_{ref}}\right)^{3/4} \quad (6.1)$$

Body height has been identified previously by de la Grandmaison as a better predictor of organ size in the majority of cases and the formula is rooted in allometric theory.(130) An exponent of ¾, although previously reported, was largely empiric for the current report, and others have used a range of values, upwards of 2, in a similar fashion.(126;134)

Blood and lymph mass means were scaled based on reference body weight (W_{ref}, Equation 6.2) as blood and lymph vessels are assumed to increase with increasing body weight as opposed to height.

$$M_0^{mean} = M_0^{ref} \times \left(\frac{W_{indiv}}{W_{ref}}\right)^{3/4} \quad (6.2)$$

Skin mass was scaled based on body surface area (BSA) as per Equation 6.3 where BSA was estimated based on Equation 6.4 and where the constant values for *a*, *b* and *c* were as proposed by Gehan and George ($a = 0.0235, b = 0.515, c = 0.422$) (135).

$$M_{skin}^{mean} = M_{skin}^{ref} \left(\frac{BSA_{indiv}}{BSA_{ref}}\right) \quad (6.3)$$

$$BSA_{indiv} = a \times (W_{indiv})^b (H_{indiv})^c \quad (6.4)$$

The total body mass (BM) of a virtual individual was then calculated as the sum of the bloodless organ masses, lymph mass, skin mass and blood mass and the BM of the final population individuals (n=1000) included only individuals within the range of 60-80 kg, consistent with the observed population. As previously suggested by Peters blood mass was partitioned as 2/3 venous and 1/3 arterial.(122)

For the derivation of organ-specific blood flows in each individual, mean perfusion values were first calculated for each organ to serve as a reference value assuming that perfusion rates would be constant across the population. Organ reference perfusion values were obtained by multiplying the cardiac output in a reference 71 kg male (115) by the blood flow fraction to that organ and then dividing the reference blood flow by the mean organ mass. Individual organ blood flows (QB) were then obtained by multiplying the organ weight of the individual by the reference perfusion value. Plasma flow (QP) was derived by multiplying QB by a factor of 1-hematocrit (hct), where hct was assumed to be log-normally distributed (Table 6.1).

Consistent with the PBPK model for a reference male, lymph flow was set at a constant fraction of blood flow (LO) where the previously employed value of 0.2% was used for all organs except skin (LS), which was set to 0.1%.(66) The fraction of 0.2% corresponds to the upper range of lymph flow reported by Swartz whereas 0.1% was obtained by optimization in the reference male model.(21)

Clearance of the pegylated protein was previously characterized by both renal (RCL) and non-renal clearance (NRCL). RCL was set at 0.1% of glomerular filtration rate (GFR) consistent with previously investigated PEG-conjugated therapeutics. To allow for incorporation of interindividual variation in GFR, the GFR was derived from the product of renal plasma flow and filtration fraction (FF) where FF was drawn from a log-normal distribution (Table 6.1).(25;66)The acronym FGFR is used to represent the fraction of glomerular filtration attributed to renal clearance. To avoid the risk of including individuals with GFRs in the impaired region of glomerular function, and to avoid extremely large values for GFR, only individuals with a GFR within the range of 90-150 mL/min were used in the simulation.(136)

For the compound in question, NRCL was assumed to occur by both macrophagic uptake of the non-pegylated moeity and by non-specific cleavage of the pegylated chain.(26) NRCL was optimized in primates in our previous model and for the current model NRCL in the primate was scaled to each simulated human based on the body weight ratio of a simulated human individual and the mean weight of the primate (3.4 kg).(66) The NRCL was then apportioned based on the relative volume of each compartment in which NRCL was assumed to occur.

6.2.4 Optimization of LDC

As the volume of drug product injected into the SC space increased, we hypothesized that there would be a proportional spreading of drug substance within the interstitial space, as opposed to expansion, thus increasing the surface area for lymphatic drainage. The volume then attributed to the LDC was considered proportional to the volume of the SC depot compartment. LDC volume was parameterized as a fraction of the SC depot compartment, denoted as Vfrac and estimated by fitting to the dose-normalized CPT data for all observed subjects. For this procedure, the PBPK model for an average human was coded into Phoenix NLME (v1.3, Certara) and estimation of the population mean Vfrac and between subject variability (as a log-normally distributed random effect) was performed using the first-order conditional estimation with interaction algorithm (FOCE-ELS).

Estimation was performed by considering the actual volume injected since the concentration varied across the five dose cohorts where all remaining parameters were fixed at the mean values previously optimized for a virtual human.(66) An additional sensitivity analysis was performed whereby the optimization of Vfrac was based solely on the CPT data obtained for a single dose level in the human investigation. An objective function calculated as the absolute, average deviation of the median predicted concentration vs. median

observed concentration at each nominal time point for each study cohort was employed to discriminate between models with and without an LDC.

6.2.5 Model Qualification

All simulations were performed using MATLAB® (v2014b, Mathworks). Adequacy of the model in describing the study population was assessed following simulation of 1000 virtual male subjects based on the study population characteristics with body weight constrained to the per protocol specified body weight (60-80 kg) and normal GFR (90-150 mL/min). Histograms were generated for height, weight and body mass index (BMI) to verify the generated population was consistent with the study population and included plausible individuals.

6.2.6 Sensitivity Analysis

A sensitivity analysis was performed to evaluate the model response to perturbation of the mean values of the parameters deemed to be the most uncertain and to evaluate the effect of incorporating or removing a distribution on certain parameters where the distribution was deemed uncertain. Mean parameter sensitivity was performed for Vfrac, σ_{sf}, σ_i, NRCL, LS and FGFR. For each perturbation, 100 individuals were simulated at the lowest dose level (45 mg) and one parameter at a time was perturbed by ±10%, except σ_{sf}, which was perturbed upwards of 1% to avoid any single organ σ_v from exceeding 1. To evaluate sensitivity, non-compartmental analysis was performed on the median (50^{th} percentile) simulated concentration vs. time profile to derive the AUC0-inf and Cmax. Change from the final model (with LDC) as a percent was expressed and plotted graphically by perturbation of the mean parameter value.

A sensitivity analysis on distributions was also performed by simulating 1000 individuals and either perturbing or removing a parameter distribution one at a time. The simulations for each scenario were plotted and compared. This analysis was completed to define the importance of specific parameter distributions on overall CPT variability.

6.3 Results

One of the primary objectives of this investigation was to develop a population generator with a lymphatic system component. As a population generator, the model produced a population consistent with the study population (Figure 6.2). With body height sampled from a normal distribution and total BM truncated to a range of 60-80 kg, the resultant BMIs fell largely within the typical range normally included in Phase 1 healthy volunteer research (18-28 kg/m^2), with only a few of the 1000 simulated individuals falling outside this range. The histogram for GFR, calculated as a product of the individual FF and renal plasma flow verified that the final population included only males with normal renal function within the specified range of 90-150 mL/min.

Figure 6.2: Model output anthropometric distribution of weight (upper left panel), height (upper right panel), body mass index (lower left panel) and derived glomerular filtration rate (lower right panel) for 1000 simulated individuals.

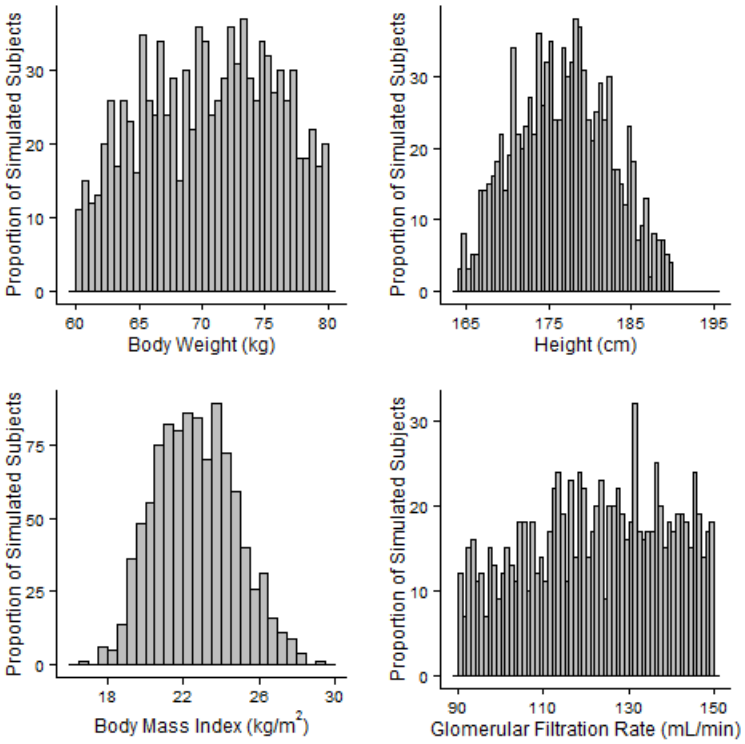

Using the mean virtual human model and the observed dose-normalized data, Vfrac was estimated with high precision (16.8%) with a mean and interindividual coefficient of variation of 0.25 (68%). This value represents the volume of LDC expressed as a fraction of the SC depot volume. Although sampled from a normal distribution, Vfrac for each individual was greater than zero for simulated individuals due to the truncation and constraining methods applied to the organ mass distributions. A sensitivity analysis confirmed that similar results were obtained regardless of whether Vfrac is sampled from a normal distribution with constraints versus sampling from a log-normal distribution suggesting the type of distribution does not influence the predictive capacity of the model.(125;126)

Figure 6.3, illustrates the comparison of the models with and without LDC when simulated for a population (n=1000, 200/dose level). Visual inspection of the log-log CPT (Figure 6.3, right panel) illustrates an over-prediction of the absorption phase when a LDC is not incorporated. Inclusion of LDC resulted in a reduction of the objective function from 107.11 to 21.10, relative to the model excluding LDC and improved the prediction of the absorption phase, particularly in the first 10 hours post-dose.

The model, with LDC, predicted the interindividual variability in all phases of the CPT (i.e. absorption, peak and elimination) with observed data points falling on either side of the 50th percentile curve and a few individual observations falling outside the 5th - 95th percentile ribbon. The one exception being a subject in the initial dose cohort (i.e. 45 mg dose) who clearly exhibited an anomalous profile, likely due to improper injection technique, as repeat analysis by the bioanalytical laboratory confirmed the measured concentration values.

Figure 6.3: Model simulated and observed plasma concentrations of a linear PEG-40 conjugated peptide versus time in humans on linear scale (left panel) and log scale (right panel). Within each panel, the left set of profiles represents the model without a lymph transit compartment and right side, with a lymph transit compartment incorporated. Closed geometric symbols represent unique individual subjects across 5 dose levels. Solid lines and grey shaded ribbon represents the median and 5th-95th percentile simulated concentrations from respective models.

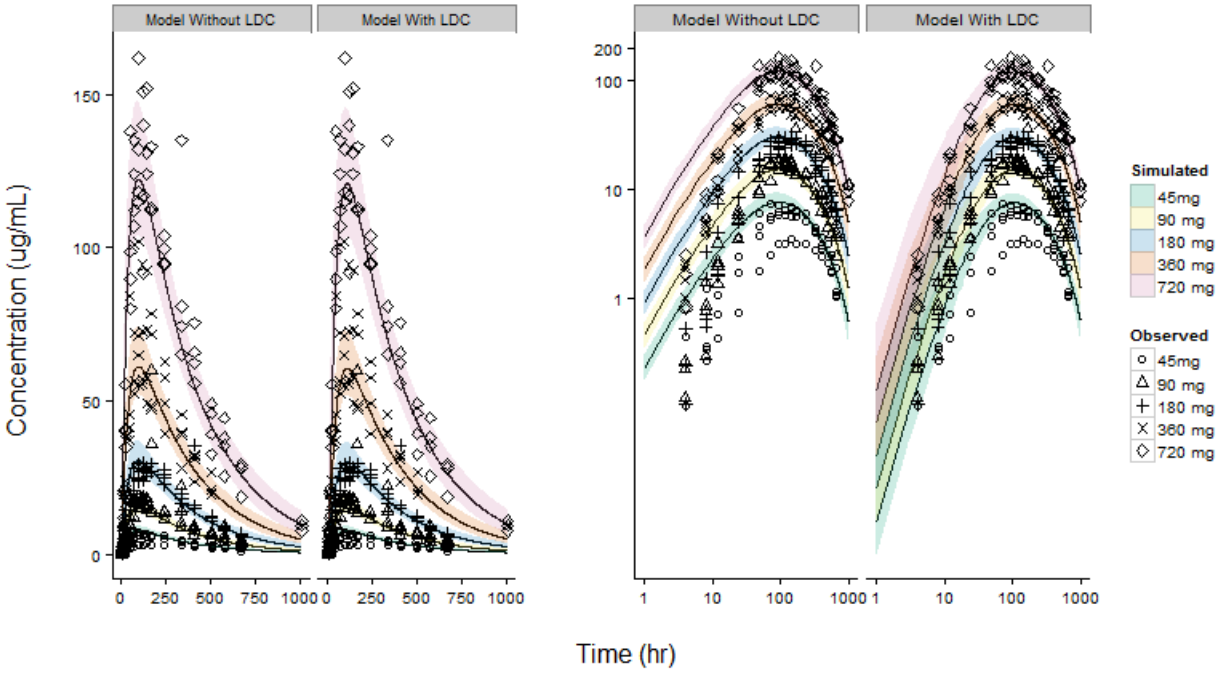

Using the one-at-a-time sensitivity test for mean parameters demonstrated that in spite of a profound influence on the early portion of the time course for this particular drug, the impact of parameter perturbation on peak and overall exposure (i.e. Cmax and AUC) was relatively small (Figure 6.4). The largest effect in terms of % change from the final model resulted from a -10% perturbation of σ_{sf} on both

Cmax and AUC. As described in the methods section, an upward perturbation was constrained to 1% to avoid any of the individual organ vascular reflection coefficients from exceeding 1. Even so, a one percent change in the mean vascular reflection coefficient scaling factor resulted in a visually detectable change in AUC and Cmax, confirming the model sensitivity to this parameter. Unsurprisingly, perturbations in FGFR and NRCL parameters, which influence renal and non-renal clearance, resulted in the next largest percent change in AUC, whilst having little influence on Cmax.

Figure 6.4: Mean parameter sensitivity perturbations vs. percent change in AUC (top left), Cmax (top right) and Tmax (bottom left) for the 50th percentile following simulation of 100 subjects. Closed geometric symbols represent perturbations as indicated in the legend.

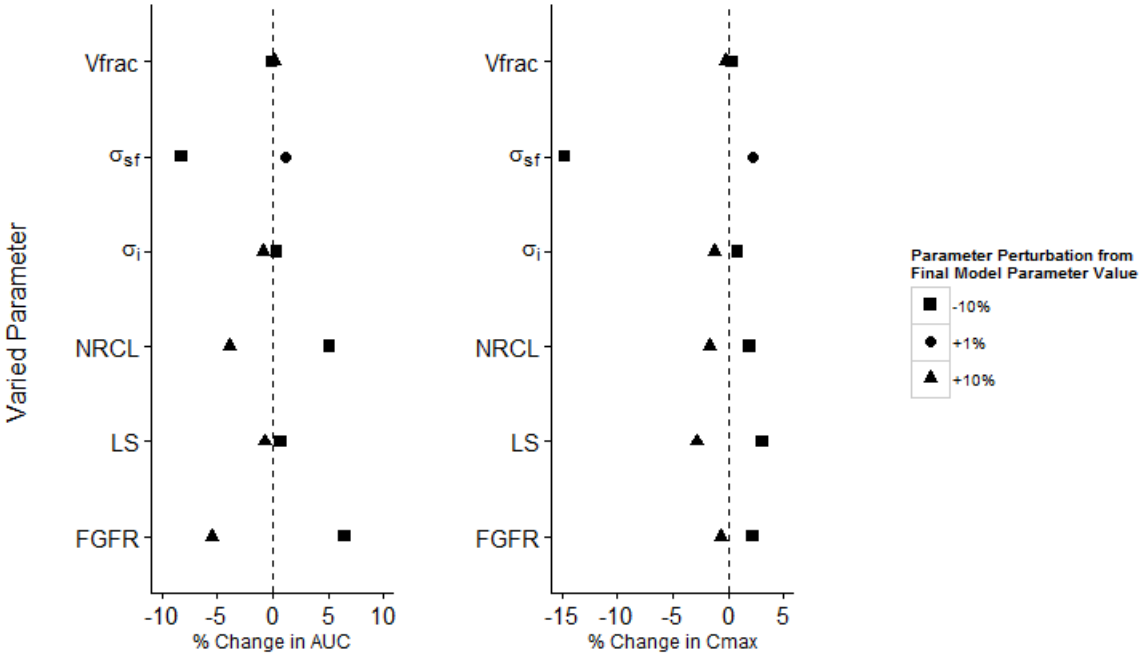

To illustrate the impact of varying parameter distribution assumptions on the three phases of the CPT, scenarios are presented on both linear and log scales (Figure 6.5). Of the parameters tested, applying a distribution assumption to LS, the parameter defining skin lymphatic flow as a fraction of skin blood flow, had the greatest influence on the interindividual variation in the absorption phase (Figure 6.5 panels 4 & 5). Whereas in the model development, only a mean valuefor LS was assumed, coefficients of variation of 10% and 50% were empirically selected and the width of the 5th-95th percentile ribbon expanded as the variability increased. In addition to LS, variability assumptions for the Vfrac parameter also influenced the interindividual variability in the absorption phase of the CPT. Halving and doubling the estimated variability

assumption from 68% to 34% and 136%, respectively resulted in a corresponding narrowing and widening of the simulated values supporting our hypothesis that the variability assumption for this parameter is important in the prediction an SC administered pegylated macromolecule CPT (Figure 6.5, panels 2 & 3). With respect to the peak portion of the CPT, variation in LS and blood volume appeared to be the most influential parameters when the distributional assumption was perturbed. For blood volume, the perturbation scenario included removing the variability in its entirety for this parameter and simulating a population based only on the mean blood volume value (Figure 6.5, panel 8). This change considerably narrowed the interindividual variability at the peak of the curve which leads to an imprecise prediction of Cmax, thus supporting the importance of including the selected blood volume variability employed in the final model.. Adding distributional assumptions to FGFR, which was assumed to be static for the final model simulations at 0.1% of GFR, resulted in an obvious broadening of the interindividual variability in the latter portion (i.e. elimination) of the CPT.(Figure 6.5, panel 11). Of the other parameters tested, none had obvious visually detectable effects across the stages of the concentration vs. time course.

Figure 6.5: Median (dashed line) and 5th-95th percentile (shaded ribbon) following simulation of 1000 virtual individuals on linear scale (left panel) and log scale (right panel). For sub-panels 1-11 in each panel, the following unique scenarios are presented: (1) Final model (2) 0.5-fold final model CV% for Vfrac (3) 2-fold final model CV% for Vfrac (4): Addition of 10% CV% on LS (5) Addition of 50% CV% on LS (6) Addition of 10% CV% on σi (7) Addition of 50% CV% on σi (8) Removing distribution on blood mass (9) Removing distribution on lymph mass (10) Removing distribution on skin mass (11) Addition of a 20% CV% on FGFR.

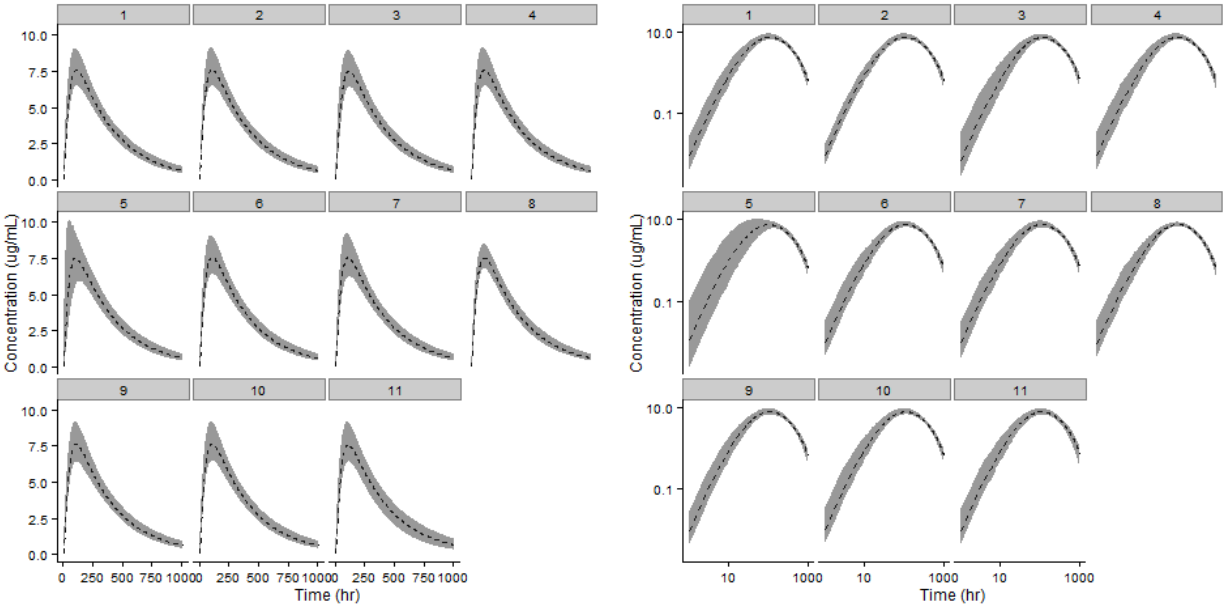

6.4 Discussion

The compound employed in the current evaluation and the base structural PBPK model were the same used in our previous publication illustrating the utility of incorporating a SC depot in the prediction of a human CPT directly from a single non-human primate species.(66) The molecule's biodistributional properties were assumed to be largely attributable to the pegylated moiety, which represents >96% of the molecular weight. The current *in silico* investigation demonstrates the scale-up from monkeys directly to a population of humans across a range of body sizes as opposed to a virtual human (weighing 70 kg).

The major objectives of this evaluation were two-fold and inter-related. The first being to develop a population PBPK model which incorporates distributional assumptions for the lymphatic system which could potentially be applied to large molecule PK predictions in a human population. The drug independent aspects of the model, being mechanistic in nature, can thus be applied to generating a population of individuals regardless of weight and height range and thus can be used to estimate the variability in a more diverse population than what was studied in the current report.

Conversion of the model to a population model was non-trivial as there is a paucity of literature to support integrating lymphatic anthropometric variability into PBPK models. Initially, we followed previous authors in terms of the distribution type (i.e. normal vs. log-normal) and, where possible, employed similar variability estimates (Table 6.1).(125;126) For some organ compartments however, either there was no information to inform said distribution or the variability appeared unusually high. It may seem counterintuitive to employ normal distributions with respect to organ sizes given the possibility of drawing implausibly small or even negative values. However, to be consistent with reported literature we elected to retain distributions as previously reported. Instead we performed an informal sensitivity analysis which concluded no appreciable difference in the prediction interval across the simulated dose cohorts regardless of whether a distribution was log-normal or not. In our final model we employed two tiers of safeguards to mitigate the risk of drawing extreme outliers or negative values when the distribution was set as normal, with the first being truncation to the 95^{th} percentile of the distribution and the second, constraining the lower bound to one tenth the mean value. Intuitively, where future data supports, population simulations should consider log-normally distributions to avoid the likelihood of negative or uncharacteristically low values being drawn from the distribution.

Prior to truncation of GFR, values within the initial population led to values interpreted as renally impaired or unusually high. After a thorough investigation, we confirmed that kidney perfusion and renal plasma flow on a per gram of tissue basis were consistently within the expected range and consequently the root cause was attributed to a larger than likely coefficient of variation for male kidney mass used as an input into the model.(125;126;130) As a further safeguard against inflated variability in kidney mass, especially given the importance of renal elimination to the drug in question, the model was set to reject any virtual individuals with GFRs less than 90 mL/min, due to being associated with renal impairment, and above 150 mL/min range, which normal healthy individuals rarely achieve, even when normalized to 1.73 kg/m^2 BSA.(137) This exercise suggests that reported values for kidney mass variability may necessitate further evaluation to ensure kidney function is appropriately simulated in the virtual population.

As described in the Methods section, we empirically assumed that the variability in lymphatic system volume would be equal to that of the variability in blood volume. Although there is not specific data to inform this hypothesis, lymphatic vessels represent a parallel circulatory system and thus an assumption of blood volume based on individual size was deemed a reasonable approach.

The second objective of this *in silico* investigation was to explore the advantage of incorporating a LDC to better represent local drainage from a SC depot space, to facilitate predictions of SC administered macromolecules.

Lymph collector vessels which run through the SC space picking up macromolecules, are reported to not reach the deep fascia until a node is reached, and from the skin can follow an unpredictable course, draining to multiple lymph nodes.(138) To address the lymphatic drainage of the drug from the SC site of administration by lymphatic capillaries, and to quantify the volume and variability in vessel volume, we elected to parameterize this compartment as a fraction of injection volume. The rationale for this approach is predicated on the assumptions that (1) there are multiple afferent vessels draining the site and (2) the drainage volume would increase as the volume of injection increases due to spreading within the interstitial space.(22) Precedent for this position is based on comparisons of high pressure SC auto injector and manual SC injection of recombinant human growth hormone, where increased pressure from the auto injector resulted in a higher and earlier CPT peak compared to a manual syringe, which was attributed to greater spread of injected material in the SC space.(139)

Other PBPK models with injection depots have employed varying assumptions for lymphatic drainage. Gill et.al. parameterized the SC depot as a fixed volume and lymph flow estimated from literature reports on

macromolecule disappearance from the SC site.(52) It's unclear why the authors, however, elected to estimate lymph flow for each study rather than rely on a standardized the lymph flow rate for skin. Lymphatic flow is a physiologic process and expected to be driven by anthropometric characteristics variability; consequently, the methods outlined by Gill do not appear to readily lend themselves to population simulations. Moreover, an assumption of a fixed volume being attributed to the SC depot is not realistic as injection volume varies from compound to compound, and study to study based on drug physicochemical properties and tolerability to the injected drug concentration. Tegenge & Mitkus, in simulated intramuscular (IM) injections of squalene-containing compounds, parameterized the lymphatic drainage by taking the total lymph node volume and applying the fraction of lymph nodes assumed to drain directly from the IM depot space.(140;141) This approach, however assumes the drainage occurs directly from injection site to a single node. However, patterns of lymphatic drainage from the skin are reported to vary substantially among individuals, even from the same area of the skin.(138)

Our model attempts to characterize local drainage by attributing a physical space representing the lymphatic capillary vessels the drug would journey through from the interstitial space to the lymph node, and is considered an additive volume to the lymphatic system as parameterized in the model proposed by Shah & Betts.(50) Although it is well established that lymphatic vessels drain from the skin, to our knowledge, an experimentally obtained value for this volume has not be determined. Consequently, it is challenging to build a purely mechanistic model describing this drainage. Gill et. al. considered the disappearance of labeled IgG from the SC space as a means of estimating the transit of drug from the injection site to the vasculature, and others have used estimation procedures to fit a transit time parameter.(50;52) However, a time parameter is not entirely mechanistic and cannot necessarily be relied upon for scaling up from preclinical species to human.

In contrast, parameterizing the LDC volume as a fraction of the injection volume represents an approach which assigns an anatomical volume to drug transit from the SC space to the lymph nodes relying on the skin lymph flow as a mechanistic driver of said transit. As this was the initial use of this methodology, no prior information was available to inform this value. Therefore we used mathematical estimation to optimize the value based on observed data obtained in the human population. Evaluation of the dose vs. exposure data suggested that the pharmacokinetic exposure was linear across the doses tested (unpublished data). Therefore we elected to perform the optimization based on all available observed data. However, as an informal sensitivity measure, we re-estimated Vfrac based on only a subset of the population which resulted in an indiscernible difference in the predicted vs. observed data (data not shown).

In the current model, the volume of the LDC was assumed to be dependent only on the injection volume, and independent of compound size. However, logically, spreading of drug particles within the SC space in theory could be influenced by the drug's physicochemical characteristics such as fluid viscosity and inactive excipients. Therefore, the utility of our methodology requires qualification with compounds across a broad pharmacologic class and molecular weight, among other characteristics, to qualify this approach for more general use.

Another consideration in developing PBPK models for PK predictions of macromolecules after SC administration is the bioavailability after SC injection. Macromolecules are reported to vary in terms of their SC bioavailability, independent of molecular weight.(18;39) The current compound was previously demonstrated to exhibit a relatively high SC bioavailability in primates at approximately 90% (data not shown). Our model was largely able to predict the exposure in humans when scaled from primates, by assuming non-renal clearance processes are proportional to the volume of the space clearance occurs in. The predictive capacity of our model requires additional work, testing broader group of macromolecules with a wide range of SC bioavailability, to be confidently applied in an a priori setting for drugs with unknown SC bioavailability.

Based strictly on a percent change in AUC and Cmax, perturbation of the mean LDC does not appear as influential in terms of peak and overall exposure. In this scenario where the half-life was on average greater than 200 hours based on non-compartmental analysis (data not shown), relying on the % change in AUC and Cmax is misleading, as inclusion of an LDC clearly was necessary to achieve the same profile shape as the observed data and resulted in a considerably smaller objective function. Inclusion of LDC only appears necessary to delay transit from the SC depot site immediately after administration. Following the initial transit through the lymphatics, drug mass that is not renally eliminated, recirculates to the organs. Drug mass that reaches the skin interstitial space that is not cleared by non-renal processes represents a relatively small proportion of the total circulating mass. Inclusion of a transit compartment draining from the full skin interstitial volume, parameterized identically to the drainage from the SC depot, consequently did not impact the model prediction (data not shown), and following the rule of parsimony, was excluded from the final model. However, incorporating lymphatic transit from the entire interstitial volume may have utility in other scenarios where multiple SC injection sites are being tested.

Despite the uncertainty in the mean and variability values included as input into the model for the lymph node compartment, the model was largely insensitive to the mean value of the lymph node. In contrast, the model exhibited the greatest sensitivity to the mean value for skin lymph flow likely as a consequence of the

route of administration being SC. This is consistent with our previously developed model for predicting the mean time course of the same drug in humans from primates.(66) We specifically observed a distinctly slower skin lymph flow was required relative to the current assumed range of 0.2-1% of blood flow to an organ (21) Lymph flow is inherently difficult to measure in humans and has been assumed to scale from animal values. As a fraction of blood flow, it may not be reasonable to assume lymph flow represents a similar fraction of blood flow across all organs, and in fact Baxter reported a wide range of organ lymph flow values in the mouse, with skin lymph flow representing the lowest rate as an absolute value across all organs reported.(101) Jones et. al. has stated that in spite of the wide range of reported lymph flows, many of the previously cited models fit the observed data well, and that this raises a fundamental question regarding model parameterization.(142) Jones goes on to state that approximately 0.07% of fluid entering the interstitial space returns to the blood via the lymph when considering net fluid recirculation. It is interesting to note that in our previous work for the same compound (66), the optimized skin lymph flow was 0.1%, very close to the 0.07% of blood flow suggested by Jones et. al. More importantly, these results reinforce the argument that models being developed for IV administration cannot simply be applied to SC administration without consideration of specific lymphatic drainage from the SC depot site.

Assuming interindividual variability of skin lymph flow resulted in a wider prediction ribbon in the absorption and peak portions of the curve. The shape of the ribbon, particularly around Cmax, confirms the vital importance of this parameter in models intended to simulate the SC profile of a macromolecule and also further supports the previously stated position that skin lymph flow may represent a smaller fraction of blood flow than previously assumed.

Further evaluation of model sensitivity suggested clearance mechanisms are important for characterizing the interindividual variability of this pegylated peptide in a population. As previously stated, despite the large molecular mass, pegylated compounds can be renally eliminated in primates and humans albeit slowly, at a rate of approximately 0.1% of GFR.(25) As renal clearance accounted for approximately one third of total body clearance we were particularly interested in whether changes in renal function would result in a change in peak and overall exposure. Perturbation of FGFR, which in the current model represents a fraction of GFR, can be interpreted as a surrogate for a change in renal function and the results of the sensitivity analysis suggested that changes in renal function precipitate a change in AUC. Whether this percent change is sufficient to warrant a change in the recommended dose however, is a function of the drug's safety profile and the relationship of exposure to safety.

6.5 Conclusion

This is the first PBPK model incorporating lymphatic system anthropometric interindividual variability for the purposes of simulating macromolecule PK in a population. As a population generator, this model is capable of simulating a population of individuals across a wide range of body weight and heights for use with other compounds with lymphatic distribution and transport. A novel proposal of incorporating an anatomical space representing lymphatic drainage by lymphatic capillaries appears critical in characterizing the early time course following drug absorption and the consequence of excluding the compartment results in poor prediction of the observed data in the early portion of the CPT. Variability in this lymph transit compartment and skin lymph flow exhibit the greatest influence on model prediction as it pertains to the absorption phase of the CPT following SC administration, whereas blood volume and renal clearance exhibit the largest apparent effect on Cmax and elimination phases of the curve, respectively.

CHAPTER 7: PREDICTION ACCURACY OF MODEL BASED METHODS, DISCUSSION AND CONCLUSIONS

7.1 Prediction Accuracy of Model Based Methods

Previous chapters proposed empirical and mechanistic model-based approaches to predict the pharmacokinetics (PK) of a pegylated peptide conjugate (PPC) following subcutaneous (SC) administration. Chapters 4-6 primarily focused on the time course prediction after SC administration, and model discrimination was based on qualitative improvements in the time course or in an objective function which was based on the difference in predicted vs. observed concentration values. To standardize the comparison of model-based and model-independent methods, a post-hoc analysis has been performed for the current chapter employing data obtained from the models described in chapter 4-6. Within the following sections a summary of the results for the model-based methods are presented (Section 7.2 and 7.3), followed by an overall comparison across model-based and model-independent methods (Section 7.4). Predictions were considered reasonable where the fold-error (FE), as described in Chapters 2 and 3, fell within a threshold of 0.7-1.3.

7.2 Prediction Accuracy of Model Based Scaling Scenarios in Chapter 4

Chapter 4 tested the utility of first fitting concentration vs. time data obtained in a single, nonhuman primate (NHP) species (i.e. cynomologus monkeys) to a population compartmental PK model, then scaling the model to human via incorporation of allometric expressions on each of the typical population values obtained in NHP. Specifically, the NHP obtained typical PK parameter value for a parameter was multiplied by the ratio of body weights of the two species, exponentiated to an empiric scaling factor. For clearance (CL) parameters (extravascular clearance, CL/F) and distributional CL, exponents of 0.85 and 1; for extravascular volume (V/F) and distributional volume an exponent of 1; and for first-order absorption processes exponents of -0.4 and 1 were each tested for prediction accuracy. Additionally, exponents for each parameter were fitted to the concentration vs. time data normalized to the initial lowest dose cohort (i.e. 45 mg) from a group of healthy male subjects participating in a first-in-human (FIH) investigation. Scenario 3, which assumed an exponent of 1 for all CL and V_d parameters, with a negative exponent of -0.4 for first-order absorption, exhibited the best visual agreement with the observed data. This scenario also resulted in the smallest objective function, which is a measure of difference between the observed and predicted results. As described in Section 7.1 of this chapter, prediction accuracy expressed by FE was the chosen metric for cross-method comparison and a FE falling within a threshold of 0.7-1.3 was considered a reasonable prediction. To facilitate the cross-method comparison, a vector of body weights (n=200 virtual human male subjects) was simulated corresponding to the range of actual body weight prescribed by the protocol for the FIH study described in Chapter 4. Concentration vs. time profiles were simulated for each virtual individual based on the model summarized in the above paragraph for Scenario 3, then non-compartmental analysis

(NCA) was used to obtain the secondary PK parameters. From the simulated NCA-derived PK parameters, an arithmetic mean value for each parameter of interest (See Table 7.1) was obtained. The simulations assumed the highest dose tested in the FIH study (i.e. 720 mg) and were compared to the arithmetic mean corresponding PK parameter from the observed data for subjects having received the same 720 mg dose (n=4). The 720 mg dose was selected as this dose resulted in concentrations which were quantifiable above the assay limit of quantitation for the longest duration of sampling post-dose.

Table 7.1: Prediction accuracy measured by fold-error within 0.7-1.3 of the arithmetic mean predicted PK parameters obtained from simulation (Chapter 4, Scenario 3) of a virtual population of male subjects (n=200) receiving a single, subcutaneous dose of 720 mg pegylated peptide conjugate compared to the arithmetic mean of the corresponding PK parameters in a group of actual human subjects receiving the same dose and regimen of a pegylated peptide conjugate in a FIH investigation

Parameter	Units	Predicted (Human)	Observed (Human)	Fold-Error	Criteria Achieved
Tmax	hr	131	126	1.00	Yes
Cmax	µg/mL	128	139	0.92	Yes
AUC0-t	µg•hr/mL	50993	56446	0.90	Yes
AUC0-inf	µg•hr/mL	53241	59742	0.89	Yes
CL/F	mL	13.6	12.2	1.10	Yes
Vz/F	mL/hr	4012	4154	0.97	Yes
$T_{1/2}$	Hr	204	235	0.87	Yes

PK parameters obtained via non-compartmental analysis

Evaluation of the FE clearly demonstrates close agreement between predicted and observed values, especially as they pertain to Tmax and Cmax. These results, which were obtained by scaling a set of population PK model parameters by empiric allometric exponents, support the hypothesis that an inverse allometric relationship exists between species body weight (or at least between small monkeys and humans) and first-order absorption rate.

7.3 Prediction Accuracy of Physiologically-Based Pharmacokinetic Models in Chapters 5 and 6

The physiologically-based pharmacokinetic (PBPK) model presented in Chapter 5 was developed with the intention to predict the PK time course of a SC administered PPC in a virtual 70 kg healthy human male subject and to compare said time course to the observed data from the first-in-human (FIH) dose escalation study. The NHP model was developed using anatomical and physiologic data corresponding to a NHP species, and simulation of the concentration vs. time profile following single-dose intravenous and subcutaneous administration of PPC to NHP demonstrated close agreement with the observed concentration data for the same species. The NHP model (was subsequently scaled to human anatomic and physiologic values for a typical 70 kg male. This model is referred to as the base PBPK model or base model for short. As described in Chapter 5, the base model did not allow for optimal characterization of the Tmax and Cmax of the observed data. Consequently the model was updated with a value for slower skin lymph flow (LS Opt model), which improved the model prediction of the time course of the drug, and particularly for Tmax. A further model revision was described in Chapter 6, developed to refine the prediction capacity of the absorption phase through incorporation of a local lymphatic drainage compartment from the SC depot space into the central lymphatics (lymphatic drainage compartment or LDC). Incorporation of a LDC (Vfrac model) resulted in a qualitative improvement based on graphical interpretation. Although the Vfrac model was originally presented in Chapter 6 in the context of a population PBPK model, to facilitate a cross-method comparison NCA-derived PK parameters were obtained for a simulation following a single-dose of PPC via the subcutaneous route for a virtual 70 kg human. Similar to the prediction accuracy assessment for the population PK model described in Section 7.2, NCA-derived PK parameters for the three PBPK model versions were compared to the mean of the observed data using the FE common metric. As with the analysis in Section 7.2 the highest dose cohort was selected for cross-method comparison of model-based methods as this dose resulted in the greatest number of concentration samples above the limit of quantitation for the longest duration post-dose.

Table 7.2: Prediction accuracy measured by fold-error within 0.7-1.3 of PBPK model versions comparing the PK parameters derived from the concentration vs. time profile obtained from a simulation for a virtual 70 kg human male and the arithmetic mean corresponding PK parameter of the observed human male subjects receiving a 720 mg single, subcutaneous dose of a pegylated peptide conjugate in a FIH investigation

		FE of predicted vs. observed					
Parameter	Units	Base	Criteria Achieved	LS Opt	Criteria Achieved	Vfrac	Criteria Achieved
Tmax	hr	0.57	No	0.76	Yes	0.95	Yes
Cmax	μg/mL	1.08	Yes	0.89	Yes	1.03	Yes
AUC0-t	μg•hr/mL	1.09	Yes	1.06	Yes	1.02	Yes
AUC0-inf	μg•hr/mL	1.33	No	1.31	No	1.28	Yes
CL/F	mL	0.79	Yes	0.80	Yes	0.82	Yes
Vz/F	mL/hr	1.11	Yes	1.14	Yes	1.27	Yes
$T_{1/2}$	hr	1.42	No	1.42	No	1.55	No

PK parameters obtained via non-compartmental analysis

Base: Base PBPK model empirically assuming skin lymph flow at 0.2% of blood flow

LS Opt: Base PBPK model with skin lymph flow optimized (0.1% of blood flow)

Vfrac: LS Opt PBPK model with a lymph drainage volume compartment parameterized as a fraction of the injection volume

Model improvements in Tmax were most obvious when the model incorporated a LDC (Vfrac model), where the improvements in prediction were largely confined to the earliest time points, and did not have a substantial adverse or positive effect in prediction of Cmax or AUC parameters relative to the other two PBPK model versions.

7.4 Cross-Method Comparison

7.4.1 Cross-Method Comparison of Key Pharmacokinetic Parameters

While CL and V_d parameters are considered critical parameters for describing the rate of removal and distribution of a drug, alone these parameters do not inform the time course of an extravascularly administered drug. In contrast, parameters such as Cmax and Tmax provide some insight into the time course and rate of drug input into the systemic circulation. Unfortunately, methods used to empirically scale a physiological process (e.g. CL) or a representation of a body compartment volume (V_d) such as single-species simplified allometry as presented in Chapter 3, do not lend themselves to comparing prediction accuracy of secondary PK parameters (e.g. Cmax and Tmax). Dedrick plots, which are considered empirical and model independent methods, however can potentially be used to predict the time course of drugs, although most frequently employed for intravenously (IV) administered compounds. This method was also employed in Chapter 3 to determine if there is potential utility in the prediction of secondary PK parameters (i.e. Cmax and Tmax) for a SC administered macromolecule. Dedrick plots rely on transformation of time and concentration scales for interspecies predictions. If the PK sample collection interval for the animal species is truncated, unusually sparse in number of samples, as is common in animal PK studies due to blood volume limitation, this can bias the estimation of the apparent elimination rate constant (λ) when using NCA methods. Consequently $T_{1/2}$ estimations would then be similarly biased since the $T_{1/2}$ is simply the natural log of 2 divided by λ. The preclinical dataset employed in this thesis for NHP terminated at 336 hours post-dose. Once the time scale was transformed to human according to the methodology outlined in Chapter 3, the predicted human dataset terminated at approximately 500 hours post-dose. This is in contrast to the observed human profile, which extended to approximately 1000 hours post-dose. Thus, Dedrick plot scaling is limited in utility in predicting the $T_{1/2}$ where the sampling time points are sparse or are prematurely terminated before a true elimination phase is characterized. Similarly, if the limit of assay quantitation is insufficient for, this case, the NHP plasma compared to human, this could also limit the utility of Dedrick plot prediction. As noted in Chapter 4 and 5, the limit of assay quantitation was the same for both human and NHP assays.

Table 7.3 illustrates cross-method comparison of model-independent and model-based methods for estimating clearance and volume parameters. With the exception of single-species allometric (SSA) methods relying on a fixed exponent for CL of 0.85, the prediction accuracy criteria of FE within 0.7-1.3 was achieved in all cases regardless of the method employed. Perhaps a more discriminating evaluation for a SC administered macromolecule is the cross-method comparison of secondary PK parameters which inform

the rate of absorption following administration (i.e. Cmax and Tmax). Table 7.4 illustrates the advantage of model-based evaluations here. Since SSA methods only consider processes and not secondary PK parameters, the SSA method is omitted for said comparison. The sheer fact that this method is incapable of informing secondary PK parameters highlights one major disadvantage. As Dedrick plots do potentially allow for estimation of secondary PK parameters, it was included as the sole model-independent method in the following comparison.

Table 7.3: Cross-method prediction accuracy of extravascular clearance (CL/F) and volume of distribution (V/F) for model-independent and model-based scaling methods measured by fold-error within 0.7-1.3

Method	Parameter	Fold-Error	Criteria Achieved
SSA	CL/F	0.67	No
Dedrick Plot	CL/F	0.72	Yes
MMSA (Scenario 3)	CL/F	1.10	Yes
PBPK (base)	CL/F	0.79	Yes
PBPK (LS Opt)	CL/F	0.80	Yes
PBPK (Vfrac)	CL/F	0.82	Yes
SSA	V/F	0.89	Yes
Dedrick Plot	V/F	0.93	Yes
MMSA (Scenario 3)	V/F	0.97	Yes
PBPK (base)	V/F	1.10	Yes
PBPK (LS Opt)	V/F	1.14	Yes
PBPK (Vfrac)	V/F	1.27	Yes

Table 7.4: Cross-method prediction accuracy of Cmax and Tmax for model-independent and model-based scaling methods measured by fold-error within 0.7-1.3

Method	Parameter	Fold-Error	Criteria Achieved
Dedrick Plot	Cmax	1.10	Yes
MMSA (Scenario 3)	Cmax	0.92	Yes
PBPK (base)	Cmax	1.10	Yes
PBPK (LS Opt)	Cmax	0.89	Yes
PBPK (Vfrac)	Cmax	1.00	Yes
Dedrick Plot	Tmax	0.67	No
MMSA (Scenario 3)	Tmax	1.00	Yes
PBPK (base)	Tmax	0.57	No
PBPK (LS Opt)	Tmax	0.76	Yes
PBPK (Vfrac)	Tmax	0.95	Yes

Where Table 7.3 suggests any of the tested methods may be appropriate for interspecies scaling prediction of the human PK for PPC, comparison of Cmax and Tmax FE as expected, are more discriminating parameters. Dedrick plots were able to predict the peak with reasonable FE, however clearly fell short on Tmax. Referring back to Chapter 3, this failure to predict is likely based on the fact that Dedrick plots do not account for any interspecies differences in absorption processes. MMSA methods (Chapter 4, Scenario 3), which assumed CL and V_d were proportional to species body weights and where first-order absorption processes where inversely proportional to body weight performed quite well in terms of Cmax and Tmax. However, it should be noted that hypothesis for MMSA based scaling was that an exponent of 0.85 would be most appropriate for CL parameters, which was not the case. Lastly, PBPK based models, when accounting for slower skin lymph flow in humans relative to NHP as a fraction of skin blood flow, performed well for both Cmax and Tmax parameters (LS Opt model) and improved considerably when further model refinement considered a lymphatic drainage compartment (Vfrac model).

7.4.2 Time Course Cross-Method Comparison

Although qualitative in nature, predicting the shape of the concentration vs. time profile after extravascular administration is of critical importance as it helps inform future study design (e.g. optimal PK sampling strategy). Of the model independent methods assessed in this thesis, only Dedrick plots (Chapter 3) facilitate

time course scaling. However, evaluation of the predicted vs. observed human time course highlights the limitation of this method. The PK sampling schedule for NHP, as described earlier in this chapter, terminated prematurely such that when scaled to a human time scale characterized approximately 50% of the elimination profile (Figure 3.4a). Upon evaluation of the log-log scale for the Dedrick plot (Figure 3.4b) a clear over-prediction is evident during the absorption phase. This is an inherent limitation of Dedrick plots in extravascular administration which do not consider scaling/normalization of absorption processes. Figures 4.4a and 4.4b illustrate the predictive capacity of the time course for the various scenarios tested and although the FE for key PK parameters suggest Scenario 3 is an accurate method, (1) this method was entirely empiric and furthermore assumed an allometric scaling factor of 1 on CL (as opposed to 0.85) and (2) exhibits clear over-prediction at the earliest portions of the absorption phase. In contrast, when optimized for lymphatic flow rate, the Vfrac PBPK model (Chapter 6) qualitatively resulted in the best prediction of the observed data, across the entire sampling time profile.

7.5 Discussion

The genesis of this project originated from a perceived need for improved macromolecule PK predictions following SC administration. Traditional methods have largely entailed scaling mean PK parameters such as total body CL across species based on empiric scaling factors. As discussed in several sections throughout this thesis, scaling of mean CL provides no information on the time course of a drug in the body following administration. Following extravascular administration, the concentration in the blood rises as drug is absorbed into the systemic circulation. With SC administration, CL at the site of administration or during lymphatic transit can potentially alter the bioavailability of the macromolecule. Additionally, the biodistribution pattern can alter the rate of transit into the systemic circulation with the contribution of lymphatic uptake as a major route of systemic absorption increasing correspondingly with molecular size of the drug.(16-18;143) Combined, these factors confer uncertainty in prediction of large molecule PK following SC administration from animal to human.

In the simplest of terms, this thesis project evaluated the utility of model-based predictions of the time course of a macromolecule in the blood stream after SC administration relative to model-independent methods. Human PK of a PPC was projected from a single NHP . Fortuitously, an industrial benefactor provided concentration vs. time data for this compound following IV and SC in NHP and SC in humans.

As with any prediction method, evaluation of a single compound is likely insufficient to draw any definite conclusions as to future predictions and is a limitation of the current thesis project. The results and

conclusions drawn from this thesis may however have broader application beyond the current molecule. The molecular weight of the pegylated moiety is approximately 44 kDa, which classifies the compound as a macromolecule. However, macromolecules vary in terms of their structural, physical and chemical properties. Being a pegylated peptide, it may be challenging to extrapolate the findings to other non-pegylated compounds or those with much smaller or much larger molecular size. Pegylation has been reported to increase the hydrodynamic radius of conjugates beyond the molecular radius, resulting in a biodistribution pattern similar to larger macromolecules such as mAbs.(12;32) As such, the observations from the current thesis may have broader application than simply to pegylated peptides with a similar molecular weight to that of the current compound.

Prior to exploring the prediction utility of computationally intensive model-based methods, a benchmark in terms of prediction accuracy had to be established. Chapter 2 reviewed a number of methods used for PK prediction from animal species, not all of which are applicable to macromolecules. As explained in the introductory chapter (Chapter 1), CL of macromolecules can occur following interaction of the drug with its target receptor. Interspecies differences in target expression and target affinity may preclude the usefulness of studying the drug PK in several species. Confirmation from the benefactor of data for the current compound confirmed that the activity of the drug is similar in NHPs and humans but not active in rodents or canine species. Consequently, only single-species methods were considered in Chapter 3 for the purposes of setting a benchmark of prediction accuracy of model independent methods.

Chapter 2 also served to introduce a metric of prediction accuracy and to establish what would constitute reasonable prediction accuracy for both model-independent methods and model-based method development. Prediction accuracy throughout this thesis has been expressed in terms of FE with a perfect prediction resulting in a value of unity (i.e. 1). FE is a logical and relatively easy method to interpret, applicable for expressing prediction accuracy of a single method for single compound; or averaged across a group of compounds to express the prediction accuracy of a single prediction method. Prediction error and root mean square error have also been reported by several authors, and is useful for rank ordering methods based on lower error, however an absolute threshold for what constitutes reasonable prediction accuracy has not been proposed.(75;96;144)

For the work embodied within this thesis, and as proposed in Chapter 2, a 2-fold error was deemed too broad a threshold of acceptance.(145) A case study example in Chapter 2 was used to illustrate that such a wide threshold could potentially produce a false positive in terms of bioequivalence potential, when applied to a biosimilar. Consequently, a FE falling within 0.7-1.3 was proposed in this thesis as a more reasonable

threshold of prediction accuracy. Such a threshold would also be expected to provide a greater degree of confidence for a novel biologic transitioning from preclinical evaluation to a FIH investigation.

In terms of single-species, model-independent methods, allometric scaling with fixed exponents, and Dedrick plots were employed to establish a benchmark for prediction accuracy. Based on the experience from several publications, Chapter 2 concluded that an exponent of 0.85-0.95 for CL and approximately 1 for V_d, are reasonable empiric scaling factors for NHP to human extrapolation when model-independent or model-based methods were employed to estimate parameters of macromolecules exhibiting linear PK.(55) For empiric, SSA, a value of 1 was indeed accurate for volume parameters and when examining the molecules in Chapter 2, 0.85 resulted in reasonable prediction accuracy of CL for the many of compounds evaluated. For PPC however, following SC administration, an empiric assumption closer 1 was required to meet the acceptance criteria; however the reason for this is unclear.

For benchmarking purposes exponents of 0.85 and 1 were initially tested for prediction accuracy of model-independent CL and V_d parameters in Chapter 3. Consistent with previous observations, the V_d similarly scaled with an exponent of 1 with FE near unity. In contrast, CL/F required a scaling factor closer to 1 (as opposed to 0.85) to achieve good prediction accuracy. Although other authors have achieved successful prediction accuracy of single-species macromolecule CL using NHP data and scaling exponents >0.75 but less than 1, no particular trend in terms of type of macromolecule and scaling exponent has been offered to improve *a priori* predictions.(61) Unsurprisingly, model-independent methods did not perform especially well in informing the absorption profile of the drug after SC administration. Although the Dedrick plot approach employed in Chapter 3 predicted Cmax reasonably well, Tmax predictions fell outside the acceptance criteria. The discussion section of Chapter 3 addresses potential sources of poor prediction in the absorption phase with this method such as inconsistent or insufficient characterization of the PK in the NHP data, however additional testing of this method with SC administered macromolecules is warranted before a definitive conclusion can be made with respect to this method.

Examination of an empiric relationship between NHP and humans in terms of macromolecule absorption from the SC space was the focus of Chapter 4. Model-based compartmental approaches proposed in Chapter 4 allowed for derivation of parameters defining absorption processes. Only a few cases of macromolecule scaling after SC absorption using compartmental approaches have been published, however where evaluated, first-order rate processes suggest an inverse relationship between species size (body weight) and absorption rate.(91;104) Derivation of NCA parameters from the model simulated concentrations in Chapter 4 exhibited excellent agreement with observed data, particularly in terms of Cmax and Tmax, when an

empirically selected exponent of -0.4 on absorption rates was used. In contrast, assumptions of an exponent ranging from 0 to 1 resulted in extremely poor prediction with the Tmax grossly under predicted as the exponent approached a value of one. The basis for this observation may be rooted in interspecies differences in skin anatomy and lymph flow from the skin, and were addressed in greater detail in Chapter 4.

Despite the successful prediction accuracy with empiric scaling factors, there is still substantial uncertainty as to which parameters scale directly with body weight and which deviate from this direct weight-based relationship. In the current thesis project, an assumption was that all model parameters would scale to some degree with body weight and the scaling factor exponents were a priori selected based on theoretical knowledge or informed from some previous literature reports. This is an inherent limitation in all empiric allometric scaling methods, however results of the current investigation suggest this empiric modeling approach may work reasonably well for the purpose of planning a FIH study.

In Chapter 5, an alternative mechanistically focused approach to scaling was attempted. At the point of writing of the work in this chapter, PBPK models capable of describing the time course of macromolecules with lymphatic uptake from the SC space had not been previously published. The absence of a predefined strategy for overcoming this uncertainty presented an opportunity to construct a novel means of addressing this problem. In contrast to several previous whole-body PBPK models incorporating lymphatic biodistribution for macromolecules following IV administration(48;50;51;101;102), the model developed as part of this thesis work offered a unique proposal whereby skin lymph flow was partitioned between the SC injection depot space and the remaining interstitial space proportionally based on the relative volume each space occupied. This modification allowed for incorporating lymph flow from the SC depot injection space whilst maintaining overall model flow balance (i.e. where flow into the lung equated to flow out of the lung compartment - see Figures 5.2 a and b and Figures 6.1 a and b).

A unique attribute of PBPK model-based scaling is that it allows for parameterization of local CL mechanisms. For the PBPK model in Chapter 5, CL was defined as both renal and non-renal processes, where the non-renal portion was estimated from the animal data and scaled based on body weight from NHP to humans. CL was then proportionally allocated to each anatomical space based on volume, which allowed for a portion to be allocated to the SC depot space. Although total non-renal CL was not mechanistically derived, apportioning of clearance was performed based on relative anatomical volume thus maintaining a mechanistic element. This base PBPK model was able to largely account for the bioavailability following SC administration to humans and produce concentrations with reasonable concordance to the observed data (Table 7.2), however failed to accurately predict the Tmax.

Prediction of bioavailability of macromolecules from animal species following SC administration historically has been challenging.(18) The root of these challenges may be in part due to a failure to adequately characterize CL processes in the animal species being studied, such that uncertainty in the scaling step is inflated.

In the current thesis project, CL was parameterized as a linear process, as the dataset provided only a single dose level following IV and SC administration in NHP. Consequently non-linear processes could not be identified. Estimating CL from a single dose level may be sufficient if the drug exhibits linear PK, however dose-dependency in absorption processes and bioavailability have been observed with therapeutic macromolecules and should be tested experimentally.(41)

Although the models in the current thesis did not incorporate non-linear processes, the workflow and processes developed in Chapters 4-6 are readily adaptable to incorporation of non-linear processes with the potential to scale across species. Chen et. al. characterized dose-dependent absorption of exenatide (approximately 4 kDa peptide) across several preclinical species with a Michaelis Mentin (MM) expression.(146) The MM constants Vmax and Km, were found to be proportional to the preclinical species and human body weight with scaling exponents of 0.392 and 0.605, respectively. Dong et. al. integrated MM expressions in clearance to characterize non-linear PK for a series of monoclonal antibodies (mAbs) in NHP for prediction in humans.(64) Vmax and Km were scaled with a theoretical exponent of 0.75 based on similar in-vitro binding of the receptor in both NHP and humans. In contrast to other reports, first order absorption processes were assumed to scale directly with body weight between NHP and humans (as opposed to inversely).

Another limitation in the model-based development, particularly as it pertains to Chapters 5 and 6, was the assumption of skin lymph flow. Zhao et. al. suggested lymph flow is the most important driver of Tmax following SC administration of mAbs.(109) The value assigned for skin lymph flow in the PBPK models was carried over from a previous platform PBPK model developed for IV administered mAbs and where the source was reported for humans, and set at a fraction of the skin blood flow.(21;50) Sensitivity analyses performed in Chapters 5 and 6 confirm lymph flow from the skin is indeed a critically important parameter in predicting Tmax following SC administration. Precise quantitation of lymph flow is difficult to verify experimentally, and therefore remains a potential source of uncertainty for future extrapolations.

Chapter 6 expanded the model development in Chapter 5 to a population-based PBPK model to explore the impact of anthropometric variability in the prediction of the drugs time course after SC absorption. Upon further review from the models in Chapter 5 it was determined that further refinement of the model was possible to improve the prediction accuracy in the early time portion. As described in Chapter 6, an anatomical volume compartment representing lymphatic vessels draining from the SC depot was introduced into the model. As PBPK models are intended to be mechanistic in nature, an attempt was made to estimate this drainage volume from the NHP data. However, the sampling time points were too sparse in the early portion of the SC time course to reliably estimate a value for this parameter in the primates. Thus, the lymphatic drainage was parameterized as a fraction of the injection volume. Integrating the drainage volume resulted in a substantial improvement in the Tmax prediction (Table 7-2), along with smaller improvements in the Cmax and AUC parameters. The validity of this method of parameterization for routine extrapolation requires further evaluation with a broader group of compounds to confirm its generalizability.

While the majority of this chapter has focused on cross-method comparisons of a mean PK parameter or mean concentration vs. time curve for a virtual human being, a major aspect of Chapter 6 was the development of a population based PBPK model. Mean PK values are inherently biased estimates. With respect to PK parameter estimation, a mean value may or may not be appropriate to use in predictions, depending on the intended application. For example, if the intention is to predict the PK of a novel drug in a relatively homogenous group of healthy male subjects for a FIH investigation, perhaps a mean virtual human prediction would suffice to guide study design and predict the dose needed to achieve a particular concentration of the drug in the blood stream intended for systemic action. However, if the intention is to apply a PBPK models in the prediction of a renally eliminated drug, for a range of renal impairment and normal renal function, prediction of a mean individual is likely insufficiently informative to guide a risk assessment.

In contrast, a population PBPK simulation facilitates estimation of an unbiased population mean for the concentration vs. time profile, as well as a range of potential outcomes for systemic exposure. For macromolecule PBPK model development, incorporation of the lymphatics is crucial as it plays an important role in the biodistribution of macromolecules. Moreover, knowledge of the interindividual variability of the lymphatic system volume is an important input into a population PBPK model intended to simulate the PK of a macromolecule. At the time of this thesis work, published PBPK models for the prediction of macromolecules PK focused solely on a virtual human subject and thus did not consider interindividual variability. Published population PBPK models, which were likely developed for small

molecules, omitted a lymphatic system compartment. Thus, there was a dearth of knowledge to inform the development of a population based PBPK model for macromolecules.

As the lymphatic system is considered a parallel circulatory system, and typically lymph vessels are collocated with blood vessels in many tissues, the interindividual variability for blood volume in humans was similarly applied to lymph volume. The resultant population PBPK model was capable of simulating the interindividual variability of the entire time course of a macromolecule following a single-dose SC administration.

The most intuitive applications of said population model are direct scaling from animals to a population of individuals as opposed to a virtual human being. The potential advantage of this simulation-based approach, particularly in the context of a FIH investigation, is greater confidence in the prediction of systemic exposure of a novel compound, particularly when the intended study population participating in the trial is not especially homogenous and exhibits a wide range of body compositions.

Returning to the example of a renally cleared drug, for PPC, renal clearance represented a significant route of elimination. By altering mechanistic aspects of the model, such as glomerular filtration rate in the virtual population, the model could be theoretically extended to predict the range of systemic exposure in individuals with various degrees of renal impairment. As the drug may be administered to individuals with renal impairment, knowledge of the anticipated exposure in an impaired population can help inform dose adjustments for clinical use, or guide the design of a formal study in varying degrees of renal impairment.

Accurate and reproducible prediction of macromolecule bioavailability across a wide range of compounds following SC administration remains elusive. The current model forms the basis for future assessment of mechanistic determinants of SC bioavailability in a population. In the event that local clearance processes in lymphatic tissue or interstitial fluid can be estimated *in-vitro* or *ex-vivo*, such processes can potentially be incorporated into the model. While evaluation of interstitial fluid has not been commonly reported, harvesting of lymph fluid in animals via cannulation techniques has been reported in the literature.(16;22)

7.6 Conclusion

Scaling the PK of a therapeutic macromolecule is fraught with uncertainty. Where empiric allometric scaling factors may be useful for predicting overall exposure of drugs exhibiting linear PK, these methods are not useful for predicting the absorption processes following SC administration nor applicable for drugs exhibiting non-linear PK. Compartmental modeling offers an opportunity to predict the overall time course of a SC administered drug, and can potentially incorporate non-linear processes, however is highly dependent on the *a priori* selection of empiric scaling factors. At this point, it is unclear whether the prediction capacity of empiric model-based methods is compound specific or broadly applicable. As such, there is greater uncertainty with such predictions, particularly with respect to absorption processes. PBPK modeling offers a mechanistic approach to interspecies scaling and where data is available to inform mechanistic processes, also provides for the least uncertainty in predicting the SC time course. With respect to the pegylated peptide conjugate employed in the current thesis project, model-based methods provided superior prediction of absorption phase of a SC administered macromolecule. Moreover, PBPK methods provide the greatest potential for *a priori* prediction of the time course following SC administration.

Bibliography

(1) A Panoramic View of the Emerging Biosimilar Landscape. Datamonitor plc; 2008. Report No.: DMHC2426.

(2) Baumann A. Nonclinical development of biopharmaceuticals. Drug Discov Today 2009 Dec;14(23-24):1112-22.

(3) Baumann A. Early development of therapeutic biologics--pharmacokinetics. Curr Drug Metab 2006 Jan;7(1):15-21.

(4) Geary RS, Norris D, Yu R, Bennett CF. Pharmacokinetics, biodistribution and cell uptake of antisense oligonucleotides. Adv Drug Deliv Rev 2015 Jun;87:46-51.

(5) U.S. Food and Drug Administration Draft Guidances for Biosimilars. FDA Website 2012 [cited 2016 May 11];Available from: URL: http://www.fda.gov/Drugs/DevelopmentApprovalProcess/HowDrugsareDevelopedandApproved/ApprovalApplications/TherapeuticBiologicApplications/Biosimilars/default.htm

(6) Questions and answers on biosimilar medicines (similar biological medicinal products). EMA Website. 2012. European Medicines Agency, Committee for Medicinal Products for Human Use. 10-27-2012.

(7) Bioavailability and BioequivalenceStudies for Orally Administered Drug Products - General Considerations. FDA Website 2003Available from: URL: http://www.fda.gov/ohrms/dockets/ac/03/briefing/3995B1_07_GFI-BioAvail-BioEquiv.pdf

(8) Guideline on the Investigation of Bioequivalence. 2010. European Medicines Agency, Committee for Medicinal Products for Human Use.

(9) Alberts B, Johnson A, Lewis J, Raff M, Roberts K, Walter P. Membrane Transport of Small Molecules and the Electrical Properties of Membranes. Molecular Biology of the Cell. 4th ed. New York: Garland Science; 2002.

(10) Rippe B, Haraldsson B. Transport of macromolecules across microvascular walls: the two-pore theory. Physiol Rev 1994 Jan;74(1):163-219.

(11) Mehta D, Malik AB. Signaling mechanisms regulating endothelial permeability. Physiol Rev 2006 Jan;86(1):279-367.

(12) Sarin H. Physiologic upper limits of pore size of different blood capillary types and another perspective on the dual pore theory of microvascular permeability. J Angiogenes Res 2010;2:14. Open access from http://www.ncbi.nlm.nih.gov/pmc/articles/PMC2928191/pdf/2040-2384-2-14.pdf.

(13) Rothschild MA, Bauman A, Yalow RS, Berson S. Tissue distribution of I131 labeled human serum albumin following intravenous administration. J Clin Invest 1955 Sep;34(9):1354-8.

(14) Tojo A, Kinugasa S. Mechanisms of glomerular albumin filtration and tubular reabsorption. Int J Nephrol 2012: Open access from http://www.hindawi.com/journals/ijn/2012/481520/.

(15) Dahlberg AM, Kaminskas LM, Smith A, Nicolazzo JA, Porter CJ, Bulitta JB, et al. The Lymphatic System Plays a Major Role in the Intravenous and Subcutaneous Pharmacokinetics of Trastuzumab in Rats. Mol Pharm 2014;11(2):496-504.

(16) Supersaxo A, Hein WR, Steffen H. Effect of molecular weight on the lymphatic absorption of water-soluble compounds following subcutaneous administration. Pharm Res 1990 Feb;7(2):167-9.

(17) Supersaxo A, Hein W, Gallati H, Steffen H. Recombinant human interferon alpha-2a: delivery to lymphoid tissue by selected modes of application. Pharm Res 1988 Aug;5(8):472-6.

(18) Richter WF, Bhansali SG, Morris ME. Mechanistic determinants of biotherapeutics absorption following SC administration. AAPS J 2012 Sep;14(3):559-70.

(19) Wang W, Chen N, Shen X, Cunningham P, Fauty S, Michel K, et al. Lymphatic transport and catabolism of therapeutic proteins after subcutaneous administration to rats and dogs. Drug Metab Dispos 2012 May;40(5):952-62.

(20) Charman SA, Segrave AM, Edwards GA, Porter CJ. Systemic availability and lymphatic transport of human growth hormone administered by subcutaneous injection. J Pharm Sci 2000 Feb;89(2):168-77.

(21) Swartz MA. The physiology of the lymphatic system. Adv Drug Deliv Rev 2001 Aug 23;50(1-2):3-20.

(22) Porter CJ, Edwards GA, Charman SA. Lymphatic transport of proteins after s.c. injection: implications of animal model selection. Adv Drug Deliv Rev 2001 Aug 23;50(1-2):157-71.

(23) Olszewski W, Engeset A, Jaeger PM, Sokolowski J, Theodorsen L. Flow and composition of leg lymph in normal men during venous stasis, muscular activity and local hyperthermia. Acta Physiol Scand 1977 Feb;99(2):149-55.

(24) O'Morchoe CC, Jones WR, III, Jarosz HM, O'Morchoe PJ, Fox LM. Temperature dependence of protein transport across lymphatic endothelium in vitro. J Cell Biol 1984 Feb;98(2):629-40.

(25) Baumann A, Tuerck D, Prabhu S, Dickmann L, Sims J. Pharmacokinetics, metabolism and distribution of PEGs and PEGylated proteins: quo vadis? Drug Discov Today 2014 Jun 11;19(10):1623-31.

(26) Caliceti P, Veronese FM. Pharmacokinetic and biodistribution properties of poly(ethylene glycol)-protein conjugates. Adv Drug Deliv Rev 2003 Sep 26;55(10):1261-77.

(27) Van der AP, Platzer E, Xu ZX, Schulz R, Feugeas O, Capdeville R, et al. Pharmacodynamics and pharmacokinetics of single doses of subcutaneous pegylated human G-CSF mutant (Ro 25-8315) in healthy volunteers: comparison with single and multiple daily doses of filgrastim. Am J Hematol 2001 Apr;66(4):245-51.

(28) Neulasta Prescribing Information. Amgen Website 2016 [cited 2016 Apr 30];Available from: URL: http://pi.amgen.com/united_states/neulasta/neulasta_pi_hcp_english.pdf

(29) Neupogen Prescribing Information. Amgen Website 2016 [cited 2016 Apr 30];Available from: URL: http://pi.amgen.com/united_states/neupogen/neupogen_pi_hcp_english.pdf

(30) Roferon-A Prescribing Information. FDA Website 2016 [cited 2016 Apr 30];Available from: URL: http://www.accessdata.fda.gov/drugsatfda_docs/label/2006/103145s5060LBL.pdf

(31) Pegasys Prescribing Information. Genentech Website 2016 [cited 2016 Apr 30];Available from: URL: http://www.gene.com/download/pdf/pegasys_prescribing.pdf

(32) Kusterle M, Jevsevar S, Porekar V. Size of Pegylated Protein Conjugates Studied by Various Methods. Acta Chim Slov 2008;55:594-601.

(33) Novel New Drug 2014. 2015. U.S. Food and Drug Administration, Center for Drug Evaluation and Research.

(34) Kolarsick BS, Kolarsick MA, Goodwin C. Anatomy and Physiology of the Skin. Oncology Nursing Society 2011 [cited 2016 Apr 30];(1):1-12. Available from: URL: https://ebooks.ons.org/book/site-specific-cancer-series-skin-cancer

(35) Kalman M, Csillag A. The Skin and Other Diffuse Sensory System. In: Csillag A, editor. Atlast of the Sensory Organs: Functional and Clinical Anatomy.New Jersey: Humana Press; 2005. p. 199-243.

(36) Frost GI. Recombinant human hyaluronidase (rHuPH20): an enabling platform for subcutaneous drug and fluid administration. Expert Opin Drug Deliv 2007 Jul;4(4):427-40.

(37) Dao L, Jacobs J, Kuebler P, Bakker B, Lippe B. Bioequivalence studies for three formulations of a recombinant human growth hormone: challenges and lessons learned. Growth Horm IGF Res 2010 Oct;20(5):367-71.

(38) Guidance on Nonclinical Safety Studies for the Conduct of Human Clinical Trials and Marketing Authorization. ICH Website 2009Available from: URL: http://www.ich.org/fileadmin/Public_Web_Site/ICH_Products/Guidelines/Multidisciplinary/M3_R2/Step4/M3_R2__Guideline.pdf

(39) Wang W, Wang EQ, Balthasar JP. Monoclonal antibody pharmacokinetics and pharmacodynamics. Clin Pharmacol Ther 2008 Nov;84(5):548-58.

(40) Gabrielsson J, Weiner D. Pharmacokinetic & Pharmacodynamic Data Analysis: Concepts and Applications. 4th ed. Stockholm: Sweedish Pharmaceutical Press; 2000.

(41) Mager DE, Neuteboom B, Efthymiopoulos C, Munafo A, and Jusko WJ. Receptor-mediated pharmacokinetics and pharmacodynamics of interferon-beta1a in monkeys. Journal of Pharmacology and Experimental Therapeutics 2003;306(1):262-70.

(42) Mager DE, and Jusko WJ. Receptor-mediated pharmacokinetic/pharmacodynamic model of interferon-beta 1a in humans. Pharmaceutical Research 2002;19(10):1537-43.

(43) Xin Y, Bai S, Damico-Beyer LA, Jin D, Liang WC, Wu Y, et al. Anti-neuropilin-1 (MNRP1685A): unexpected pharmacokinetic differences across species, from preclinical models to humans. Pharm Res 2012 Sep;29(9):2512-21.

(44) Bonate PL. Pharmacokinetic-Pharmacodynamic Modeling and Simulation. 2nd ed. New York: Springer; 2011.

(45) Parrott N, Paquereau N, Coassolo P, Lave T. An evaluation of the utility of physiologically based models of pharmacokinetics in early drug discovery. J Pharm Sci 2005 Oct;94(10):2327-43.

(46) Lave T, Levet-Trafit B, Schmitt-Hoffmann AH, Morgenroth B, Richter W, and Chou RC. Interspecies scaling of interferon disposition and comparison of allometric scaling with concentration-time transformations. J Pharm Sci 1995;84(11):1285-90.

(47) Baxter LT, Zhu H, Mackensen DG, Butler WF, and Jain RK. Biodistribution of monoclonal antibodies: scale-up from mouse to human using a physiologically based pharmacokinetic model. Cancer Research 1995;55(20):4611-22.

(48) Davda JP, Jain M, Batra SK, Gwilt PR, Robinson DH. A physiologically based pharmacokinetic (PBPK) model to characterize and predict the disposition of monoclonal antibody CC49 and its single chain Fv constructs. Int Immunopharmacol 2008 Mar;8(3):401-13.

(49) Urva SR, Yang VC, and Balthasar JP. Physiologically based pharmacokinetic model for T84.66: a monoclonal anti-CEA antibody. J Pharm Sci 2010;99(3):1582-600.

(50) Shah D, Betts A. Towards a platform PBPK model to characterize the plasma and tissue disposition of monoclonal antibodies in preclinical species and human. Journal of Pharmacokinetics and Pharmacodynamics 2012 Feb 1;39(1):67-86.

(51) Ferl GZ, Wu AM, DiStefano JJ, III. A predictive model of therapeutic monoclonal antibody dynamics and regulation by the neonatal Fc receptor (FcRn). Ann Biomed Eng 2005 Nov;33(11):1640-52.

(52) Gill KL, Gardner I, Li L, Jamei M. A Bottom-Up Whole-Body Physiologically Based Pharmacokinetic Model to Mechanistically Predict Tissue Distribution and the Rate of Subcutaneous Absorption of Therapeutic Proteins. AAPS J 2015 Sep 25. Open access from http://link.springer.com/article/10.1208%2Fs12248-015-9819-4.

(53) Boxenbaum H. Interspecies pharmacokinetic scaling and the evolutionary-comparative paradigm. Drug Metab Rev 1984;15(5-6):1071-121.

(54) Gayon J. History of the Concept of Allometry. American Zoologist 2000 Oct 1;40(5):748-58.

(55) Offman E, Edginton AN. Contrasting toxicokinetic evaluations and interspecies pharmacokinetic scaling approaches for small molecules and biologics: applicability to biosimilar development. Xenobiotica 2013 Jun;43(6):561-9.

(56) Mahmood I. Pharmacokinetic allometric scaling of coagulation factors and tissue-type plasminogen activators. Haemophilia 2009;15(5):1109-17.

(57) Mahmood I. Pharmacokinetic allometric scaling of antibodies: application to the first-in-human dose estimation. J Pharm Sci 2009;98(10):3850-61.

(58) Mordenti J, Chen SA, Moore JA, Ferraiolo BL, and Green JD. Interspecies scaling of clearance and volume of distribution data for five therapeutic proteins. Pharmaceutical Research 1991;8(11):1351-9.

(59) Swanson SJ, Bussiere J. Immunogenicity assessment in non-clinical studies. Curr Opin Microbiol 2012 Jun;15(3):337-47.

(60) Huh Y, Smith DE, Feng MR. Interspecies scaling and prediction of human clearance: comparison of small- and macro-molecule drugs. Xenobiotica 2011 Nov;41(11):972-87.

(61) Ling J, Zhou H, Jiao Q, and Davis HM. Interspecies scaling of therapeutic monoclonal antibodies: initial look. Journal of Clinical Pharmacology 2009;49(12):1382-402.

(62) Wang W, and Prueksaritanont T. Prediction of human clearance of therapeutic proteins: simple allometric scaling method revisited. Biopharmaceutics & Drug Disposition 2010;31(4):253-63.

(63) Deng R, Iyer S, Theil FP, Mortensen DL, Fielder PJ, and Prabhu S. Projecting human pharmacokinetics of therapeutic antibodies from nonclinical data: what have we learned? Therapeutic monoclonal antibodies 2011;3(1):61-6.

(64) Dong JQ, Salinger DH, Endres CJ, Gibbs JP, Hsu CP, Stouch BJ, et al. Quantitative prediction of human pharmacokinetics for monoclonal antibodies: retrospective analysis of monkey as a single species for first-in-human prediction. Clin Pharmacokinet 2011 Feb 1;50(2):131-42.

(65) Offman E, Edginton AN. Pharmacokinetic Time Course Scaling of a Subcutaneously Administered Pegylated Peptide Conjugate for a First-in-Human Investigation. Eur J Drug Metab Pharmacokinet 2016 Feb 2. Online first publication.

(66) Offman E, Edginton AN. A PBPK workflow for first-in-human dose selection of a subcutaneously administered pegylated peptide. J Pharmacokinet Pharmacodyn 2015 Apr;42(2):135-50.

(67) Offman E, Phipps C, Edginton AN. Population physiologically-based pharmacokinetic model incorporating lymphatic uptake for a subcutaneously administered pegylated peptide. *In Silico* Pharmacol 2016 Dec;4(1):3.

(68) Beyond the Generics Horizon. Datamonitor plc; 2009 Jun. Report No.: DMHC2477.

(69) European Medicines Agency Scientific Guidelines on Biosimilars. EMA Website 2012 [cited 2016 May 11];Available from: URL: http://www.ema.europa.eu/ema/index.jsp?curl=pages/regulation/general/general_content_000408.jsp&mid=WC0b01ac058002958c&jsenabled=true

(70) Guideline on Similar Biological Medicinal Products Containing Biotechnology-Derived Proteins as Active Substance:Non-Clinical and Clinical Issues. 2006. European Medicines Agency, Committee for Medicinal Products for Human Use.

(71) Rituxamab, Biologic license Application. Preclinical and Clinical Pharmacology Review. 1997.; [cited 2016 May 11];Available from: URL: http://www.fda.gov/downloads/Drugs/DevelopmentApprovalProcess/HowDrugsareDevelopedandApproved/ApprovalApplications/TherapeuticBiologicApplications/ucm113334.pdf

(72) Mascelli MA, Zhou H, Sweet R, Getsy J, Davis HM, Graham M, et al. Molecular, Biologic, and Pharmacokinetic Properties of Monoclonal Antibodies: Impact of These Parameters on Early Clinical Development. The Journal of Clinical Pharmacology 2007 May 1;47(5):553-65.

(73) Schellekens H. Biosimilar therapeutics-what do we need to consider? NDT Plus 2009;2(Suppl_1):i27-i36.

(74) Obach RS, Baxter JG, Liston TE, Silber BM, Jones BC, MacIntyre F, et al. The prediction of human pharmacokinetic parameters from preclinical and in vitro metabolism data. Journal of Pharmacology and Experimental Therapeutics 1997;283(1):46-58.

(75) Ring BJ, Chien JY, Adkison KK, Jones HM, Rowland M, Jones RD, et al. PhRMA CPCDC initiative on predictive models of human pharmacokinetics, part 3: Comparative assessement of prediction methods of human clearance. J Pharm Sci 2011 May 3;100(10):4090-110.

(76) Wajima T, Fukumura K, Yano Y, Oguma T. Prediction of human pharmacokinetics from animal data and molecular structural parameters using multivariate regression analysis: oral clearance. J Pharm Sci 2003 Dec;92(12):2427-40.

(77) Wajima T, Yano Y, Fukumura K, Oguma T. Prediction of human pharmacokinetic profile in animal scale up based on normalizing time course profiles. J Pharm Sci 2004 Jul;93(7):1890-900.

(78) Tang H, Hussain A, Leal M, Mayersohn M, and Fluhler E. Interspecies Prediction of Human Drug Clearance Based on Scaling Data from One or Two Animal Species. Drug Metabolism and Disposition 2007;35(10):1886-93.

(79) Mahmood I. Role of fixed coefficients and exponents in the prediction of human drug clearance: how accurate are the predictions from one or two species? J Pharm Sci 2009;98(7):2472-93.

(80) Kleiber M. Body size and metabolism. Hilgardia 1932;6(11):315-53.

(81) West GB, Brown JH. The origin of allometric scaling laws in biology from genomes to ecosystems: towards a quantitative unifying theory of biological structure and organization. Journal of Experimental Biology 2005 May 1;208(9):1575-92.

(82) Mahmood I, Balian JD. Interspecies scaling: predicting clearance of drugs in humans. Three different approaches. Xenobiotica 1996 Sep;26(9):887-95.

(83) Boxenbaum H, Fertig JB. Scaling of camptothecin plasma protein binding in 24 species. Biopharm Drug Dispos 1984 Oct;5(4):405-8.

(84) Boxenbaum H. Time concepts in physics, biology, and pharmacokinetics. J Pharm Sci 1986 Nov;75(11):1053-62.

(85) Dedrick R, Bischoff KB, Zaharko DS. Interspecies correlation of plasma concentration history of methotrexate (NSC-740). Cancer Chemother Rep 1970 Apr;54(2):95-101.

(86) Boxenbaum H, Ronfeld R. Interspecies pharmacokinetic scaling and the Dedrick plots. Am J Physiol 1983 Dec;245(6):R768-R775.

(87) Mahmood I, Yuan R. A comparative study of allometric scaling with plasma concentrations predicted by species-invariant time methods. Biopharm Drug Dispos 1999 Apr;20(3):137-44.

(88) Boxenbaum H, Fertig JB. Scaling of antipyrine intrinsic clearance of unbound drug in 15 mammalian species. Eur J Drug Metab Pharmacokinet 1984 Apr;9(2):177-83.

(89) Oitate M, Nakayama S, Ito T, Kurihara A, Okudaira N, Izumi T. Prediction of Human Plasma Concentration-Time Profiles of Monoclonal Antibodies from Monkey Data by Species-Invariant Time Method. Drug Metab Pharmacokinet 2011 Dec 6.

(90) Akabane T, Tabata K, Kadono K, Sakuda S, Terashita S, and Teramura T. A Comparison of Pharmacokinetics between Humans and Monkeys. Drug Metabolism and Disposition 2010;38(2):308-16.

(91) Woo S, and Jusko WJ. Interspecies comparisons of pharmacokinetics and pharmacodynamics of recombinant human erythropoietin. Drug Metabolism and Disposition 2007;35(9):1672-8.

(92) Thygesen P, Macheras P, and Van Peer A. Physiologically-based PK/PD modelling of therapeutic macromolecules. Pharmaceutical Research 2009;26(12):2543-50.

(93) Espie P, Tytgat D, Sargentini-Maier ML, Poggesi I, Watelet JB. Physiologically based pharmacokinetics (PBPK). Drug Metab Rev 2009;41(3):391-407.

(94) Shargel L, Yu A. Applied Biopharmaceutics and Pharmacokinetics. 3rd ed. Norwalk: Appleton & Lange; 1993.

(95) Yates JW, Arundel PA. On the volume of distribution at steady state and its relationship with two-compartmental models. J Pharm Sci 2008 Jan;97(1):111-22.

(96) Vuppugalla R, Marathe P, He H, Jones RD, Yates JW, Jones HM, et al. PhRMA CPCDC initiative on predictive models of human pharmacokinetics, part 4: Prediction of plasma concentration-time profiles in human from in vivo preclinical data by using the Wajima approach. J Pharm Sci 2011 Apr 7.

(97) Woodburn KW, Fong KL, Wilson SD, Sloneker S, Strzemienski P, Solon E, et al. Peginesatide clearance, distribution, metabolism, and excretion in monkeys following intravenous administration. Drug Metab Dispos 2013 Apr;41(4):774-84.

(98) Oitate M, Masubuchi N, Ito T, Yabe Y, Karibe T, Aoki T, et al. Prediction of human pharmacokinetics of therapeutic monoclonal antibodies from simple allometry of monkey data. Drug Metab Pharmacokinet 2011;26(4):423-30.

(99) Davies B, Morris T. Physiological parameters in laboratory animals and humans. Pharm Res 1993 Jul;10(7):1093-5.

(100) Mahmood I. Interspecies scaling of protein drugs: prediction of clearance from animals to humans. J Pharm Sci 2004;93(1):177-85.

(101) Baxter LT, Zhu H, Mackensen DG, Jain RK. Physiologically based pharmacokinetic model for specific and nonspecific monoclonal antibodies and fragments in normal tissues and human tumor xenografts in nude mice. Cancer Res 1994 Mar 15;54(6):1517-28.

(102) Garg A, Balthasar JP. Physiologically-based pharmacokinetic (PBPK) model to predict IgG tissue kinetics in wild-type and FcRn-knockout mice. J Pharmacokinet Pharmacodyn 2007 Oct;34(5):687-709.

(103) Mahmood I. Pharmacokinetic allometric scaling of oligonucleotides. Nucleic Acid Ther 2011 Oct;21(5):315-21.

(104) Jolling K, Perez Ruixo JJ, Hemeryck A, Vermeulen A, Greway T. Mixed-effects modelling of the interspecies pharmacokinetic scaling of pegylated human erythropoietin. Eur J Pharm Sci 2005 Apr;24(5):465-75.

(105) R: A language and environment for statistical computing [computer program]. Version 3 R Foundation for Statistical Computing; 2013.

(106) Wickham H. ggplot2: Elegant graphics for data analysis. New York: Springer; 2009.

(107) Knibbe CA, Zuideveld KP, Aarts LP, Kuks PF, Danhof M. Allometric relationships between the pharmacokinetics of propofol in rats, children and adults. Br J Clin Pharmacol 2005 Jun;59(6):705-11.

(108) Hope WW, Kaibara A, Roy M, Arrieta A, Azie N, Kovanda LL, et al. Population pharmacokinetics of micafungin and its metabolites M1 and M5 in children and adolescents. Antimicrob Agents Chemother 2015 Feb;59(2):905-13.

(109) Zhao L, Ji P, Li Z, Roy P, Sahajwalla CG. The antibody drug absorption following subcutaneous or intramuscular administration and its mathematical description by coupling physiologically based absorption process with the conventional compartment pharmacokinetic model. J Clin Pharmacol 2013 Mar;53(3):314-25.

(110) Richter WF, Jacobsen B. Subcutaneous absorption of biotherapeutics: knowns and unknowns. Drug Metab Dispos 2014 Nov;42(11):1881-9.

(111) Jolling K, Ruixo JJ, Hemeryck A, Piotrovskij V, and Greway T. Population pharmacokinetic analysis of pegylated human erythropoietin in rats. J Pharm Sci 2004;93(12):3027-38.

(112) Rippe B, Haraldsson B. Fluid and protein fluxes across small and large pores in the microvasculature. Application of two-pore equations. Acta Physiol Scand 1987 Nov;131(3):411-28.

(113) Kagan L, Mager DE. Mechanisms of subcutaneous absorption of rituximab in rats. Drug Metab Dispos 2013 Jan;41(1):248-55.

(114) Zheng Y, Tesar DB, Benincosa L, Birnbock H, Boswell CA, Bumbaca D, et al. Minipig as a potential translatable model for monoclonal antibody pharmacokinetics after intravenous and subcutaneous administration. MAbs 2012 Mar;4(2):243-55.

(115) Graf JF, Scholz BJ, Zavodszky MI. BioDMET: a physiologically based pharmacokinetic simulation tool for assessing proposed solutions to complex biological problems. J Pharmacokinet Pharmacodyn 2012 Feb;39(1):37-54.

(116) Kawai R, Mathew D, Tanaka C, Rowland M. Physiologically based pharmacokinetics of cyclosporine A: extension to tissue distribution kinetics in rats and scale-up to human. J Pharmacol Exp Ther 1998 Nov;287(2):457-68.

(117) Iwama R, Sato T, Sakurai K, Takasuna K, Ichijo T, Furuhama K, et al. Estimation of Glomerular Filtration Rate in Cynomolgus Monkeys (Macaca fascicularis). J Vet Med Sci 2014 Jul 7;76(10):1423-6.

(118) Gordon S. Alternative activation of macrophages. Nat Rev Immunol 2003 Jan;3(1):23-35.

(119) Li Z, Rana TM. Therapeutic targeting of microRNAs: current status and future challenges. Nat Rev Drug Discov 2014 Aug;13(8):622-38.

(120) Bacher G, Szymanski WW, Kaufman SL, Zollner P, Blaas D, Allmaier G. Charge-reduced nano electrospray ionization combined with differential mobility analysis of peptides, proteins, glycoproteins, noncovalent protein complexes and viruses. J Mass Spectrom 2001 Sep;36(9):1038-52.

(121) Pease LF, III, Elliott JT, Tsai DH, Zachariah MR, Tarlov MJ. Determination of protein aggregation with differential mobility analysis: application to IgG antibody. Biotechnol Bioeng 2008 Dec 15;101(6):1214-22.

(122) Peters SA. Evaluation of a generic physiologically based pharmacokinetic model for lineshape analysis. Clin Pharmacokinet 2008;47(4):261-75.

(123) Mordenti J. Man versus beast: pharmacokinetic scaling in mammals. J Pharm Sci 1986 Nov;75(11):1028-40.

(124) Lubach D, Ludemann W, Berens von RD. Recent findings on the angioarchitecture of the lymph vessel system of human skin. Br J Dermatol 1996 Nov;135(5):733-7.

(125) McNally K, Cotton R, Hogg A, Loizou G. PopGen: A virtual human population generator. Toxicology 2014 Jan 6;315:70-85.

(126) Willmann S, Hohn K, Edginton A, Sevestre M, Solodenko J, Weiss W, et al. Development of a physiology-based whole-body population model for assessing the influence of individual variability on the pharmacokinetics of drugs. J Pharmacokinet Pharmacodyn 2007 Jun;34(3):401-31.

(127) Craig P, Halavatau V, Comino E, Caterson I. Differences in body composition between Tongans and Australians: time to rethink the healthy weight ranges? Int J Obes Relat Metab Disord 2001 Dec;25(12):1806-14.

(128) Heymsfield SB, Gallagher D, Mayer L, Beetsch J, Pietrobelli A. Scaling of human body composition to stature: new insights into body mass index. Am J Clin Nutr 2007 Jul;86(1):82-91.

(129) Feldschuh J, Enson Y. Prediction of the normal blood volume. Relation of blood volume to body habitus. Circulation 1977 Oct;56(4 Pt 1):605-12.

(130) de la Grandmaison GL, Clairand I, Durigon M. Organ weight in 684 adult autopsies: new tables for a Caucasoid population. Forensic Sci Int 2001 Jun 15;119(2):149-54.

(131) Jacob M, Annaheim S, Boutellier U, Hinske C, Rehm M, Breymann C, et al. Haematocrit is invalid for estimating red cell volume: a prospective study in male volunteers. Blood Transfus 2012 Oct;10(4):471-9.

(132) Ritz E, Benck U, Franek E, Keller C, Seyfarth M, Clorius J. Effects of smoking on renal hemodynamics in healthy volunteers and in patients with glomerular disease. J Am Soc Nephrol 1998 Oct;9(10):1798-804.

(133) Basic anatomical and physiological data for use in radiological protection: reference values. A report of age- and gender-related differences in the anatomical and physiological characteristics of reference individuals. ICRP Publication 89. Ann ICRP 2002;32(3-4):5-265.

(134) Bosgra S, van EJ, Bos P, Zeilmaker M, Slob W. An improved model to predict physiologically based model parameters and their inter-individual variability from anthropometry. Crit Rev Toxicol 2012 Oct;42(9):751-67.

(135) Gehan EA, George SL. Estimation of human body surface area from height and weight. Cancer Chemother Rep 1970 Aug;54(4):225-35.

(136) Delanaye P, Schaeffner E, Ebert N, Cavalier E, Mariat C, Krzesinski JM, et al. Normal reference values for glomerular filtration rate: what do we really know? Nephrol Dial Transplant 2012 Jul;27(7):2664-72.

(137) K/DOQI clinical practice guidelines for chronic kidney disease: evaluation, classification, and stratification. Am J Kidney Dis 2002 Feb;39(2 Suppl 1):S1-266.

(138) Uren RF, Howman-Giles R, Thompson JF. Patterns of lymphatic drainage from the skin in patients with melanoma. J Nucl Med 2003 Apr;44(4):570-82.

(139) Verhagen A, Ebels JT, Dogterom AA, Jonkman JH. Pharmacokinetics and pharmacodynamics of a single dose of recombinant human growth hormone after subcutaneous administration by jet-injection: comparison with conventional needle-injection. Eur J Clin Pharmacol 1995;49(1-2):69-72.

(140) Tegenge MA, Mitkus RJ. A first-generation physiologically based pharmacokinetic (PBPK) model of alpha-tocopherol in human influenza vaccine adjuvant. Regul Toxicol Pharmacol 2015 Apr;71(3):353-64.

(141) Tegenge MA, Mitkus RJ. A physiologically-based pharmacokinetic (PBPK) model of squalene-containing adjuvant in human vaccines. J Pharmacokinet Pharmacodyn 2013 Oct;40(5):545-56.

(142) Jones HM, Mayawala K, Poulin P. Dose selection based on physiologically based pharmacokinetic (PBPK) approaches. AAPS J 2013 Apr;15(2):377-87.

(143) Porter CJ, Charman SA. Lymphatic transport of proteins after subcutaneous administration. J Pharm Sci 2000 Mar;89(3):297-310.

(144) Jones RD, Jones HM, Rowland M, Gibson CR, Yates JW, Chien JY, et al. PhRMA CPCDC initiative on predictive models of human pharmacokinetics, part 2: Comparative assessment of prediction methods of human volume of distribution. J Pharm Sci 2011 Mar 30.

(145) Characterization adn application of physiologically based pharmacokinetic models in risk assessment. World Health Organization; 2010. Report No.: International Programme on Chemical Safety, Harmonization document No.9.

(146) Chen T, Mager DE, Kagan L. Interspecies modeling and prediction of human exenatide pharmacokinetics. Pharm Res 2013 Mar;30(3):751-60.

8 Appendices

8.1 Chapter 5 Appendix 5.1

Representative Mass Balance Equations for a Generic PBPK Model for SC Administration of a Pegylated Protein Conjugate with Renal and Non-Specific Clearance

Venous Plasma Circulation

$$Vven\frac{Cven}{dt} = (Q_{heart} - L_{heart})* C_{pla,organ} + (Q_{adipose} - L_{adipose})* C_{pla,adipose} + (Q_{muscle} - L_{muscle})* C_{pla,muscle} + (Q_{kidney} - L_{kidney})* C_{pla,kidney} + (Q_{bone} - L_{bone})* C_{pla,bone} + (Q_{skin} - L_{skin})* C_{pla,skin} + (Q_{thymus} - L_{thymus})* C_{pla,thymus} + (Q_{other} - L_{other})* C_{pla,other} + ((Q_{liver} - L_{liver}) + (Q_{smallintestines} - L_{smallintestines}) + (Q_{largeintestines} - L_{largeintestines}) + (Q_{spleen} - L_{spleen}) + (Q_{pancreas} - L_{pancreas}))*C_{pla,liver} + (L_{lymph}*C_{lymph}) - (Q_{lung}*C_{ven}) - NRCL_{ven}*C_{ven}$$

Arterial Plasma Circulation

$$Vart\frac{Cart}{dt} = ((Q_{lung}-L_{lung})*C_{pla,lung}) - ((Q_{heart} + Q_{adipose} + Q_{muscle} + Q_{kidney} + Q_{bone} + Q_{thymus} + Q_{skin} + Q_{brain} + Q_{liver} + Q_{smallintestines} + Q_{largeintestines} + Q_{spleen} + Q_{pancreas} + Q_{other}) *C_{art}) - NRCL_{art}*C_{art}$$

Lymph

$$Vlymph\frac{Clymph}{dt} = \Sigma (L_{organ}*(1-\sigma_{isf})*C_{isf,organ}) - (L_{lymph}*C_{lymph})$$

Lung Vascular

$$Vpla,lung\frac{Cpla,lung}{dt} = (Q_{lung}*C_{ven}) - (L_{lung}*(1-(\sigma_{v,sf}*\sigma_{v,lung}))*C_{pla,lung}) - ((Q_{lung}-L_{lung})*C_{pla,lung}) - NRCL_{pla,lung}*C_{pla,lung}$$

Lung Interstitial

$$Visf,lung\frac{Cisf,lung}{dt} = (L_{lung}*(1-(\sigma_{v,sf}*\sigma_{v,lung}))*C_{pla,lung}) - (L_{lung}*(1-\sigma_{isf})*C_{isf,lung}) - NRCL_{isf,lung}*C_{isf,lung}$$

Kidney Vascular

$$Vpla,kidney\frac{Cpla,kidney}{dt} = (Q_{kidney}* C_{art}) - (L_{kidney}*(1-(\sigma_{v,sf}*\sigma_{v,kidney}))*C_{pla,kidney}) - ((Q_{kidney}-L_{kidney})* C_{pla,kidney}) - (GFR*FGFR*C_{pla,kidney}) - (NRCL_{pla,kidney} * C_{pla,kidney})$$

Kidney Interstitial

$$Visf,kidney\frac{Cisf,kidney}{dt} = (L_{kidney}*(1-(\sigma_{v,sf}*\sigma_{v,kidney}))*C_{pla,kidney}) - (L_{kidney}*(1-\sigma_{isf})*C_{isf,kidney}) - NRCL_{isf,kidney}*C_{isf,kidney}$$

Skin Vascular

$$Vpla,skin\frac{Cpla,skin}{dt} = (Q_{skin}* C_{art}) - ((L_{skin} + L_{depot})*(1-(\sigma_{v,sf}*\sigma_{v,skin}))*C_{pla,skin}) - ((Q_{skin}-(L_{skin} + L_{depot}))*C_{pla,skin}) - NRCL_{pla,skin}$$

Skin Interstitial

$$Visf,skin\frac{Cisf,skin}{dt} = (L_{skin} *(1-(\sigma_{v,sf}* \sigma_{v,skin}))*C_{pla,skin}) - (L_{skin}*(1-\sigma_{isf})*C_{isf,skin}) - NRCL_{isf,skin}*C_{isf,skin}$$

Skin Subcutaneous Depot

$$Vdepot\frac{Cdepot}{dt} = (L_{depot} *(1-(\sigma_{v,sf}* \sigma_{v,skin}))*C_{depot}) - (L_{depot}*(1-\sigma_{isf})*C_{depot}) - NRCL_{depot}*C_{depot}$$

Liver Vascular

$$Vpla,liver\frac{Cpla,liver}{dt} = = (Q_{liver} * C_{art}) + ((Q_{smallintestines}-L_{smallintestines})*C_{pla,smallintestines}) + ((Q_{largeintestines}-L_{largeintestines})*C_{pla,largeintestines}) + ((Q_{spleen}-L_{spleen}) * C_{pla,spleen}) + ((Q_{pancreas}-L_{pancreas})*C_{pla,pancreas}) - (L_{liver} * (1-(\sigma_{v,sf} * \sigma_{v,liver}))*C_{pla,liver}) - ((((Q_{liver}-L_{liver}) + (Q_{smallintestines}-L_{smallintestines}) + (Q_{largeintestines}-L_{largeintestines}) + (Q_{spleen}-L_{spleen}) + (Q_{pancreas}-L_{pancreas}))*C_{pla,liver}) - NRCL_{pla,liver}*C_{pla,liver}$$

Liver Interstitial

$$V_{isf,liver}\frac{C_{isf,liver}}{dt} = = (L_{liver} * (1-(\sigma_{v,sf} * \sigma_{v,liver}))*C_{pla,liver}) - (L_{liver}*(1-\sigma_{isf})*C_{isf,liver}) - NRCL_{isf,liver}*C_{isf,liver}$$

Remaining Organs Vascular

$$V_{pla,kidney}\frac{C_{pla,kidney}}{dt} = (Q_{organ}* C_{art}) - (L_{organ}*(1-(\sigma_{v,sf}*\sigma_{v,organ}))*C_{pla,organ}) - ((Q_{organ}-L_{organ})* C_{pla,organ}) - (GFR*FGFR*C_{pla,organ}) - (NRCL_{pla,organ} * C_{pla,organ})$$

Remaining Organs Interstitial

$$V_{isf,kidney}\frac{C_{isf,kidney}}{dt} = (L_{organ}*(1-(\sigma_{v,sf}*\sigma_{v,organ}))*C_{pla,organ}) - (L_{organ}*(1-\sigma_{isf})*C_{isf,organ}) -NRCL_{isf,organ}*C_{isf,organ}$$

Abbreviations

FGFR: Fraction of glomerular filtration rate attributed to renal clearance
GFR: Glomerular filtration rate
ISF (subscripted): Interstitial space
L: Lymph flow
NRCL: Non-Renal clearance
Pla (subscripted): Plasma
Q: Blood Flow
V_{art}, V_{ven}: Volume of the arterial and venous plasma space
V_{lymph}: Volume of the lymph node space
$V_{isf,organ}$: Volume of the organ interstitial space
$V_{pla,organ}$: Volume of the organ plasma vascular space
$\sigma_{v,sf}$: Vascular reflection coefficient, scaling factor
$\sigma_{v,organ}$: Organ vascular reflection coefficient
$\sigma_{v,isf}$: Interstitial reflection coefficient

8.2 Chapter 5 Appendix 5.2:

Monkey and Human Anatomical and Physiological Values

	Monkey		Human			
	Volume (mL per kg)	Blood Flow Fraction of Cardiac Output	Volume (per kg)	Blood Flow Fraction of Cardiac Output	Fraction Vascular	Fraction Interstitial
Organ						
heart	4.56	0.03	4.80	0.043	0.262	0.1
lung	24.78	1	32.31	1	0.262	0.188
muscle	527.96	0.18	423.63	0.188	0.026	0.12
skin	108.77	0.11	48.00	0.065	0.019	0.302
adipose	24.91	0.01	189.65	0.063	0.01	0.135
bone	153.52	0.01	143.17	0.015	0.041	0.1
brain	15.16	0.07	20.41	0.12	0.039	0.18
kidney	4.40	0.15	4.67	0.204	0.105	0.2
liver	30.13	0.06	30.18	0.074	0.115	0.163
smallintestine	31.85	0.16	10.86	0.069	0.024	0.094
largeintestine	45.27	0.16	15.43	0.072	0.024	0.094
pancreas	2.01	0.02	1.46	0.017	0.2	0.173
thymus	0.34	0.01	0.09	0.002	0.03	0.15
spleen	0.96	0.01	3.12	0.036	0.282	0.15
other	14.96	0.04	7.07	0.032	0.103	0.154
lymph	4.04		3.86			
Blood	4.56		80.05			
Other: bladder, stomach, gallbladder, adrenals, thyroid						

Additional Physiological Parameters	Monkeys	Humans	
Cardiac Output (mL/hr/kg)	6472.26	4564.22	
Hematocrit	0.41	0.44	

8.3 Chapter 6 Appendix 6.1

Representative Mass Balance Equations for a Generic PBPK Model for SC Administration of a Pegylated Protein Conjugate with Renal and Non-Specific Clearance

Venous Plasma Circulation

$$V_{ven} * \frac{dC_{ven}}{dt} = (Q_{heart} - L_{heart}) * C_{pla,heart} + (Q_{adipose} - L_{adipose}) * C_{pla,adipose} + (Q_{muscle} - L_{muscle}) * C_{pla,muscle} + (Q_{kidney} - L_{kidney}) * C_{pla,kidney} + (Q_{bone} - L_{bone}) * C_{pla,bone} + (Q_{skin} - L_{skin}) * C_{pla,skin} + (Q_{thymus} - L_{thymus}) * C_{pla,thymus} + (Q_{other} - L_{other}) * C_{pla,other} + (Q_{brain} - L_{brain}) * C_{pla,brain} + \left[(Q_{liver} - L_{liver}) + (Q_{smallintestines} - L_{smallintestines}) + (Q_{largeintestines} - L_{largeintestines}) + (Q_{spleen} - L_{spleen}) + (Q_{pancreas} - L_{pancreas})\right] * C_{pla,liver} + L_{lymph} * C_{lymph} - Q_{lung} * C_{ven} - NRCL_{ven} * C_{ven}$$

Arterial Plasma Circulation

$$V_{art} * \frac{dC_{art}}{dt} = (Q_{lung} - L_{lung}) * C_{pla,lung} - (Q_{heart} + Q_{adipose} + Q_{muscle} + Q_{kidney} + Q_{bone} + Q_{thymus} + Q_{skin} + Q_{brain} + Q_{liver} + Q_{smallintestines} + Q_{largeintestines} + Q_{spleen} + Q_{pancreas} + Q_{other}) * C_{art} - NRCL_{art} * C_{art}$$

Lymph

$$V_{lymph} * \frac{dC_{lymph}}{dt} = \sum\left(L_{organ} * (1 - \sigma_i) * C_{isf,organ}\right) + L_{depot} * C_{LDC} - L_{lymph} * C_{lymph}$$

Lung Vascular

$$V_{pla,lung} * \frac{dC_{pla,lung}}{dt} = Q_{lung} * C_{ven} - L_{lung} * \left(1 - \sigma_{sf} * \sigma_{v,lung}\right) * C_{pla,lung} - \left(Q_{lung} - L_{lung}\right) * C_{pla,lung} - NRCL_{pla,lung} * C_{pla,lung}$$

Lung Interstitial

$$V_{isf,lung} * \frac{dC_{isf,lung}}{dt} = L_{lung} * \left(1 - \sigma_{sf} * \sigma_{v,lung}\right) * C_{pla,lung} - L_{lung} * (1 - \sigma_i) * C_{isf,lung} - NRCL_{isf,lung} * C_{isf,lung}$$

Kidney Vascular

$$V_{pla,kidney} * \frac{dC_{pla,kidney}}{dt} = Q_{kidney} * C_{art} - L_{kidney} * \left(1 - \sigma_{sf} * \sigma_{v,kidney}\right) * C_{pla,kidney} - \left(Q_{kidney} - L_{kidney}\right) * C_{pla,kidney} - \mathrm{GFR} * \mathrm{FGFR} * C_{pla,kidney} - NRCL_{pla,kidney} * C_{pla,kidney}$$

Kidney Interstitial

$$V_{isf,kidney} * \frac{dC_{isf,kidney}}{dt} = L_{kidney} * (1 - \sigma_{sf} * \sigma_{v,kidney}) * C_{pla,kidney} - L_{kidney} * (1 - \sigma_i) * C_{isf,kidney} - NRCL_{isf,kidney} * C_{isf,kidney}$$

Skin Vascular

$$V_{pla,skin} * \frac{dC_{pla,skin}}{dt} = Q_{skin} * C_{art} - \left(L_{skin} + L_{depot}\right) * \left(1 - \sigma_{sf} * \sigma_{v,skin}\right) * C_{pla,skin} - \left(Q_{skin} - \left(L_{skin} + L_{depot}\right)\right) * C_{pla,skin} - NRCL_{pla,skin} * C_{pla,skin}$$

Skin Interstitial

$$V_{isf,skin} * \frac{dC_{isf,skin}}{dt} = L_{skin} * \left(1 - \sigma_{sf} * \sigma_{v,skin}\right) * C_{pla,skin} - L_{skin} * (1 - \sigma_i) * C_{isf,skin} - NRCL_{isf,skin} * C_{isf,skin}$$

Skin Subcutaneous Depot

$$V_{depot} * \frac{dC_{depot}}{dt} = L_{depot} * \left(1 - \sigma_{sf} * \sigma_{v,skin}\right) * C_{depot} - L_{depot} * (1 - \sigma_i) * C_{depot} - NRCL_{depot} * C_{depot}$$

Skin Depot Lymph Drainage Compartment (LDC)

$$V_{LDC} * \frac{dC_{LDC}}{dt} = L_{depot} * (1 - \sigma_i) * C_{depot} - L_{depot} * C_{LDC}$$

Liver Vascular

$$V_{pla,liver} * \frac{dC_{pla,liver}}{dt} = Q_{liver} * C_{art} + (Q_{smallintestines} - L_{smallintestines}) * C_{pla,smallintestines} + \left(Q_{largeintestines} - L_{largeintestines}\right) * C_{pla,largeintestines} + \left(Q_{spleen} - L_{spleen}\right) * C_{pla,spleen} + \left(Q_{pancreas} - L_{pancreas}\right) * C_{pla,pancreas} - L_{liver} * \left(1 - \sigma_{v,sf} * \sigma_{v,liver}\right) * C_{pla,liver} - \left[(Q_{liver} - L_{liver}) + (Q_{smallintestines} - L_{smallintestines}) + \left(Q_{largeintestines} - L_{largeintestines}\right) + \left(Q_{spleen} - L_{spleen}\right) + \left(Q_{pancreas} - L_{pancreas}\right)\right] * C_{pla,liver} - NRCL_{pla,liver} * C_{pla,liver}$$

Liver Interstitial

$$V_{isf,liver} * \frac{dC_{isf,liver}}{dt} = L_{liver} * \left(1 - \sigma_{sf} * \sigma_{v,liver}\right) * C_{pla,liver} - L_{liver} * (1 - \sigma_i) * C_{isf,liver} - NRCL_{isf,liver} * C_{isf,liver}$$

Remaining Organs Vascular

$$V_{pla,organ} * \frac{dC_{pla,organ}}{dt} = Q_{organ} * C_{art} - L_{organ} * \left(1 - \sigma_{sf} * \sigma_{v,organ}\right) * C_{pla,organ} - \left(Q_{organ} - L_{organ}\right) * C_{pla,organ} - NRCL_{pla,organ} * C_{pla,organ}$$

Remaining Organs Interstitial

$$V_{isf,organ} * \frac{dC_{isf,organ}}{dt} = L_{organ} * \left(1 - \sigma_{sf} * \sigma_{v,organ}\right) * C_{pla,organ} - L_{organ} * (1 - \sigma_i) * C_{isf,organ} - NRCL_{isf,organ} * C_{isf,organ}$$

Notation
FGFR: Fraction of glomerular filtration rate attributed to renal clearance
GFR: Glomerular filtration rate
isf (subscripted): Interstitial fluid
L: Lymph flow
NRCL: Non-Renal clearance
pla (subscripted): Plasma
Q: Blood Flow
Vfrac: Fraction of injection volume attributed to the lymph drainage vessels
V_{art}, V_{ven}: Volume of the arterial and venous plasma space

V_{lymph}: Volume of the lymph node space
$V_{isf,organ}$: Volume of the organ interstitial space
$V_{pla,organ}$: Volume of the organ plasma vascular space
σ_{sf}: Vascular reflection coefficient, scaling factor
$\sigma_{v,organ}$: Organ vascular reflection coefficient
σ_i: Interstitial fluid reflection coefficient

9 Copyright/permissions for reprinting published materials

9.1 Chapter 1 reprint of Figure 1.1 permission

Rightslink® by Copyright Clearance Center

Sunday, May 01, 2016
1:02 PM

Title:	Recombinant human hyaluronidase (rHuPH20): an enabling platform for subcutaneous drug and fluid administration	Logged in as: Elliot Offman
Author:	Gregory I Frost	
Publication:	Expert Opinion on Drug Delivery	
Publisher:	Taylor & Francis	Account #: 3000928668
Date:	Jul 1, 2007	
Copyright © 2007 Taylor & Francis		

Thesis/Dissertation Reuse Request

Taylor & Francis is pleased to offer reuses of its content for a thesis or dissertation free of charge contingent on resubmission of permission request if work is published.

9.2 Chapter 2 reprint permission

9.3 Chapter 4 reprint permission

SPRINGER LICENSE
TERMS AND CONDITIONS

Apr 24, 2016

This is a License Agreement between Elliot M Offman ("You") and Springer ("Springer") provided by Copyright Clearance Center ("CCC"). The license consists of your order details, the terms and conditions provided by Springer, and the payment terms and conditions.

All payments must be made in full to CCC. For payment instructions, please see information listed at the bottom of this form.

License Number	3855420042349
License date	Apr 24, 2016
Licensed content publisher	Springer
Licensed content publication	European Journal of Drug Metabolism and Pharmacokinetics
Licensed content title	Pharmacokinetic Time Course Scaling of a Subcutaneously Administered Pegylated Peptide Conjugate for a First-in-Human Investigation
Licensed content author	Elliot Offman
Licensed content date	Jan 1, 2016
Type of Use	Thesis/Dissertation
Portion	Full text
Number of copies	1
Author of this Springer article	Yes and you are the sole author of the new work
Order reference number	None
Title of your thesis / dissertation	De-risking Biologic and Biosimilar Development
Expected completion date	Jul 2016
Estimated size(pages)	250
Total	0.00 CAD
Terms and Conditions	

9.4 Chapter 5 reprint permission

SPRINGER LICENSE
TERMS AND CONDITIONS

Apr 24, 2016

This is a License Agreement between Elliot M Offman ("You") and Springer ("Springer") provided by Copyright Clearance Center ("CCC"). The license consists of your order details, the terms and conditions provided by Springer, and the payment terms and conditions.

All payments must be made in full to CCC. For payment instructions, please see information listed at the bottom of this form.

License Number	3855411358685
License date	Apr 24, 2016
Licensed content publisher	Springer
Licensed content publication	Journal of Pharmacokinetics and Pharmacodynamics
Licensed content title	A PBPK workflow for first-in-human dose selection of a subcutaneously administered pegylated peptide
Licensed content author	Elliot Offman
Licensed content date	Jan 1, 2015
Volume number	42
Issue number	2
Type of Use	Thesis/Dissertation
Portion	Full text
Number of copies	1
Author of this Springer article	Yes and you are the sole author of the new work
Order reference number	None
Title of your thesis / dissertation	De-risking Biologic and Biosimilar Development
Expected completion date	Jul 2016
Estimated size(pages)	250
Total	0.00 CAD
Terms and Conditions	

9.5 Chapter 6 reprint permission

Offman et al. In Silico Pharmacology (2016) 4:3
DOI 10.1186/s40203-016-0018-5

In Silico Pharmacology
a SpringerOpen Journal

ORIGINAL RESEARCH Open Access

Population physiologically-based pharmacokinetic model incorporating lymphatic uptake for a subcutaneously administered pegylated peptide

Elliot Offman, Colin Phipps and Andrea N. Edginton*

Abstract

Purpose: Physiologically-based pharmacokinetic (PBPK) models provide a rational mechanistic approach for predicting the time course of macromolecules in plasma. Population PBPK models for large molecules necessitate incorporation of lymphatic circulation to mechanistically account for biodistribution. Moreover, characterization of subcutaneous absorption requires consideration of the microvascular transit from the injection site to the systemic circulation. A PBPK model for a pegylated peptide conjugate, previously developed for primates, was modified to describe the lymphatic uptake in a population of humans by incorporation of interindividual variability in the lymphatic circulation and a unique lymphatic drainage compartment (LDC). The model was then used to simulate the time course of the drug in a population of humans and compared to the same drug administered to a group of human subjects participating in a first-in-human study.

Methods: Organ, blood and lymph masses for the population were sampled from either normal or log-normal distributions. Blood flows were calculated for each organ based on mean organ perfusion per gram of organ tissue and lymphatic flow was set as a fixed fraction of blood flow. Interindividual variability in lymphatic volume was assumed to be similar to that of blood volume. The volume of the LDC was parameterzed as a fraction of the injection volume. Sensitivity analysis was performed to study uncertain parameters and distribution assumptions.

Results: The population generator was capable of simulating a virtual population incorporating the lymphatic circulation. Incorporation of a LDC resulted in similar line shape relative to the observed data and incorporation of anthropometric variability accounted for individual differences in the absorption and elimination phases across all dose cohorts. Line shape was sensitive to the inclusion of LDC while peak and elimination portions of the time course were influenced by the magnitude of variance assumed for blood volume and renal clearance, respectively.

Conclusion: Lymphatic circulation can be incorporated into a population PBPK model assuming similar interindividual variability as observed for blood volume. Incorporation of an LDC, where the volume of this transit compartment is proportional to the SC injection volume may be an important mechanistic means of predicting the transit from the SC depot to the systemic circulation.

Keywords: Physiologically-based pharmacokinetic model, Subcutaneous, Peptide, Pegylated, Lymph

* Correspondence: aedginto@uwaterloo.ca
School of Pharmacy, University of Waterloo, 200 University Ave W, Waterloo, ON N2L 3G1, Canada